

***Arabidopsis* Tandem Zinc Finger 9, a Mitogen Activated Protein Kinase substrate, binds RNA and mediates immunity**

Dissertation

Zur Erlangung des akademischen Grades

Doctor rerum naturalium (Dr. rer. nat)

Vorgelegt der

Naturwissenschaftlichen Fakultät I
Biowissenschaften

Der Martin-Luther-Universität Halle-Wittenberg

Von

Naheed Tabassum

Geb. am: 27 Januar 1989 in Jharkhand, India

Gutacher /in

1. Prof. Dierk Scheel, Leibniz Institute of Plant Biochemistry (IPB), MLU Halle
2. Prof. Sven-Erik Behrens, MLU Halle
3. Prof. Natalia Requena, KIT Karlsruhe

Verteidigungsdatum: 24.04.2018

Table of Contents

List of abbreviations.....	i
1 Introduction.....	1
1.1 Plant defense system: a general introduction.....	1
1.2 PAMP-triggered immunity (PTI).....	2
1.3 MAPK signaling cascade.....	3
1.3.1 Identification of MAPK substrates.....	4
1.3.2 Role of MAPK substrates in various cellular processes.....	6
1.3.3 <i>Arabidopsis</i> MAPK substrates are involved in immunity at transcriptional and post-transcriptional level.....	7
1.4 Processing Bodies (p-bodies or PB).....	7
1.5 Tandem Zinc-finger (TZFs) proteins in <i>Arabidopsis</i>	8
1.5.1 TZF9 (Tandem Zinc Finger 9).....	11
1.6 Aim of the study.....	12
2 Materials and Methods.....	13
2.1 Materials.....	13
2.1.1 Plants.....	13
2.1.2 Bacteria.....	13
2.1.3 Medium.....	14
2.2 Methods.....	14
2.2.1 Protoplast transient assays.....	14
2.2.2 Molecular cloning processes.....	16
2.2.3 Extraction of <i>Arabidopsis</i> genomic DNA and selection of knockout lines 18	
2.2.4 RNA Extraction.....	18
2.2.5 DNase I treatment.....	19
2.2.6 Synthesis of cDNA from mRNA.....	19
2.2.7 Quantitative real-time PCR (qRT-PCR).....	19
2.2.8 Protein purification and related assays.....	19
2.2.9 <i>In-vitro</i> RNA binding assays.....	22
2.2.10 Determination of ROS.....	24
2.2.11 Isolation and purification of total mRNA for microarray.....	24
2.2.12 Isolation and purification of polysomal mRNA for microarray.....	24
2.2.13 Microarray.....	25

3	Results.....	27
3.1	TZF9 as MPK3/6 substrate in PTI	27
3.1.1	TZF9 shows mobility shift upon flg22 treatment.....	27
3.1.2	TZF9 shows phosphorylation at multiple sites	27
3.1.3	A phosphonull version of TZF9 does not show flg22 induced mobility shift 29	
3.1.4	TZF9 shows mobility shift due to phosphorylation after flg22 elicitation.	30
3.1.5	TZF9 is phosphorylated by activation of MKK5-MPK3/6 pathway post flg22 elicitation.....	31
3.1.6	TZF9 interacts with MPK3 and MPK6	32
3.1.7	TZF9 phosphorylation by MAPKs alters its stability	33
3.1.8	TZF9 relocates upon flg22 treatment.....	34
3.2	TZF9 localizes within Processing Bodies (PB).	36
3.3	TZF9 interacts with RNA <i>in-vitro</i>	36
3.3.1	TZF9 shows affinity to poly U and poly G ribohomopolymers	37
3.3.2	TZF9 binds specifically to pentaprobe 2 among other RNA sequences.	38
3.4	TZF9 interacts with a calmodulin binding protein annotated as a putative RNA ligase39	
3.4.2	Validation of interaction between TZF9 and putative RNA ligase by Co- immunoprecipitation (CoIP)	40
3.4.3	Ankyrin domain of TZF9 is required for interaction with putative RNA ligase 41	
3.4.4	TZF9 interacts with putative RNA ligase predominantly in cell cytoplasm 42	
3.4.5	Putative RNA ligase is localized in cytoplasm.....	43
3.5	TZF9 and plant immunity	44
3.5.1	Attenuated defense response in <i>tzf9</i> knockout line: ROS assay.....	44
3.5.2	Omics studies to characterize TZF9.....	45
4	Discussion	58
4.1	TZF9 is a MAPK substrate.....	58
4.2	Phosphosite mapping of TZF9: Challenges and prospects	59
4.3	Localization studies suggest the dynamic nature of TZF9.....	60
4.4	TZF9 binds to specific RNA sequences:.....	61
4.5	TZF9 interaction with putative RNA ligase.....	63
4.6	Global gene expression changes regulated by TZF9: omics approach	65

4.7	TZF9 as possible post-transcriptional regulator of gene expression.....	66
4.8	CCCH-TZFs are involved in stress-response: a future perspective.....	67
5	Summary	69
6	References	71
7	Appendix I.....	77
8	Appendix II (Data provided in CD)	0

List of abbreviations

ABA	Abscisic acid
ActD	Actinomycin D
AGO1	ARGONAUTE 1
AMD	ARE (AU-rich element)-mediated mRNA decay
ANK	Ankyrin
ARE	AU-rich element
AtCPSF30	Cleavage and polyadenylation specificity factor
Avr	Avirulence
BAK1	BRI1-associated receptor kinase
BiFC	Bimolecular fluorescence complementation assay
BIK1	Botrytis-induced kinase 1
BIR2	BAK1 interacting receptor-like kinase
C/G/Y/RFP	Cyan/green/yellow/red fluorescent protein
CaCl ₂	Calcium chloride CaCl ₂
CaM	Calmodulin binding proteins
CCCH	Cysteine Cysteine Cysteine Histidine
CDPK	Ca ²⁺ -dependent protein kinases
CoIP	Co-immunoprecipitation
Col-0	Arabiopsis accessions Columbia
DABG	detection above background calls
DCP1	Decapping 1
DEGs	Differentially expressed genes
DEPC	Diethylpyrocarbonate
ETI	Effector triggered immunity
ETS	Effector-triggered susceptibility
flg22	Flagellin 22
FLS2	Flagellin insensitive 2
GA	Gibberellic acid
GhZFP1	Cotton Zinc Finger Protein 1
HA	Hemagglutinin
hCIN85	Human Cbl-interacting protein 85
HR	Hypersensitive response
hTTP	Human tristetraprolin
IOS1	Impaired oomycete susceptibility 1
IP	Immunoprecipitation

ko	Knockout
L/RP	left/right primer
MAPK/MPK	Mitogen activated protein kinases
MARD1	Mediator of ABA-Regulated Dormancy 1
MBP	Maltose binding protein
MeJA	Methyl jasmonate
MEKK	Mitogen activated protein kinases kinase kinase
MKK	Mitogen activated protein kinases kinase
MKS1	Mitogen activated protein kinase substrate 1
NES	Nuclear export signal
NLR	Nucleotide-binding and leucine-rich repeat domain
NLS	Nuclear localization signal
NMD	Nonsense mediated mRNA decay
NTA	Nickel-Nitrilo Triacetic Acid
PAD3	PHYTOALEXIN DEFICIENT 3
PARN	Deadenylation enzymes
PAT1	Protein associated with topoisomerase II
PB	Processing Bodies
PR1	PATHOGENESIS RELATED 1
PRR	Pattern recognition receptor
PS mut	Phosphosite mutant
pUBQ10	Promoter, ubiquitin10
qRT-PCR	quantitative real time PCR
rA, rC, rG, rU	Ribohomopolymers of adenine, cytosine, guanine, uracil
RD21A	Responsive to Dehydration 21A
RDR6	RNA-dependent RNA polymerase
RLCK	Receptor like cytoplasmic kinase
RLK	Receptor like kinase
RLUs	Relative luminescence units
RNA	Ribonucleic acid
ROS	Reactive oxygen species
RPL18	Ribosomal protein L-18
R-protein	Resistant protein
SAR	Systemic acquired resistance
SG	Stress granules
SGS3	Suppressor of Gene Silencing 3
siRNA	Short interfering

SP	Serine Proline
SPCH	Speechless
TZFs	Tandem zinc finger proteins
UPF	Up-frame shift proteins
UTR	Untranslated region
VIP1	VirE1-interacting protein1
wt	Wild-type
XRN4	Exoribonuclease

1 Introduction

1.1 Plant defense system: a general introduction

Plants are constantly being challenged by both abiotic and biotic stresses. Abiotic stresses include all the environmental conditions that can damage plants such as drought, flood, high or low temperature, salinity, insufficient nutrition, excess or insufficient light. Biotic stresses can be imposed by pathogenic bacteria, fungi, viruses, mycoplasmas, protists, invertebrates or even parasitic plants. In order to combat these biotic stress, plants have developed sophisticated levels of defense responses. In general, the very first level of defense includes anatomical barriers, the morphological system that precludes other organisms to access the living cells. These barriers include cuticle (composed of cutin and waxes) and the cell wall (composed of cellulose, hemicellulose, pectin, proteins) (Somerville et al., 2004; Yeats and Rose 2013). The second level of defense includes a range of antimicrobial proteins/chemicals generally called phytoanticipins. They are usually generated as secondary products during the growth and development of plants. Some examples are defensin or defensin-like proteins, terpenes, phenolics, and alkaloids (Osbourn 1996; Tierens et al., 2001; Jones and Dangl 2006). These two lines of preformed defense provide plants a generalized resistance to almost all the organisms. However, potential pathogens might breach these barriers. So, plants have adapted the third level of inducible defense against these phytopathogens. Briefly, plants recognize specific pathogen/microbe-associated molecular patterns (PAMP/MAMPs) by membrane-localized pattern recognition receptors (PRR). P/MAMPs are pathogen-derived molecules that can be proteins/ carbohydrate/ lipopolysaccharides (Albert 2013; Kunze et al., 2004)

The recognition of PAMPs via PRRs induces so-called PAMP-triggered immunity (PTI) and thereby triggering a complex network of downstream signaling pathways (Boller and Felix 2009; Yamaguchi and Huffaker 2011). Some pathogens, however, deliver specialized virulence factors or effectors directly into the plant cells to overcome PTI. This causes disease in susceptible plants commonly termed as effector-triggered susceptibility (Sasabe et al., 2011). However, some resistant plants have evolved to recognize effectors via intracellular nucleotide-binding and leucine-rich repeat proteins (NLRs) proteins and counterattack by inducing Effector-triggered immunity (ETI) (**Fig. 1**). These intracellular receptors are sometimes also called resistant (R) proteins. Many effector encoding genes were first called as avirulence genes because they are recognized by cognate resistant (*R*) gene generating the R-gene mediated defense. For example, *Pseudomonas* AvrPto effector causes avirulence (lack of disease) in tomato lines that carry corresponding *Pto* resistance gene. The general overview of induced immunity including PTI, ETS, and ETI is depicted in **Fig. 1a**. These phases could be illustrated in a zig-zag model (**Fig. 1b**) where the amplitude of defense in each phase

is shown in overall plant immune system (Jones and Dangl 2006). The amplitude and acceleration of ETI are faster than PTI, usually causing a localized cell death called hypersensitive response (HR) at the infection site. Pathogens and hosts are believed to be in a co-evolutionary arms race of natural selection. For example, pathogens could evade ETI either by diversifying the recognized effector genes or by acquiring an additional repertoire of effectors. However, natural selection favours new plant *R*-alleles that recognize these newly acquired effectors, resulting again in ETI (**Fig. 1b**). Activation of local defense signaling might lead to the induction of intercellular signals that produce a systemic response known as systemic acquired resistance (SAR). SAR provides an enhanced resistance to a subsequent pathogenic challenge and could be described as the fourth level of the defense response.

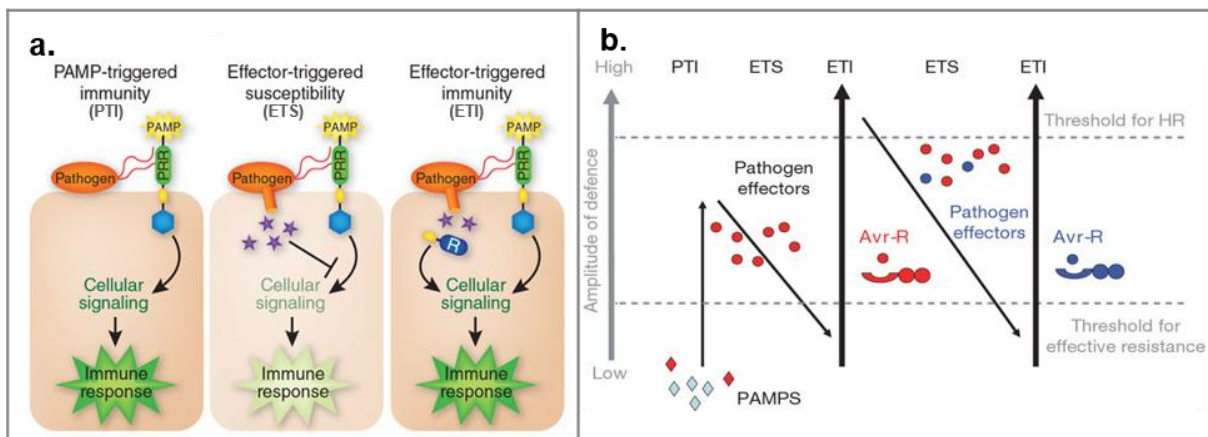


Fig. 1: A general depiction of induced defense response in the plant cell. **(a)** PAMP recognition by plant PRR receptors induces basal immune signaling known as PAMP-triggered immunity (PTI). Successful pathogen directly delivers proteins (effectors) in the plant cell causing effector-triggered susceptibility (Sasabe et al., 2011). Resistant plants recognize effectors by intracellular receptors thereby inducing effector-triggered immunity (ETI) (Source: Pieterse et al., 2009) **(b)** A zig-zag model of plant immunity showing the quantitative output of different phases of plant immune responses (Source: Jones and Dangl 2006).

1.2 PAMP-triggered immunity (PTI)

The present study is dedicated to understand a part of downstream signaling mechanism in PTI. One of the well-known PAMP is a 22-amino-acid long epitope at the N-terminal end of *Pseudomonas aeruginosa* flagellin (flg22). Flg22 is recognized by a specific PRR called FLS2 (Gomez-Gomez and Boller 2000). FLS2 (flagellin insensitive2) is a receptor-like kinase (RLK), comprising of three regions, an extracellular receptor domain-containing leucine-rich repeats or LRR, a transmembrane region and a cytoplasmic kinase domain. In the absence of flg22, FLS2 and its co-receptor BRI1-associated receptor kinase (BAK1) are constitutively associated with Botrytis-induced kinase 1 (BIK1), a receptor-like cytoplasmic kinase (RLCK) (**Fig. 2**) (Roux et al., 2011; Segonzac et al., 2011; Sun et al., 2013; Lu et al., 2010). Other RLCKs involved in signaling are PBS1 (AvrPphB susceptible 1) and PBS1-like (PBL) proteins. BIR2 (BAK1 interacting receptor-like kinase), an RLK has been found to interact with BAK1 in the absence

of PAMP and negatively regulates BAK1-FLS2 interaction (Halter et al., 2014). Perception of flg22 induces rapid auto- and trans-phosphorylation and thereby, dissociation of BIK1 from FLS2 and BAK1 leading to the instantaneous formation of immune receptor complex (Lu et al., 2010; Macho and Zipfel 2014). Another RLCK, BSK1, is found to be associating with FLS2, upon flg22 perception. BSK1 and BIK1 positively regulate FLS2 mediated oxidative burst. A few number of other PAMP-PRR pair have been identified. For example, bacterial PAMP elf18 is perceived by EFR while fungal chitin is perceived by CERK1. It has been shown that BIK1 and PBLs integrate immune signaling from multiple PRR including EFR and CERK (Zhang et al., 2010).

Flg22 perception, in general, leads to various physiological changes in the plant cell. Among them, one of the earliest responses is Ca^{2+} burst (starts at ~30 s to 2 min and reaches a peak around 4-6 min), and oxidative burst (starts at ~2 to 3 min and reaches a peak around 10-14 min). Other changes include ion fluxes, transcriptional reprogramming, production and activation of phytohormones, activation of G-proteins, 14-3-3 proteins and Calmodulin-binding proteins (CaM) (Bigeard et al., 2015). More importantly, two group of kinase cascades, Ca^{2+} -dependent protein kinases (CDPK) and mitogen-activated protein kinases (MAPKs) get activated during PTI (Bigeard et al., 2015). CDPKs are not found in mammals whereas MAPKs are conserved in all eukaryotes.

1.3 MAPK signaling cascade

A typical MAPK cascade consists of a map kinase (MPK), an activator of MPK (MAPKK or MKK) and another activator of MKK (MAPKKK or MEKK) (**Fig. 2**). MAPKKs (MEKKs) are serine or threonine kinases which upon PRR activation phosphorylate downstream MAPKK at conserved S/T-X3-5-S/T motif. Upon activation, MAPKK, in turn, phosphorylates downstream MAPK at threonine or tyrosine residues in their activation loop. Activated MAPKs phosphorylate their substrate(s) at the unique site(s)-usually a serine/threonine followed a proline residue. The *Arabidopsis* genome encodes ~60 MAPKKs, 10 MAPKKs, and 20 MAPKs, which suggests scope for cross-talk between different signal-transduction pathways (MAPK Group 2002). The formation and integrity of a particular MAPK cascade are explained by involvement of scaffold or adaptor proteins that might share their docking domains (Bardwell et al., 2001; Takekawa et al., 2005). Studies indicate that MAPK cascade is involved in hormonal responses, cell cycle regulation, growth, development, abiotic and biotic signaling. (Tena et al., 2001; Xu and Zhang 2015). However, the complete mechanism or pathway of MAPK cascade in particular cellular processes is not fully understood. For example, upon flg22 elicitation, two modules of MAPKs downstream of BIK1 and PBLs are activated, one being MKK4/MKK5-MPK3/MPK6 (two partially redundant MPKs) (Asai et al., 2002) and the other MEKK1-MKK1/2-MPK4 (Qiu et al., 2008b; Rodriguez et al., 2010). MPK11, a homolog of MPK4

is also found to be elicited by flg22 (Bethke et al., 2012). Recently, MPK1 and 13 are shown to be activated by flg22 but their upstream kinases and downstream substrates are not known (Nitta et al., 2014). The known PAMP responsive MPKs, MPK3, -6, and -4 phosphorylate various substrates and thereby, change their properties or localization. These substrates then execute their function in several pathways like defense gene activation and camalexin (a phytoalexin, defense-related secondary metabolite) biosynthesis (**Fig. 2**).

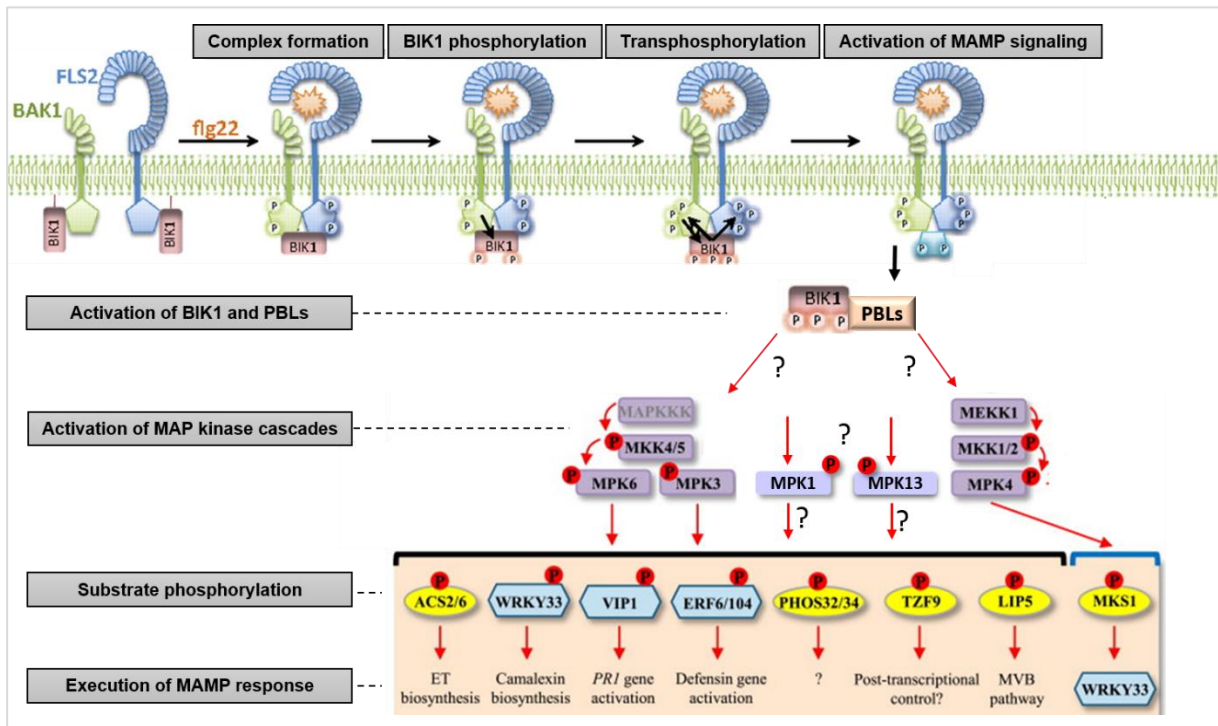


Fig. 2: Activation of MAMP/PAMP signaling and execution of immune response. At resting stage, FLS2 and BAK1 are associated with BIK1. Upon flg22 perception, FLS2 and BAK1 heterodimeric complex undergo transphosphorylation and dissociation of BIK1 occur leading to activation of MAPK pathway. MAPKs phosphorylate their substrates to execute the immune response (Modified from Lu et al., 2010; Bigeard et al., 2015).

1.3.1 Identification of MAPK substrates

To understand the mechanism by which a MAPK executes the cellular process(es) and signaling response(s), identifying substrates of a given MAPK has been of particular interest in past decades. Various screening methods are employed to find putative substrates of MAPKs. After a screening, validation techniques are usually employed to confirm a putative substrate as MAPK substrate. The further steps include mapping the phosphosite(s) in a given substrate, which is important to check the effect of phosphorylation on the substrate. These techniques are summed up in **Table 1**.

Table 1: Techniques used for the identification and validation of MAPK substrates

Screening techniques	
Method	Description
Yeast two-hybrid (Y2H)	MAPK is used as a bait to screen a plant cDNA library of interest to find MAPK interactors
Protein microarray	A protein microarray is incubated with MAPK and γ^{32} -P and subsequent detection of phosphorylated substrates
Mass Spectrometry (MS) based screen:	<i>In-vivo</i> transphosphorylation approach and phospho-peptide identification by MS
<ul style="list-style-type: none"> Phosphoproteomics 	Global phosphorylations are compared between MPK activated/inactivated plants
<ul style="list-style-type: none"> Affinity purification-MS 	Affinity-based co-purification of proteins from plant extract expressing tagged kinase, subsequent identification by MS
<ul style="list-style-type: none"> ATP-analogue-kinase assay 	Kinase substrates are labelled with an ATP analogue and purified on the basis of immunoaffinity
Validation techniques	
<i>In-vitro</i> kinase assay, (radioactive)	The putative substrate is mixed with the kinase of interest in the presence of γ^{32} -P, run on a gel and analysed by autoradiography
ProQ diamond staining, (non-radioactive kinase assay)	In tube kinase assay, proteins are then electrophoresed on SDS-PAGE gel, the gel is stained with the ProQ diamond solution which specifically stains phosphorylated proteins
<i>In-vivo</i> interaction assays:	
<ul style="list-style-type: none"> BiFC (Bimolecular fluorescence complementation assay) 	The putative substrate is expressed as a fusion with an N-terminal fragment of the yellow fluorescent protein (YFP) and other kinase of interest is expressed as a fusion with a C-terminal fragment of the YFP or vice versa. The interacting proteins bring two fragments of YFP protein to close proximity and reconstitute the YFP-fluorescence, detected by YFP channel in fluorescent microscopy
<ul style="list-style-type: none"> FRET (Förster resonance energy transfer) 	Like BiFC, this method is also based on fluorescence. Each of the putative interacting proteins is tagged with different fluorophores such that emission wavelength of one is the excitement wavelength of the other. If two proteins are close enough to transfer the resonance signal then the second emission wavelength is detected
<ul style="list-style-type: none"> Co-IP (Co-immunoprecipitation) 	In immunoprecipitation (IP), an immobilized antibody against an antigen (kinase of interest) forms an immune complex with the target protein in the crude extract. This immune complex is precipitated or captured and analysed on denaturing SDS-PAGE gel and western blot is performed to verify the identity of antigen. CoIP is an extension of IP that is based on the identification of other protein (substrate) bound to the antigen (kinase) by native interactions in the crude extract
Co-localization	Putative substrate and kinase of interest tagged with a different fluorescent gene (CFP/GFP/RFP/YFP) are expressed under native or moderate promoter (pUBQ10). The detection is done by fluorescence microscopy

Phosphosite mapping	
MS-based mapping	The phosphorylation of substrate by kinase can be detected by mass spectrometry (Dephoure et al., 2013)
Mutagenesis approach	The putative phosphosite (S/T) is mutagenized to phospho-null (to A) or phosphomimic mutants (to D/E) and can be analysed by kinase assay

1.3.2 Role of MAPK substrates in various cellular processes

Using the above-mentioned methods, a handful of MAPK substrates have been found and it is deciphered that MAPKs are associated with various physiological, hormonal, developmental and stress responses. The phosphorylation of substrates can alter their localization/stability/activity/ interaction pattern, leading to physiological responses. Though some progress has been made in identifying MAPK substrates, future work is needed for further understanding of the biological roles of MAPK substrates. This can be achieved by characterizing the substrate and deciphering the effect of phosphorylation. In the context of the present study, some of the well-characterized PTI responsive-MAPK substrates in *Arabidopsis* are listed in **Table 2**.

Table 2: Examples of MAPK substrates and their possible role(s)

Substrate	MPKs	Screening/validation techniques	Function	References
MKS1	MPK4	Y2H, Co-IP, co-localization	Interacts with MPK4 and WRKYs in defense response	(Andreasson et al., 2005)
PAT1	MPK4	Y2H, Co-IP	Relocalize to cytoplasmic foci after phosphorylation	(Roux et al., 2015)
MEKK2	MPK4	Y2H, Co-IP	Regulation of cell-death	(Kong et al., 2012)
ASR3	MPK4	Mobility shift, mutagenesis	Phosphorylation suppresses DNA-binding activity of ASR3	(Li et al., 2015)
MPK65-1/2/3	MPK4	In-vitro kinase assay, co-localization	Role in cytokinesis	(Sasabe et al., 2011)
EIN3	MPK4,-3, -6	In-vitro phosphorylation, Co-IP	Phosphorylation affects stability	(Yoo et al., 2008)
VIP	MPK3	Y2H, Co-IP	Translocation to nucleus	(Djamei et al., 2007)
DCP1	MPK6	In-vitro kinase assay	Interacts with DCP5, involved in mRNA turnover regulation	(Xu and Chua, 2012)
ACS6	MPK6	In-gel kinase assay	Induces ethylene biosynthesis.	(Liu and Zhang, 2004)
SPCH	MPK6	In-vitro kinase assay	Stomatal development	(Lampard et al., 2008)
WRKY33	MPK6	Mobility shift	Camalexin biosynthesis in defense	(Mao et al., 2011)
HD2B	MPK3	Phosphoproteomics, kinase assay	Regulation of expression of biotic stress response genes	(Latrasse et al., 2017)

1.3.3 *Arabidopsis* MAPK substrates are involved in immunity at transcriptional and post-transcriptional level

Transcriptional level: As indicated in **Table 2**, many MPK substrates are transcription factors. For example, VIP1 (VirE1-interacting protein1) is a bZIP transcription factor phosphorylated by MPK3 (Djamei et al., 2007). Phosphorylation of VIP1 results in its translocation to the nucleus. VIP1 then binds to the promoter of the defense-related gene, *PR1* (Djamei et al., 2007), and enhance its expression. However, this mechanism is hijacked by *Agrobacterium* to facilitate nuclear import of VirE2/T-DNA complex during *Agrobacterium*-infection in plants (Tzfira et al., 2001). Another nuclear protein, MKS1 (MAP kinase 4 substrate 1) which interacts with WRKY transcription factors, is phosphorylated by MPK4. Phosphorylation of MKS1 by MPK4 is required for the release of the WRKY33 transcription factor. WRKY33 (which also binds its own promoter) activates the expression of *PAD3* (*PHYTOALEXIN DEFICIENT 3*), which is required for camalexin synthesis (Qiu et al., 2008a). In other words, MPK4 may use MKS1 as a mediator to control immunity responses. In other studies, WRKY33 has been shown to be phosphorylated by MPK3 and MPK6 to mediate the biosynthesis of camalexin (Mao et al., 2011). Other WRKY transcription factors, like WRKY22, -28, -29 have been shown to be downstream targets of MPKs (Asai et al., 2002).

Post-transcriptional level: MAPK substrates also regulate gene expression at post-transcriptional level. mRNA after being transcribed and processed (capping and polyadenylation) in the nucleus are exported to the cytoplasm. In the cytoplasm, the stability of mRNA can be changed by deadenylation (shortening of poly-A tail) by 3' to 5' exoribonuclease and decapping (removal of 5' cap) by decapping complex. DCP1 (decapping 1), a part of decapping complex, stimulates decapping activity of DCP2 (Xu et al., 2006). Under dehydration stress, phosphorylation of DCP1 by MPK6 promotes interaction with DCP5 and thereby promotes mRNA decapping (Xu and Chua 2012). This provides a link between MAPK signaling and mRNA turnover. PAT1 (protein associated with topoisomerase II) another enzyme from yeast and animal decapping complex also assist DCP2 in decapping and regulation of mRNA levels (Kulkarni et al., 2010). In *Arabidopsis*, PAT1 is phosphorylated by MPK4 at specific sites after flg22 elicitation as identified by MS. The phosphorylation results in the relocalization of PAT1 to cytoplasmic foci called processing bodies for mRNA regulation (Roux et al., 2015).

1.4 Processing Bodies (p-bodies or PB)

Processing bodies (PBs) are protein/RNA complexes that reside in the cytosol of eukaryotic cells. They control the decapping, degradation, and storage of mRNA molecules and are usually visualized as speckle-like structures inside the cell (Kedersha et al., 2005; Parker and Sheth, 2007) (**Fig. 3a**). A number of studies in yeast and animal system have been performed

that associate PB with nonsense-mediated mRNA decay (NMD), ARE (AU-rich element)-mediated mRNA decay (AMD) and miRNA (microRNA)-induced mRNA silencing (Kulkarni et al., 2010). These decay processes are associated with different types of mRNAs and performed by different proteins. For example, NMD is the rapid degradation of aberrant mRNAs that contain a premature termination codon. AMD is associated with those mRNAs (many cytokine and proto-oncogene mRNA) that have AREs in their 3'UTR (untranslated region). The formation of PB is dependent on the availability of free mRNAs or mRNAs not associated with polysomes (actively translating ribosomes bound to mRNA). The numbers and sizes of PBs are variable, for example, the diameter of the oxidative stress-induced PB in the human cell is 10-15 nm (Souquere et al., 2009).

The composition and dynamics of PB are poorly studied in plants. In *Arabidopsis*, PB and PB-resident proteins showed important roles in immune responses (Maldonado-Bonilla et al., 2014), post-embryonic development (Xu and Chua, 2009; Xu et al., 2006) and salt stress tolerance (Steffens et al., 2015). Interestingly, several PB proteins were found to be potential MPK substrates (Lee et al., 2015). Many, but not all, PB components are known in *Arabidopsis* but so far independent studies showed that they are co-localizing as foci in the plant cells (**Fig. 3a**) (Xu et al., 2006; Xu and Chua, 2009). PB have been shown to contain subunits of decapping complex (DCP1, DCP2, DCP5 and VCS), activator of decapping complex (Sm-like proteins or LSM components), 5' exoribonuclease (XRN4), deadenylation enzymes (PARN), miRNA-associated protein (ARGONAUTE 1 or AGO1), NMD components (up-frame shift proteins or UPFs) and tandem zinc-finger proteins (TZFs) (Maldonado-Bonilla et al., 2014) (**Fig. 3b**).

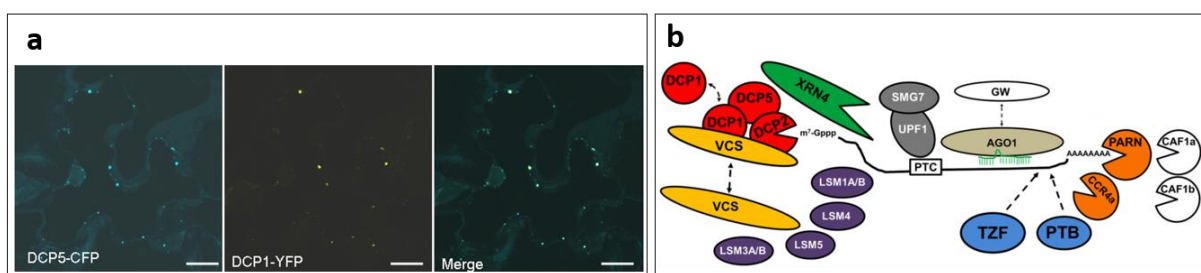


Fig. 3: PB speckle in plant cells. **(a)** Co-localization of *Arabidopsis* DCP5 and DCP1 expressed in *Nicotiana* cells (Source: Xu and Chua, 2009). **(b)** The composition of PB in *Arabidopsis* showing mRNA processing components like decapping and deadenylation (Source: Maldonado-Bonilla 2014).

1.5 Tandem Zinc-finger (TZFs) proteins in *Arabidopsis*

Tandem Zinc-finger (TZF) proteins are characterized by zinc-finger motifs in which zinc ion is coordinated by three cysteine and one histidine residues hence the name CCCH-TZF (**Fig. 4**). TZF proteins from plants are known to localize in PBs and interestingly, the CCCH-type proteins from the animal are known to localize in PB and to bind RNA as well. *Arabidopsis*

genome encodes 68 CCCH-type TZF genes. They have been phylogenetically divided into 11 subfamilies (Wang et al., 2008). Out of these, subfamily IX has 11 members, all of which have two tandemly repeated zinc-finger motifs separated by 16 amino acids (C-x7/8-C-x5-C-x3-H-16-C-x5-C-x4-C-x3-H) and an arginine-rich (RR) motif. Additionally, the last 5 members, TZF7,-8,-9,-10,-11 have long C termini and the N termini with two predicted ankyrin (ANK) repeat motifs (**Fig. 4**) (Pomeranz et al., 2010a).

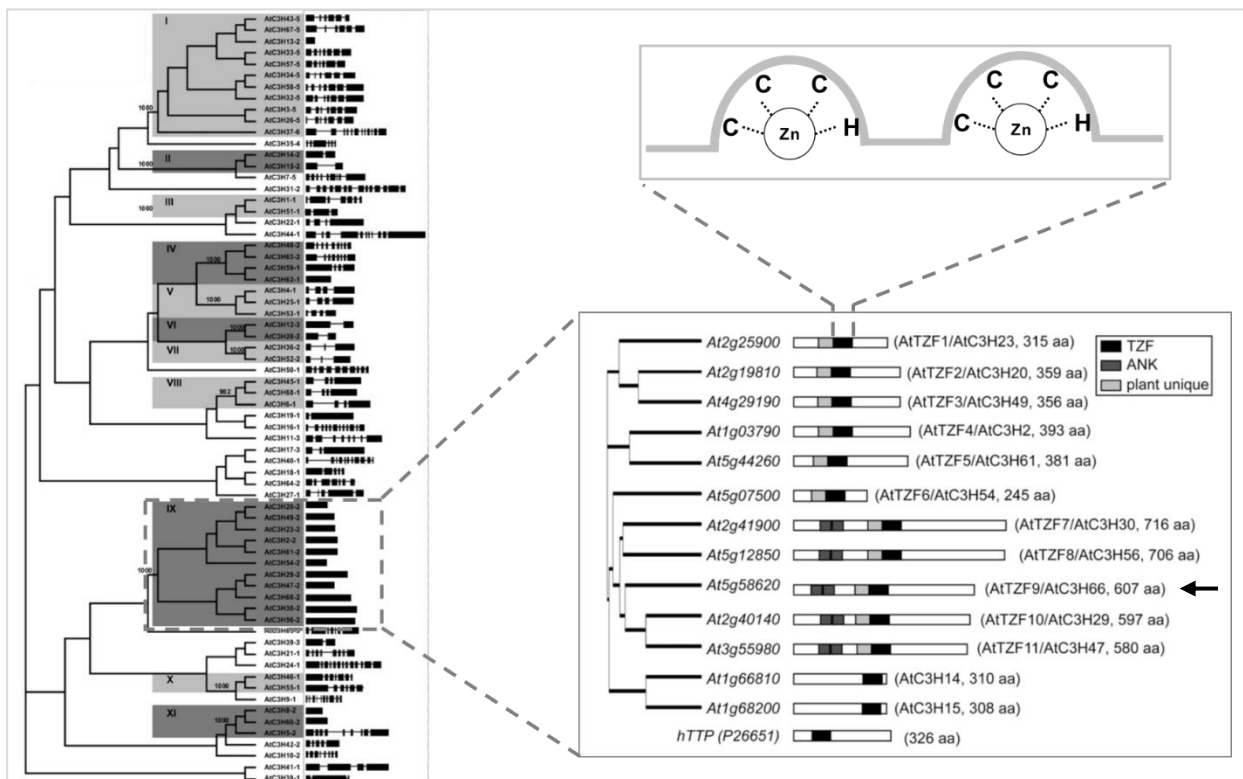


Fig. 4: Phylogenetic tree of XI subfamilies of *Arabidopsis* CCCH-TZFs. All the 68 CCCH-TZF are classified into 11 subfamilies, 11 members of the subfamily IX are shown in enlarged view. TZF9, the candidate of the present study shown by an arrow belongs to this group. TZF9 and related members have two CCCH type zinc-finger domains (Wang et al., 2008; Pomeranz et al., 2010b).

Localization: When transiently expressed, all the 11 members of subfamily IX were shown to be localized in cytoplasmic foci, which are thought to be PB or stress granules (SG) (Pomeranz et al., 2010a) (**Fig. 5**). However, other studies have shown altered/variable subcellular localization such as nucleus, cytoplasm, and plasma membrane. Deletion or mutation of CCCH or ANK coding region might alter the localization of the protein and supposedly lead to different function in different compartments (Blanvillain et al., 2011). Additionally, the temporal and spatial expression pattern of *TZF4,-5,-6* is shown in seeds (Bogamuwa and Jang, 2013).

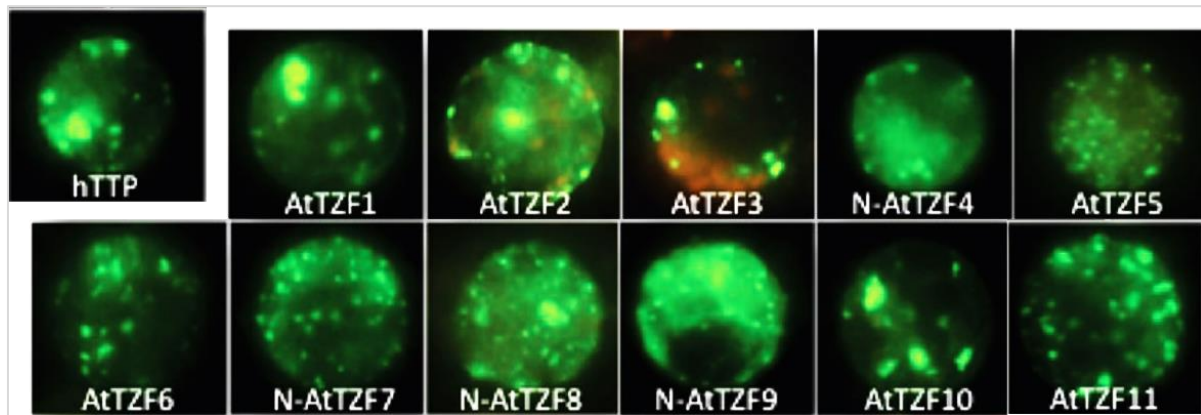


Fig. 5: Transient expression of hTTP (human tristetruprolin, mammalian homolog of TZFs) and *Arabidopsis* TZFs of subfamily IX in protoplast shows foci like structures (Source: Pomeranz et al., 2010a).

Molecular function: The molecular function of TZFs is not fully understood. However, the mammalian putative homolog of these proteins (Tristetraprolin or TTP) has been extensively studied. TTP is considered to be important for the assembly of PB. TTP binds to class II AU-rich elements (ARE) in 3'-UTR of specific mRNAs and promotes their degradation (Fenger-Gron et al., 2005; Lykke-Andersen and Wagner, 2005). In *Arabidopsis*, TZF1 of subfamily IX has been shown to bind RNA *in-vitro* (Pomeranz et al., 2010b; Qu et al., 2014). TZF2 and 3 are known to show RNase activity (Lee et al., 2012). In contrast, TZF7 acts as a transcriptional activator (Blanvillain et al., 2011). However, a dual activity of other TZFs as a transcriptional activator in nucleus and mRNA metabolic regulator in cytoplasm has not been determined yet. TZF4 and 5 also show interaction with stress-related proteins (Bogamuwa and Jang, 2016). The localization and known molecular functions of TZFs are summarized in **Table 3**.

Table 3: CCCH-TZFs of subfamily IX in *Arabidopsis*

TZFs	Other names	Localization	Positive regulation for	Negative regulation for	References
TZF1	ZFP1	PB/SG, nucleus	ABA, sugar, salt stress	GA	(Han et al., 2014; Lin et al., 2011)
TZF2	OZF1	PM, cytoplasm, cytoplasmic foci	ABA, ROS, salt stress	JA	(Huang et al., 2011; Huang et al., 2012; Lee et al., 2012)
TZF3	OZF2	PM, cytoplasm, cytoplasmic foci	-----	JA	(D'Orso et al., 2015; Huang et al., 2011; Huang et al., 2012; Lee et al., 2012)
TZF4	SOMNUS	PB/SG, nucleus	ABA	GA and seed germination	(Bogamuwa and Jang, 2013, 2016; Kim et al., 2008)

TZF5		PB/SG, nucleus	----"----	----"----	(Bogamuwa and Jang, 2013, 2016)
TZF6	PEI1	PB/SG, nucleus	----"----	----"----	(Bogamuwa and Jang, 2013, 2016)
TZF7	OX2	cytoplasm, cytoplasmic foci, nucleus	vegetative growth and abiotic stress	stress-induced flowering	(Blanvillain et al., 2011)
TZF8	O2L1	cytoplasmic foci	----"----		(Blanvillain et al., 2011)
TZF9	O2L2	Cytoplasmic foci, nucleus	----"----	stress induced flowering	(Blanvillain et al., 2011; Maldonado-Bonilla et al., 2014)
TZF10	SZF2/O2L4	Cytoplasmic foci (nucleus?)	----"----	----"----	(Blanvillain et al., 2011)
TZF11	SZF1/O2L3	cytoplasmic foci, nucleus	----"----	----"----	(Blanvillain et al., 2011)

----"---- means same as above.

1.5.1 TZF9 (Tandem Zinc Finger 9)

As MPK3 and 6 are two main PTI responsive MAPKs, it is interesting to know their downstream substrates to decipher the overall mechanism of signal transduction. In order to hunt for the potential MPK substrates, several screening methods were used (**Table 1**). TZF9 was identified as a putative MPK3 and -6 substrate in a protein array screen (Feilner et al., 2005). To validate TZF9 as MPK3 and-6 substrate, pro-Q diamond staining was performed to show *in-vitro* phosphorylation in our lab (Maldonado-Bonilla et al., 2014). Also, TZF9 was shown to be positively involved in both early and late PTI responses. For example, a *tzf9* knockout (ko) line showed attenuated MAPK activation compared to the wild-type (Col-0) plants. In late PTI, the *tzf9* ko line also showed attenuated defense response as compared to Col-0. This was reflected by more bacterial (*Pseudomonas syringae*) growth, compromised inhibition of root growth in the presence of PAMP and reduced expression of defense-related genes, *FRK1* in *tzf9* line. TZF9, when transiently expressed in the protoplast, was localized in cytoplasmic foci, PB. These results provided a background knowledge for this thesis as it was intriguing to further understand the mechanism by which TZF9 is involved in PTI.

(The domain organization and sequence information of TZF9 are given in **Appendix Fig. A1** and **A2** respectively. *In-silico* prediction of MAPK-target phosphorylation sites are given in **Appendix Fig A3** and those detected by Mass spectrometry summarized in **Appendix A4**).

1.6 Aim of the study

Mechanistic understanding of how TZF9 controls PTI and whether this involves PB functions are largely unknown. The objective of this study is an in-depth functional characterization of TZF9, with the aim to decipher the mechanism behind TZF9 mediated-regulation of PTI. In this regard, the major objectives of the current study are:

- To validate phosphorylation of TZF9 by MAPKs.
- To validate interaction of TZF9 with MAPKs.
- To study the fate of TZF9 post MAPK phosphorylation.
- To confirm the localization of TZF9 in PB and test RNA binding capacity.
- To study interacting partner(s) of TZF9.
- To understand the role of TZF9 in flg22-induced gene expression at the transcriptome and translome level.

2 Materials and Methods

2.1 Materials

2.1.1 Plants

Arabidopsis thaliana (ecotype Col-0) were grown in a short-day condition (8 hours light). For transcriptomics experiment, about 6-week old wild-type (WT), *tzf9* knockout plants were used. For the translomics experiment, *A. thaliana* expressing FLAG-tagged ribosomal gene L-18 (*RPL18*) under *CaMV* 35S promoter was used (Zanetti et al., 2005). This *p35S::RPL18* transgenic line was crossed with the *tzf9* knockout line and homozygous lines were selected in the F2 generation. For microarray study, Col-0 WT, *tzf9*, *p35S::RPL18* and *p35S::RPL18/tzf9* lines were infiltrated with 1 μ M flg22 in the abaxial side of leaves using sterile syringe and harvested after 1 hour. The flg22 peptide (QRLSTGSRINSAKDDAAGLQIA) used for the treatment was synthesised according to the consensus sequence for the most highly conserved region in the N-terminus of flagellin (Felix et al. 1999). The flg22 peptide was synthesized using Abimed EPS221 (Abimed, Germany). The plant lines used in the study are summarized in **Table 4**.

Table 4: Salk IDs of the lines used in the study

Gene description	AGI code	NASC stock number	T-DNA position	Given name
<i>TZF9</i>	At558620	SALK_010842	exon	<i>tzf9</i>
<i>Putative RNA ligase</i>	At5g40190	SALK_084396	5'-UTR	<i>Putative RNA ligase-1</i>
<i>Putative RNA ligase</i>	At5g40190	SALK_084402	exon	<i>Putative RNA ligase-2</i>
Lines used for crossing with <i>tzf9</i>				
<i>TZF7</i>	At2G41900	SALK_120825	exon	<i>tzf7</i>
<i>TZF8</i>	At5G12850	SALK_004272	exon	<i>tzf8-1</i>
<i>TZF8</i>	At5G12850	SALK_091474	exon	<i>tzf8-2</i>
<i>TZF10</i>	At2G40140	SALK_024800	exon	<i>tzf10</i>
<i>TZF11</i>	At3G55980	SALK_141550	5'-UTR	<i>tzf11</i>

2.1.2 Bacteria

E.coli (DH5 α) cells were used for normal cloning procedures. For protein expression, *E.coli* (KRX) cells were used (Promega).

2.1.3 Medium

For the growth of *E.coli*, LB medium (10% w/v bacto-tryptone, 10% w/v bacto yeast extract and 5% w/v NaCl, 15% w/v agar) was used. To grow seedlings ½ MS medium (Duchefa Biochemie) (0.22% MS salt, 0.25% sucrose) was used.

2.2 Methods

2.2.1 Protoplast transient assays

2.2.1.1 Preparation and transfection of *Arabidopsis* protoplasts

The method was adapted from Yoo et al (2007). Well-expanded leaves from 3 to 4 weeks old plants were chosen for the isolation of mesophyll protoplasts. About 1 mm leaf strips were cut with a fine razor blade and transferred in the cell wall digesting enzyme solution (0.4 M mannitol, 20 mM KCl, 20 mM MES (pH 5.7), 10 mM CaCl₂, 0.1% (w/v) BSA, 0.4% (w/v) macerozyme R10 (Yakult pharmaceuticals), 1.5% (w/v) cellulose R10 (Yakult pharmaceuticals)). The enzyme solution was vacuum infiltrated in the dark for 30 min using a desiccator. The digestion was performed for 2.5 h at 18-20°C in the dark. For the optimum release of protoplasts, the leaf-enzyme solution was gently swirled for 30 min. The green protoplast suspension was filtered through the 100 µm nylon mesh. The tube was centrifuged at 200x g for 1 min and the protoplast pellet was resuspended in 2 ml W5 solution (154 mM NaCl, 125 mM CaCl₂, 2 mM MES (pH 5.7), 5 mM KCl) by gently inverting the tube. The tubes were placed on ice and the protoplasts were allowed to settle by gravity for 40 min in the dark. The supernatant was removed and protoplast pellet was again resuspended in W5 solution. The protoplast suspension was again incubated on ice for 40 min in dark and allowed to settle by gravity. The supernatant was removed and protoplast pellet was diluted with MMG solution, (0.4 M mannitol, 15 mM MgCl₂, 4 mM MES (pH 5.7) prior to the transformation to a concentration of about 2×10⁵ protoplasts/ml. The plasmid (DNA concentration 10 µg for 100 µl protoplast) was mixed with protoplast and gently mixed. The transformation was mediated by adding 1:1 vol (volume) of PEG solution (40% (w/v) PEG4000, 0.2 M mannitol, 100 mM CaCl₂) and incubating for 10 min at 18-20°C. The transformation was stopped by adding 4.4 vol of the W5 solution. The protoplast tubes were centrifuged at 200x g for 1 min and the supernatant was removed. Finally, the transformed protoplasts were resuspended in 1 vol of WI solution (0.5 M mannitol, 20 mM KCl, 4 mM MES pH 5.7) and were incubated at 18-20°C overnight to enable gene expression from the transfected constructs.

2.2.1.2 Bimolecular Fluorescence Complementation (BiFC) or Split YFP assay

For the protein-protein interaction study, the one protein of interest was expressed as a fusion with the N-terminal fragment of YFP and other with the C-terminal fragment of YFP. They were transformed into *Arabidopsis* protoplast for the transient expression. The interacting proteins

bring two fragments of YFP protein to the close proximity and reconstitute the YFP-fluorescence, which was detected via the YFP channel of fluorescent microscopy LSM710 (Zeiss, Germany).

2.2.1.3 Localization Study

Localization study of the proteins were expressed under moderate promoter (pUBQ10) with either C or N terminal fluorescent tag {cyan(C)/green(G)/red(R)/yellow(Y)}. The vectors used to study the localization are given **Appendix Fig. A5** The plasmids were transfected and were allowed to express overnight. The detection of the protein was performed using fluorescent microscopy, LSM710 (Zeiss). For time-series assays, the protoplasts were treated with water/flg22 and scanned under the microscope by selecting time-points and position.

2.2.1.4 *In-vivo* mobility shift assay

Mobility shift assay was performed to check post-translational modification of the protein. For this purpose, a protein of interest was expressed as a fusion with hemagglutinin (HA) tag. After overnight expression of the protein, protoplasts were treated with flg22 and harvested at selected time points. Untreated protoplasts were used as a control. Protoplasts were lysed and protoplast extract was loaded in the SDS-PAGE for electrophoresis. The proteins were transferred onto the nitrocellulose membrane and western blot was performed using the respective antibodies. To show that the mobility shift of protein in flg22 treated samples were due to phosphorylation, the protein extract was treated with lambda-phosphatase (1X buffer, 10mM DTT, 1U enzyme (NEB)) for 10 min at 30°C. The protein extract was then loaded onto the gel and western blot was performed as mentioned. Band of modified protein shows reduced mobility in the gel. Besides the clear experimental evidence of the method, it is important to mention that the exact principle behind the lag in mobility due to phosphorylation is not known.

2.2.1.5 Pull-down assay and CoIP

CoIP assays were performed to confirm the interaction of proteins. Briefly, TZF9 and its variants (in fusion with YFP and HA) were co-expressed with RNA ligase (in fusion with HA) in protoplast. The protoplast samples were harvested after and were lysed for 10 min using 2 ml lysis buffer (10 mM Tris pH 7.5, 150 mM NaCl, 0.5 mM EDTA, 0.1% NP-40) with constant shaking. The samples were centrifuged at 16000x g for 10 min and supernatants were collected in new tubes. 50 µl of protein lysate was separated in 1.5 ml tube (to show the expression of transfected constructs in the protoplast on the western blot) while rest of the supernatants were diluted to 3:1 using dilution buffer/wash buffer (10 mM Tris pH 7.5, 150 mM NaCl, 0.5 mM EDTA). Commercially available GFP trap beads (Chromotek) were washed with the wash buffer and added to the samples (~15µl bead per sample). To inhibit proteases, protease-inhibitor Mix P (Serva) was added in 1:100 dilution. The samples were incubated for 2 hours at 4°C with constant shaking. After 2 hours, tubes were centrifuged at 2000xg and

supernatants were discarded. The beads were carefully washed 3 times with the wash buffer. For gel electrophoresis, 40 μ l of 2X SDS loading dye was directly added to the bead and boiled at 95°C for 5 min. The beads were briefly centrifuged and the protein supernatants were loaded on the 12% SDS-PAGE gel. The samples were transferred to NCL membrane and blotted against α -HA antibody (1:1000).

2.2.2 Molecular cloning processes

2.2.2.1 Polymerase Chain Reaction (PCR)

A list of all the primers used for PCR in the study are given in **Appendix Table A1**. A high-fidelity Phusion DNA Polymerase with 3' to 5' proofreading activity (ThermoFisher) was used for gene amplification (PCR conditions are given in **Appendix Table A4**) whereas other amplifications like genotyping (**Appendix Table A3**), colony PCR (**Appendix Table A2**) etc. were performed using DreamTaq DNA polymerase (ThermoFisher). The final reaction mix of 20 μ l in both the cases had concentrations as follows: 1X buffer (including 2 mM MgCl₂ provided by ThermoFisher with enzymes), 200 μ M dNTPs, 1 μ M forward and reverse primers, 10-100 ng template DNA and 0.5 U of the enzyme. The PCR cycling conditions were set based on the melting temperature (T_m) of the primers, length of the sequence to be amplified, GC content performed as per the manufacturer's recommendations (ThermoFisher).

2.2.2.2 Site-Directed mutagenesis

Mutagenesis was performed by generating a mutation in DNA sequence that would translate to alanine or glycine instead of serine and threonine (followed by proline). The method is based on the combination of Typell with Typells restriction enzymes (Palm-Forster et al., 2012). PCR reaction using mutated primers was performed to amplify the desired sequence using pENTR-*TZF9* as a template. For this, 50 μ l final reaction mix for the PCR reaction containing 1X HF buffer, 0.5 U Phusion Taq, 200 μ M dNTP, 1 μ M forward and reverse primers, 100 ng/ μ l template was used and PCR (15 cycles of amplification, condition: **Appendix Table A4**) was performed. The PCR products were purified by gel extraction kit (Qiagen) after agarose electrophoresis and eluted in 30 μ l water. The 20.5 μ l purified PCR product was incubated with 20 U *DpnI* (ThermoFisher) with 2.5 μ l buffer (final volume 25 μ l) at 37°C overnight. The final ligation-restriction reaction was prepared as 25 μ l *DpnI* digested product, 1U *DpnI*, 4U *BpiI* (typells restriction enzyme, ThermoFisher), 1.5 U T4 DNA ligase (ThermoFisher), 0.75 μ l ATP (20 mM), 0.5 μ l restriction buffer (1X), 1.75 μ l water. The mixture was incubated in a thermocycler at 37°C for 5 min, 16°C for 5 min (10X). Then 4 μ l of the reaction mix was transformed into DH5 α cells and colonies were selected from kanamycin-LB plates. A few colonies were randomly selected, cultured for plasmid isolation. Isolated plasmids were

digested using *Typell* restriction enzyme, *KasI* and positive colonies were confirmed by sequencing.

2.2.2.3 Purification of PCR products

Prior to digestion and subsequent ligation of a gene into a vector, the amplified PCR product was purified to remove excess primers and salts. For this, the PCR mix was electrophoresed in EtBr containing (0.5 µg/ml) 1% agarose gel. The desired band was excised under UV light and the DNA was purified using commercially available column (Invisorb Spin DNA Extraction Kit, Stratec).

2.2.2.4 Cloning into Gateway Entry and Destination vectors

Blunt end PCR products were cloned into entry vector (pENTR™, Gateway® system, ThermoFisher) by mixing in a 1:1 ratio. The reaction mix was transformed into *E.coli* (DH5α) cells (method of transformation is described in section 2.2.2.5) and selected on an antibiotic-containing LB-agar plate (e.g., Kan at 50 µg/ml). The selected colonies were checked for the inserts either by colony PCR or by digesting the plasmid mini-prep with type II restriction enzymes (methods described below). The selected plasmid (entry clone) was then cloned into the destination vector by Gateway LR reaction (ThermoFisher). For this, ~100ng Entry clone (0.5-4 µl); ~150 ng Destination vector (0.5 µl); TE buffer: pH 8.0 (to 4 µl) and 1 µl LR Clonase™ II enzyme-mix were mixed in the tube and incubated at 25°C for 4 hours. The reaction mix was transformed into DH5α cells. For the protein expression related experiments, the plasmids isolated from DH5α cells were re-transformed into KRX competent cells (Promega).

2.2.2.5 Transformation in *E.coli* (DH5α and KRX) cells and colony PCR

The competent cells were prepared by as described in Inoue et al (1990). For transformation, the cloning reaction was mixed with 50 µl cells and thawed on ice for 30 min. The cells were subjected to heat-shock at 42°C for 30 sec and snap-chilled on ice. 250 µl LB medium was added to the cells and incubated at 37°C for 1 hour with shaking (120 rpm). The cells were pelleted at 1000x *g* for 1 min and suspended in fresh LB medium. The cells were then spread on the respective antibiotic containing LB-agar plate for the selection. The plate was incubated at 37°C overnight. For colony PCR, randomly selected overnight grown colonies were suspended in 50 µl autoclaved water and lysed at 95°C for 10 min. The colony PCR was performed using 1 µl of the lysed extract and DreamTaq DNA polymerase reaction mix in 50 µl of final PCR reaction volume. The PCR condition is given in **Appendix Table A3**.

2.2.2.6 Extraction of plasmid from *E.coli* (DH5α)

For cloning or restriction-digestion purpose, plasmid-minipreps were used. For this, 2 ml of LB medium (with selected antibiotic) was inoculated with a bacterial colony. The culture was incubated at 37°C overnight with shaking (120 rpm). The plasmid was isolated through

Invisorb® Spin Plasmid Mini Two kit as per the prescribed protocol. For other purposes, like protoplast transient transformation, plasmid-midipreps (from 50 ml of bacterial culture) or maxipreps (from 250 ml of bacterial culture) were prepared using commercial kit provided by Qiagen.

2.2.2.7. Restriction digestion and DNA sequencing analysis

Plasmid miniprep (~1µg DNA) was used for the restriction digestion. The 20 µl of final reaction mix had 1X of recommended buffer and 5-10 U of restriction enzyme (ThermoFisher). The mixture was incubated for 1-16 hour at recommended temperature for optimum digestion. The selected plasmids were sequenced (Sanger sequencing, Eurofins-genomics/GATC-biotech Ltd).

2.2.3 Extraction of *Arabidopsis* genomic DNA and selection of knockout lines

Crude extraction of genomic DNA was performed from *Arabidopsis* leaves. 2-3 fully expanded leaves were ground in 1 ml of extraction buffer (100 mM Tris pH=8, 50 mM EDTA, 500 mM NaCl, 1.5% SDS). Samples were vortexed and centrifuged at 10000x for 5 min. Supernatant was mixed with 1:1 vol of isopropanol and centrifuged again at 16000x for 10 min. The pellets were washed with 70% ethanol, dried and dissolved in 10 mM Tris-Cl. For the selection of knockout T-DNA Salk-lines, DNA from these plants was amplified with 5' T-DNA border primer (Lba1) and gene-specific 3' right primer. On other hand, lines showing amplicon with gene-specific left primer (LP) and right primer were not selected as they did not contain the T-DNA inserted into their gene body. The PCR conditions for the genotyping are given in **Appendix Table A2**.

2.2.4 RNA Extraction

The total RNA from leaves was isolated using monophasic lysis reagent (TRIzol: 0.8 M Guanidine thiocyanate, 4 M Ammonium thiocyanate, 0.1 M Na-Acetate, 5% Glycerol, 38% Phenol (Aqua-Roti-Phenol from Roth)). 1-2 *Arabidopsis* leaves were pulverized in RNase free tubes and 1 ml TRIzol reagent was added. The tubes were incubated at room temperature for 10 min with constant shaking. 200 µl chloroform was added to the samples, mixed and incubated for 5 min at room temperature for the separation of organic phase from the aqueous phase. The samples were centrifuged at 14000x g for 15 min at 4°C. The upper aqueous phase was carefully transferred into a new sterile tube without disturbing lower protein-organic phase or DNA-interface. 1 volume of isopropanol was added to the aqueous phase, mixed and incubated at room temperature for 10 min for RNA precipitation. The mixtures were centrifuged at 16000x g for 15 min at 4°C to isolate RNA as a pellet. The RNA pellets were washed with 70% ethanol and centrifuged again for 10 min. The pellets were dried completely and dissolved in 20 µl DEPC-treated water. The absorbance was measured at 260 nm (A₂₆₀) to determine

the concentration of RNA. The ratio of A260/A280 was checked (1.8-2.0) to ensure the purity of RNA samples.

2.2.5 DNase I treatment

The extracted RNA samples were treated with DNaseI (1X buffer, 2U DNaseI (ThermoFisher)). DNaseI is a non-specific endonuclease enzyme that cleaves both double and single stranded DNA by hydrolyzing phosphodiester bonds. The extracted RNA samples were added to the DNase I buffer and enzyme and volume were adjusted to 20 μ l (final concentration: 1X DNaseI buffer and \sim 0.5 μ l DNaseI (1 U of enzyme per 2 μ g of RNA)) and incubated for 30 min at 37°C. To stop the enzyme activity, EDTA was added to a final concentration of 2.5 mM and incubated at 65°C for 10 min. EDTA is added to the samples before heat inactivation because RNA degradation takes place at a high temperature in the presence of divalent cations.

2.2.6 Synthesis of cDNA from mRNA

The first strand of cDNA was synthesized by RevertAid H Minus cDNA synthesis kit as per manufacturer's instructions (Fermentas). Briefly, the reaction mix was prepared to the final concentrations of 1X reaction buffer, 2 mM dNTP, 0.5 μ g oligo(dT)18, 1 μ l Ribolock, 1 μ l RevertAid enzyme (200 U/ μ l) and added to the RNA template. The cDNA was synthesized by incubating the mixture at 42°C for 1 hour and the reaction was stopped by increasing the temperature to 70°C for 10 min.

2.2.7 Quantitative real-time PCR (qRT-PCR)

qRT-PCR was performed in 10 μ l reaction volume, using 2 μ g of reverse transcribed total RNA, 0.3 μ M of each gene-specific primer, and 5x QPCR Mix EvaGreen® (Bio&Sell). The reaction protocol is described in (**Appendix Table A4**). To calculate relative transcription levels, the delta of threshold cycle (Δ Ct) values were calculated by subtracting the arithmetic mean Ct values of the target gene from the arithmetic mean Ct value of the normalizing PP2A, (At1g69960) which was obtained from the two technical replicates. The relative transcription level ($2^{-\Delta$ Ct) was calculated from the sample obtained from three biological replicates.

2.2.8 Protein purification and related assays

2.2.8.1 Induction and purification of recombinant protein from *E.coli* (KRX) cells

Full-length *TZF9* and zinc-finger motif deleted *TZF9* (*TZF9 Δ CCCH*) were cloned in the pDEST-C102 vector while *putative RNA ligase* was cloned in pDEST-N110. (Dyson et al., 2004). Vector pDEST N110 has a 10X His tag at N- terminal and pDEST-C102 has two tags, maltose binding protein (MBP) and 10X His, at C-terminal. These vectors were transformed into *E. coli* protein expression strain KRX. About 250 ml LB medium containing ampicillin, (final concentration 100 μ g/ml) was inoculated and incubated at 37°C with shaking (120 rpm) until

OD600 of 0.5 was achieved. The protein expression was induced with the addition of 0.1% Rhamnose and incubated overnight at 24°C with shaking (120 rpm). The culture was then centrifuged at 4000x g for 20 min and the supernatant was discarded.

The cells were resuspended in 10 ml sodium-phosphate buffer (0.1 M NaH₂PO₄, 0.3 M NaCl, 10 mM Imidazole, 1:100 protease inhibitor HP mix (Serva GmbH)). For lysis of the cells, lysozyme was added to the final concentration of 2 mg/ml and placed on ice for 30 min with a gentle back and forth shaking every 10 min. The cell suspension was then sonicated 3 times, each for 10 sec with 15 sec interval. This was followed by the addition of Triton X-100 (0.1%), DNaseI (5 µg/ml) and RNaseA (final concentration 5 µg/ml) and placed on the ice again for 30 min. The lysed cells were centrifuged at 16000x g for 30 min. The supernatant was collected in 15 ml precooled conical centrifuge tube.

The purification of the protein was done by immobilized metal affinity chromatography (IMAC). It is based on the affinity of polyhistidine tracts for divalent metal cations (Ni²⁺) immobilized with the chelating ligand Nitrilo Triacetic Acid (NTA) coupled to a cross-linked 6% agarose resin (Ni-NTA agarose). TZF9 and TZF9ΔCCCH expressed with 10X His-tag were purified with Ni-NTA-Agarose (ThermoFisher). About 50µl of Ni-NTA bead slurry was washed three times with the lysis buffer and added to the protein supernatant. The tubes were incubated with Ni-NTA resins at 4°C for 1 hour with constant rocking. The resins were centrifuged and washed once with 2 ml wash buffer (0.1 M NaH₂PO₄, 0.3 M NaCl, 40 mM Imidazole, 1:100 protease inhibitor HP mix). The second wash was performed with high salt wash buffer (0.1 M NaH₂PO₄, 0.5 M NaCl, 40 mM Imidazole, 1:100 protease inhibitor HP mix). The third wash was performed with the first wash buffer (0.1 M NaH₂PO₄, 0.3 M NaCl, 40 mM Imidazole, 1:100 protease inhibitor HP mix). The beads were then resuspended in 50 µl 10 mM Tris pH 7.5 and stored in -20°C.

For ribohomopolymers-EMSA (described in section 2.2.9.3), TZF9-MBP-His and TZF9ΔCCCH-MBP-His were purified in two steps, first using Ni-NTA beads (ThermoFisher) and subsequently with amylose beads (New England Biolabs). For the first step of protein purification, proteins bound to Ni-NTA agarose beads were eluted in 30 µl elution buffer (0.1 M NaH₂PO₄, 0.3 M NaCl, 250 mM Imidazole, 1:100 protease inhibitor HP mix) by incubating at 4°C for 10 min. The eluted protein solution was then mixed with 50 µl amylose bead slurry, incubated for 1 hour at 4°C with gentle shaking for 10 min, centrifuged briefly and supernatants were removed. For the second step of protein purification using amylose bead, Tris-elution buffer (200 mM NaCl, 20 mM Tris-HCl, 1 mM EDTA, 1 mM DTT, 20 mM maltose) was used. Crucially, the second step was required to avoid co-purification of unspecific RNA binding *E.coli* KRX protein. The equivalent volume of bacterial protein extract from untransformed *E.coli* KRX was also purified with the two-step affinity purification to use as a negative control in ribohomopolymer-EMSA. However, for pentaprobe-EMSA, the Ni-NTA purification was optimized to avoid binding of any unspecific protein to Ni-NTA beads. This was achieved by

increasing imidazole concentration in the supernatant up to 40 mM prior to Ni-NTA bead binding of the protein. In this case, the second purification step with amylose beads was not required. For both the RNA-EMSA studies, eluted proteins were dialyzed to eliminate buffer salts and smaller molecules, by using Slide-A-Lyzer MINI dialysis Unit (ThermoFisher). The dialysis was performed for 2 hours at 4°C and dialyzed proteins were collected at 4°C. The proteins were quantified by Bradford protein assay (Biorad) using spectrophotometer (TECAN infinite F50).

2.2.8.2 SDS-PAGE and immunoblotting

SDS-PAGE and immunoblotting were performed as per described method (Sambrook et al., 1989). Antibodies used in the study are summarised in **Table 5**.

Table 5: Antibodies used in the study

Antibody	α -HA	α -myc	α -His	α -GFP	α -mouse	α -rabbit
Concentration	1:1000	1:2000	1:3000	1:5000	1:10000	1:5000
Provider	Biozol	Sigma	Amersham	ThermoFisher	Living colors	BioRad

2.2.8.3 Coomassie and silver staining

SDS-PAGE gels were stained with Coomassie staining solution (0.05% Coomassie Brilliant Blue R-250, 50% methanol, 10% glacial acetic acid) for 2 hours. The gels were then destained with destaining solution (30% methanol, 10% glacial acetic acid) for 2-4 hours. Alternatively, the Colloidal blue staining kit (Invitrogen) was used. For silver staining, the SDS-PAGE gels were incubated with fixation solution (40% v/v ethanol, 10% v/v acetic acid) for 2 hours. It was followed by washing steps, two times with 30% v/v ethanol for 20 min and one-time water for 20 min. After the washes, gels were treated with 0.02% w/v sodiumthiosulfate solution for 1 min, rinsed with water for three times and stained with the silver staining solution (0.2% w/v silver nitrate, 0.075% v/v formaldehyde) for 15 min. The gel was then rinsed with water three times and put in the developing solution (3% w/v sodium carbonate, 0.05% v/v formaldehyde, 0.0004% w/v sodiumthiosulfate) for less than 5 min until the bands became visible. 7% v/v acetic acid was used to stop the developing reaction. The gel was again rinsed two times with water and preserved in 25% ethanol, 3% glycine solution.

2.2.9 *In-vitro* RNA binding assays

2.2.9.1 Isolation and labelling of ribohomopolymers

The four ribohomopolymers were custom synthesized from MWG Biotech. To remove the synthesis contaminants, the ribohomopolymers were purified by urea-PAGE gel electrophoresis (15% acrylamide, 8 M urea). The gel was stained with Serva-G staining. The RNA bands were excised and incubated at 37°C overnight in extraction buffer (10 mM Tris pH 8, 1 mM EDTA, 0.5% SDS) with gentle shaking. Acrylamide was removed by centrifugation and the eluted RNA was precipitated with isopropanol, washed with 70% (v/v) ethanol and resuspended in diethylpyrocarbonate (DEPC)-treated water. The ribohomopolymers were radiolabelled with T4 polynucleotide kinase (Fermentas) and γ -³²P ATP (3,000 Ci mmol⁻¹; Hartmann Analytic) according to Sambrook et al (1989). The unincorporated radioactivity was removed using 'mini quick spin oligo columns'. RNA labelling was assessed by analytic denaturing PAGE (15% acrylamide/8M urea) and autoradiography.

2.2.9.2 Purification and labelling of pentaprobases

The 12 pentaprobases (100bp long probes, cloned in pcDNA3.1) were provided by Mackey's lab, University of Sydney, Australia (Bendak et al., 2012). The working procedure starts with isolating 12 pentaprobe-plasmids from *E.coli* cells by commercially available kit (Invisorb® Spin Plasmid Mini Two kit, Stratec molecular). The plasmids were linearized with *Apa*I (1X buffer, 5U *Apa*I, 5 µg DNA) and separated on 1% agarose gel. The linearized-DNA-bands were excised and the gel particles were removed (using Invisorb® Fragment Cleanup, Stratec molecular). The 3' overhang, generated due to the *Apa*I restriction digestion, was filled using DNA polymerase I large (Klenow) fragment (NEB) (1X buffer, 0.1 mM dNTP, 2 U Klenow mix, 5 µg DNA). These 12 linear DNA-pentaprobe strands were used as a template for the generation of respective RNA pentaprobe. Transcription was carried out using an *in-vitro* transcription kit (RiboMAX™ large-scale RNA production system-T7, Promega). The final reaction mixture (1X buffer, 7.5 mM rNTP, 0.1 µl T7 enzyme mix and ~ 3 µg DNA) was incubated at 37°C for 3 hours. The reaction mixture was treated with DNase I (1 U/µg of the template) at 37°C for 15 min. The RNA pentaprobases were then precipitated and extracted with 1 volume of phenol: chloroform: isoamyl alcohol (25:24:1). The mixture was vortexed and centrifuged for 2 minutes. The upper aqueous phase was mixed with 1 volume of chloroform: isoamyl alcohol (24:1). 0.1 volume of 3 M Sodium Acetate (pH 5.2) and 1 volume of isopropanol was added to the tube, mixed and placed on ice for 5 min. The mixture was then centrifuged at 15000x g for 10 minutes. The supernatant was aspirated and the pellet was washed with 1 ml of 70% ethanol. The RNA-pentaprobe pellet was dried, dissolved in 15 µl DEPC-water and stored at -80°C. The concentration of RNA was determined by UV-Vis spectrophotometer

(Nanodrop, ThermoFisher) and the integrity of RNA was determined by running on an agarose gel.

Afterwards, radioactive 5' end-labelling of pentaprobe was performed. For this, 5'-phosphate group was removed by using 2 μ l (2U) alkaline phosphatase (with 2 μ l of 10X phosphatase buffer, 0.2 μ l (8U) of RNase inhibitor (RiboLock) and 15 μ l RNA (~150 μ g) in 20 μ l reaction) by incubating at 37°C for 30 min. The RNAs were then extracted with 1 volume of phenol: chloroform: isoamyl alcohol (25:24:1) and precipitated as described. The dephosphorylated pentaprobe was then phosphorylated at 5'-end using γ -³²P ATP (Hartmann analytic). For this, the reaction mix was prepared with 1 μ l of 10X kinase buffer, 1 μ l polynucleotide kinase 0.5 μ l ribolock (ThermoFisher), 1 μ l γ -³²P ATP, and 70 μ g RNA in 10 μ l and incubated at 37°C for 30 min. The enzyme was heat-inactivated by incubating at 75°C for 10 min. The unincorporated radioactivity was removed using 'mini quick spin RNA columns'. The schematic representation of pentaprobe generation and labelling is shown in **Fig. 6**. The 5' end labelled pentaprobe was then used for EMSA experiment (method described).

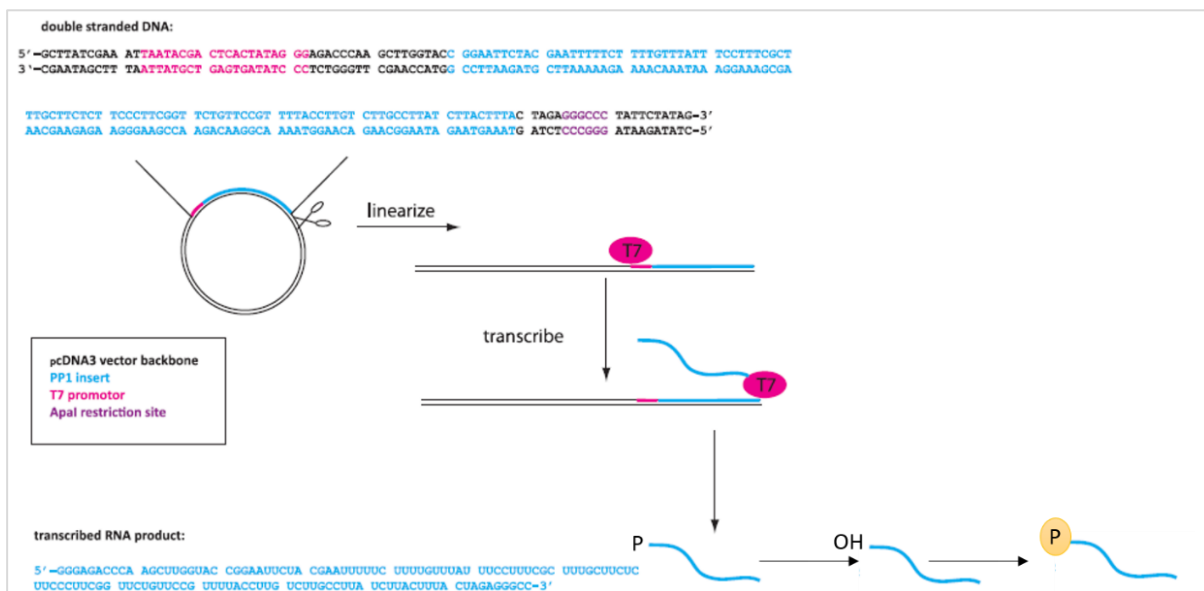


Fig. 6: Schematic representation of ssRNA pentaprobe generation and labelling. Plasmid containing a dsDNA pentaprobe sequence (blue) under the T7 promoter (pink) is linearized by restriction digestion at *ApaI* site (purple). The pentaprobe is *in-vitro* transcribed and 5' phosphate was removed using phosphatase. The 5' end of the pentaprobe was then radiolabelled using γ -ATP (Source Bendak et al., 2012).

2.2.9.3 Ribohomopolymers/Pentaprobe-EMSA

RNA binding and separation of unbound probes on non-denaturing PAGE was performed according to Brewer et al (2004). Briefly, recombinant proteins (~5 ng) were pre-incubated with binding buffer (10 mM Tris pH 8, 100 mM KCl, 2 mM DTT, 0.1 mg/ml bovine serum albumin, 10% glycerol, 5 mM ZnCl₂) for 20 min at room temperature and, afterwards, approximately 0.2

nmol of ^{32}P -labeled ribohomopolymers were added to the reaction in a final volume of 15 μl . The reaction was incubated on ice for 15 min and then separated on a native 5% non-denaturing gel (37.5: 1 acrylamide/bisacrylamide) in 1X TAE buffer (40 mM Tris, 20 mM acetic acid, 1 mM EDTA) at 4°C. After electrophoresis, gels were dried and exposed to phosphor-screens and scanned using a Typhoon phosphor imager scanner (GE Healthcare, <http://www.gelifesciences.com/>).

2.2.10 Determination of ROS

Production of ROS was assayed as described (Gomez-Gomez et al., 1999) using 3 mm leaf discs. The leaf-discs were floated adaxial-side up in 96-well plates containing 200 μl dH_2O and incubated overnight in the dark. Next day, dH_2O was removed using vacuum pump. 10 μl luminol–HRP mix {5 μM luminol (L-012, WAKO) and 2U HRP (Sigma) in 10ml dH_2O)} was added to each leaf-discs and background light emission was measured. To measure flg22-induced ROS production, 200nM flg22 was mixed to luminol-HRP solution and added to the leaf-discs using an injector in the luminometer (Luminoskan Ascent 2.1). Each set of measurement (measured at 2 min intervals) was normalized to the background level and the statistical significance of the differences was tested by Kruskal–Wallis test ($P < 0.05$) using Graph Pad Prism software.

2.2.11 Isolation and purification of total mRNA for microarray

The total RNA was isolated by the Trizol method as described in Chomczynski and Sacchi, 1987. The RNA was further purified using columns provided in the RNeasy mini kit (Qiagen) as per described protocol. 100 ng of total RNA was used for cDNA synthesis (already described) to perform microarray.

2.2.12 Isolation and purification of polysomal mRNA for microarray

About 6-8 week old *p35S::RPL18* and *p35S::RPL18/tzf9* lines were infiltrated with 1 μM flg22 and harvested after 1 hour. About 3 ml of pulverized tissues were mixed with 6 ml of polysomal extraction buffer (PEB: 0.2 M Tris (pH 9), 0.2 M KCl, 0.025 M EGTA, 0.035 M MgCl_2 , 1% detergent mix (1% (w/v) polyethylene (23) lauryl ether (Brij-35), 1% (v/v) Triton X-100, 1% (v/v) octophenyl-polyethylene glycol (lgapel CA 630), 1 % (v/v) polyoxyethylene sorbitan monolaurate (tween 20), 1% polyoxyethylene 10 tridecyl ether (PTE), 1% sodium deoxycholate, 5 mM DTT, 1 mM PMSF, 50 $\mu\text{g/ml}$ cycloheximide, 50 $\mu\text{g/ml}$ chloramphenicol, 0.5 mg/ml Heparin). The samples were allowed to thaw on ice for 10 min. The samples were centrifuged at 4°C at 15000x g for 15 min and supernatants were filtered through Miracloth (Millipore) into the new sterile tube. The above centrifugation step was repeated. 50 μl of α -FLAG M2 agarose beads (Sigma) was washed three times with 1 ml of wash buffer (0.2 M Tris (pH 9), 0.2 M KCl, 0.025 M EGTA, 0.035 M MgCl_2 , 5 mM DTT, 1 mM PMSF, 50 $\mu\text{g/ml}$

cycloheximide, 50 µg/ml chloramphenicol, 10U RiboLock). Washed beads were added to the clarified extract and incubated for 2 hours at 4°C with gentle back-and-forth shaking to allow the binding of the epitope-tagged ribosome (and associated mRNAs) to the affinity matrix. After 2 hours, the beads were centrifuged for 1 min at 2000x g at 4°C. The supernatants were removed and beads were carefully washed five times with 5 ml of wash buffer. The α-FLAG M2 agarose beads directly proceeded for extraction of FLAG-RPL18-associated mRNA. This was done by addition of 400 µl RLT buffer (provided with RNeasy kit, Qiagen) and 4 µl β-mercaptoethanol directly to the beads to denature the protein. The mixture was vortexed, 200 µl ethanol was added and mixed. The mixture was centrifuged at 2000 rpm for 15 sec and supernatant was transferred into pink column provided in the Qiagen RNAsy kit. Rest of the steps were followed as recommended by the manufacturer (Qiagen). The integrity of eluted RNA was checked with the Qiaxcel machine (Qiagen) which shows 28s and 18s ribosomal bands.

2.2.13 Microarray

About 100 ng of total RNA and 150 ng of polysomal mRNA was processed for cDNA synthesis using the kit provided by Affymetrix and the probes were prepared for the microarray. All of the steps were followed according to the protocol provided by Affymetrix. The simplified assay workflow is shown in **Fig. 7** below.

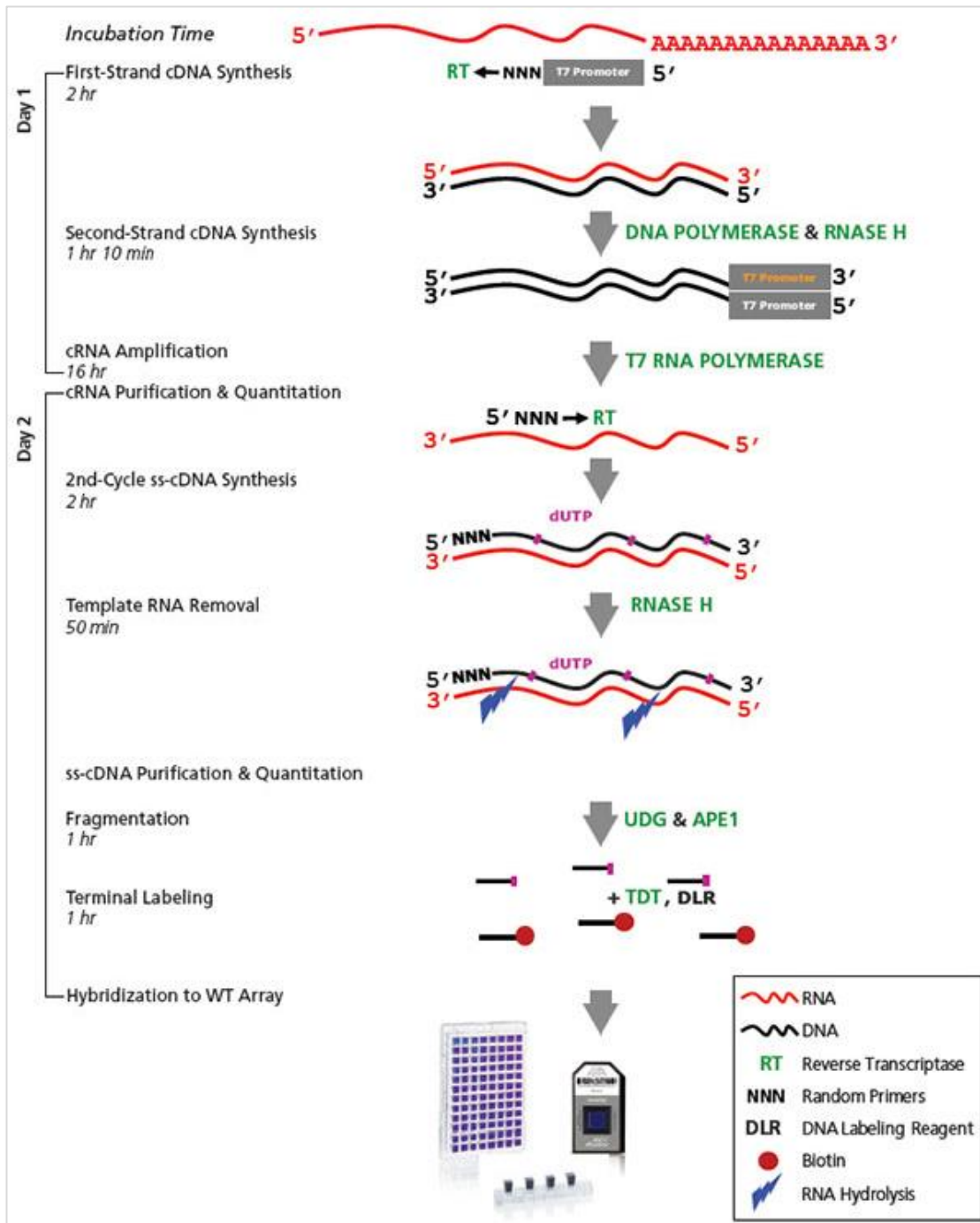


Fig. 7: Simplified workflow of Affymetrix Microarray Assay. Hybridization was performed on the commercially available chip (Affymetrix 1.1 ST array). The chip-compatible GeneAtlas® system was available in-house (Figure adapted from the user manual, GeneAtlas®).

3 Results

3.1 TZF9 as MPK3/6 substrate in PTI

3.1.1 TZF9 shows mobility shift upon flg22 treatment

Many defense-related proteins are post-translationally modified when PTI is triggered *in-vivo* upon flg22 elicitation. A mobility shift assay was employed to detect the flg22-induced post-translational modification of the TZF9 protein. A mobility shift is observed as modified proteins move slower in a PAGE gel as compared to their non-modified counterparts. For this, protoplasts were transfected with plasmid encoding/expressing epitope-tagged wild-type TZF9 (TZF9-WT). In this assay, TZF9 was expressed in fusion with hemagglutinin (HA) tag. After an overnight expression, the protoplasts were treated with 100 nM flg22 and harvested after 10 min and 60 min. Untreated transformed protoplasts were used as a control. The protoplasts were then lysed, extracts were run on SDS-PAGE gel and western blotting was performed. As shown in **Fig. 8**, a reduced mobility shift of TZF9 band was observed after flg22 treatment for the indicated times. Hence, TZF9 was suggested to be a potential target for post-translational modifications upon flg22 treatment.

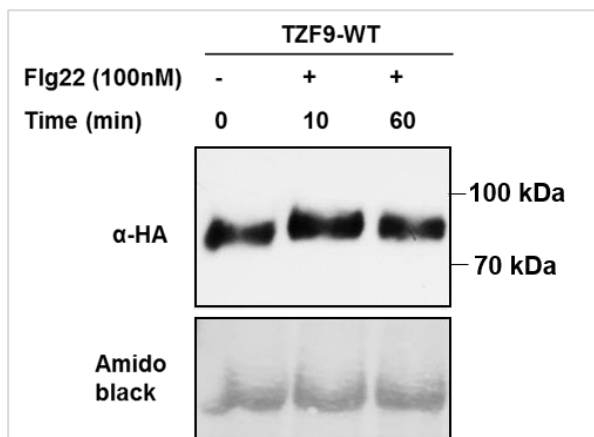


Fig. 8: *In-vivo* post-translational modification of TZF9. Protoplasts expressing TZF9 WT-HA were treated with flg22 for indicated time periods, lysed, extracts were run on a SDS-PAGE gel and blotted against α -HA antibody. A mobility shift of protein is observed after flg22 treatment (as shown in α -HA blot). Amido black staining of the membrane is shown as the loading control

3.1.2 TZF9 shows phosphorylation at multiple sites

Protein phosphorylation is one of the vital post-translational modifications. TZF9 contains 14 putative MAPK phosphorylation sites (**Appendix Fig. A2**). To identify MAPK-targeted sites, several experiments were performed in previous (Maldonado-Bonilla et al., 2014) and the current study.

In the previous studies done in our lab, recombinantly expressed and purified TZF9 was *in-vitro* phosphorylated by MPK3 and -6 protein and phosphorylated sites were identified by mass spectrometry. Out of 14 putative MAPK phosphosites, six phosphosites were identified as phosphorylation sites of MPK3. These sites are S³²³, T³⁷⁷, S⁴⁰⁸, S⁴¹⁵, S⁴¹⁹ S⁴³⁵ and S⁴⁷². Only two sites (S³²³, S⁴³⁵) were found to be phosphorylated by MPK6 in MS (**Appendix Fig. A4**).

Another approach used to map the phosphosites was based on site-directed mutagenesis analysis. Using this method, several mutant versions of TZF9 were generated where serine or threonine was replaced by alanine or glycine (Ser/Thr→Ala/Gly). The method of mutagenesis was adapted from Palm-Forster et al (2012). Recombinant proteins were purified from *E.coli* and were used for kinase assay. For kinase assay, proteins were analysed for *in-vitro* phosphorylation using MAPKs as the kinases in presence of kinase buffer containing radiolabelled γ -³²P ATP. Wild-type protein was used as the control in these kinase assays. A comparison of signal intensity between wild-type and the mutant protein was performed (Master thesis, Martina Brode). The result of these assays is summarized in **Table 6**. Collectively, this data suggested that multiple phosphosites in TZF9 could be targeted by MAPKs.

Table 6: Putative MPK3/6 phosphorylation sites of TZF9, their identification and validation

Position of amino acid	Respective number	Identified by Mass spectrometry		Confirmed by <i>in-vitro</i> kinase assay	
		Against MPK3	Against MPK6	Against MPK3	Against MPK6
T60	M (Mutation)1	no	no	no	no
S141	M2	no	no	no	no
S181	M3	no	no	yes	yes
S323	M4	yes	yes	yes	yes
S343	M5	no	no	yes	yes
T352	M6	no	no	yes	yes
S356	M7	no	no	yes	yes
S362	M8	no	no	yes	yes
T377	M9	yes	no	yes	yes
S408	M10	yes	no	yes	yes
S415	M11	yes	no	no	no
S419	M12	yes	no	no	no
S435	M13	yes	yes	no	no
S472	M14	yes	no	no	no

Based on these studies, a phosphomutant variant of TZF9 was generated in which eight (out of 14) putative phosphorylation sites were mutated. Those consecutive sites are T³⁵² S³⁵⁶, S³⁶², T³⁷⁷, S⁴⁰⁸ S⁴¹⁵, S⁴¹⁹ and S⁴³⁵ (Master thesis, Martina Brode). This version of TZF9 was referred to as TZF9 PS T³⁵²A-S⁴³⁵A (PS stands for phosphosite). A mobility shift assay using this variant was performed to check if there are modifications at other putative-MAPK targeted sites. For this, protoplasts were transfected with plasmid harbouring HA tagged TZF9-WT and TZF9-PS mut S³⁵²A-T⁴³⁵A, protoplasts were treated with flg22 (100nM) and harvested after 10 min. The protoplasts extracts were run in SDS-PAGE gel and western blot was performed. As expected, a reduced mobility shift of TZF9-WT band was observed however, a subtle shift was observed in TZF9 PS T³⁵²A-S⁴³⁵A band suggesting some additional MAPK-targeted sites could be modified (**Fig. 9**).

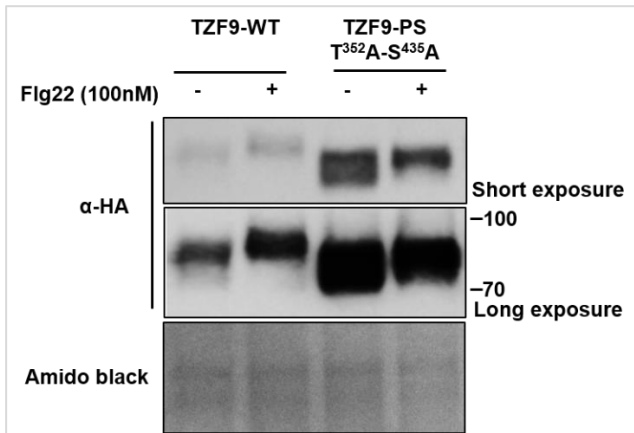


Fig. 9: Post-translational modification of TZF9-WT and TZF9 PS mut S⁴³⁵A-T³⁵²A. Protoplasts expressing TZF9-WT-HA and TZF9 PS mut T³⁵²A-S⁴³⁵A-HA were treated with 100 nM flg22 for 10 min. Protein extracts were subjected to SDS-PAGE and blotted with the α-HA antibody. The blot shows flg22-induced mobility shift in both the proteins. Amido black staining of the membrane shows equal loading.

3.1.3 A phosphonull version of TZF9 does not show flg22 induced mobility shift

Based on the aforementioned results (Fig. 9), a mutant version of TZF9, in which all the putative MAPK targeted phospho-sites were mutated (phosphonull TZF9), was generated. This creates a non-phosphorylatable (phosphonull version) TZF9. For simplicity, the 14 phosphosites are consecutively represented as sequential number from M1 to M14 (Table 6). To generate phosphonull version of the protein, site directed mutagenesis was performed to change the Ser and Thr amino acids to Ala and Gly (Palm-Forster et al., 2012) (Fig. 10). Here, four phosphomutant variants of TZF9 generated previously in the lab were used. Three of them were carrying mutation in one phosphosite and one was carrying mutation in eight phosphosites. As shown in Fig. 10, primers carrying mutation (red arrows) on the phosphosites were used to generate more mutation in the resulting amplicons. Golden gate-cloning compatible primers were designed in such a way that 4 unique overhangs were produced after *Bpil* enzyme digestion. This allowed the digested amplicons to ligate in the correct orientation in one go. The positive constructs were selected on appropriate antibiotics after transformation.

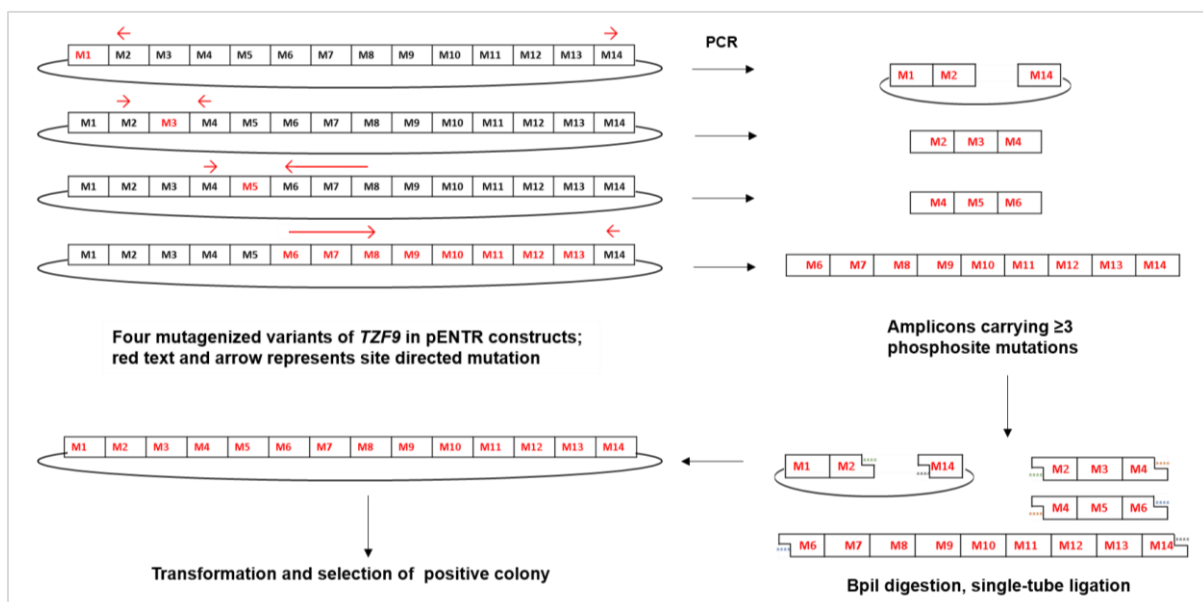


Fig. 10: Workflow for the generation of phosphonull mutant of TZF9. First construct carrying mutation at 1st phosphosite (M1) was amplified with the primers carrying mutation in 2nd and 14th phosphosite (M2 and M14). Likewise, second construct carrying M3 and third construct carrying M5 were amplified with the primers M2/M4 and M4/M6-8 respectively. The fourth construct carrying mutation at multiple sites (M6-M13) was amplified using primers M6-8/M14. PCR amplicons were digested by *BpiI*, ligated with T4 DNA ligase, transformed in *E. coli* cells and subsequently selected.

Protoplasts were transfected with plasmid harbouring HA tagged TZF9-PS mut. After overnight incubation, protoplasts were treated with flg22 and harvested after 10 min. The protoplasts were then lysed, extracts were run in SDS-PAGE gel and western blot was performed. No mobility shift was observed upon flg22 elicitation, which indicated that the mobility shift is caused by modifications at the putative MAPK-targeted sites (**Fig. 11**).

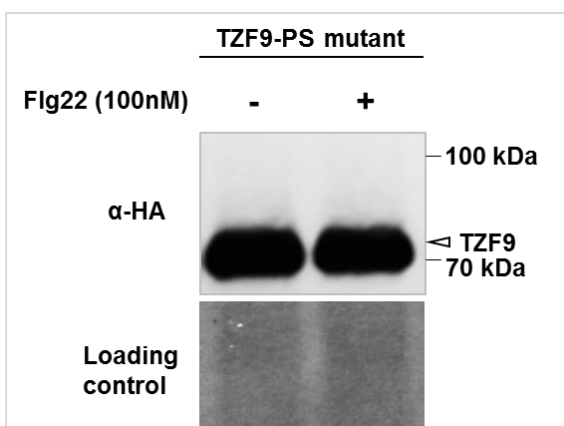


Fig. 11: TZF9 phosphonull mutant protein does not show mobility shift after flg22 elicitation. Plasmid carrying *TZF9 PS mut-HA* was transformed in protoplast and after overnight incubation, protoplasts were elicited with flg22. Extracted proteins were subjected to SDS-PAGE and blotted with α-HA antibody. Both untreated and flg22 treated samples migrated to the same position in the gel showing lack of any mobility shift.

3.1.4 TZF9 shows mobility shift due to phosphorylation after flg22 elicitation

PAMP-induced MAP kinase activation and subsequent phosphorylation of their substrates is one of the known examples of post-translational modification. However, many proteins undergo post-translational modifications upon PAMP-treatment. These modifications could include phosphorylation, glycosylation, ubiquitination, acetylation and so forth. To show that the mobility shift of a protein is only due to phosphorylation, the protein extract was treated with λ-phosphatase. The λ-phosphatase releases phosphate group from phosphorylated serine, threonine and tyrosine residue in a protein.

Since TZF9 PS mutant did not show a mobility shift, it was used as a control in the following assay. Plasmids encoding wild-type (WT) or phosphosite mutated (PS mut) TZF9 were transfected into *Arabidopsis* protoplasts. After an overnight incubation, protoplasts were treated with flg22 and harvested after 10 min. Afterwards, protein extracts from the one of the flg22 elicited samples were treated with λ-phosphatase. As expected, TZF9-PS mut did not show any mobility shift upon flg22 (and/or λ-phosphatase treatment). Compared with the TZF9-PS mut, TZF9-WT showed a different mobility in the non-elicited protoplasts (possibly due to basal phosphorylation) and a higher mobility shift after 10 min of flg22 elicitation (**Fig. 12**).

However, both basal and flg22 dependent shifts in TZF9-WT were reduced to the PS mut level when treated with λ -phosphatase. This proved that the mobility shift observed in TZF9-WT is due to phosphorylation at putative MAPK phosphorylation sites.

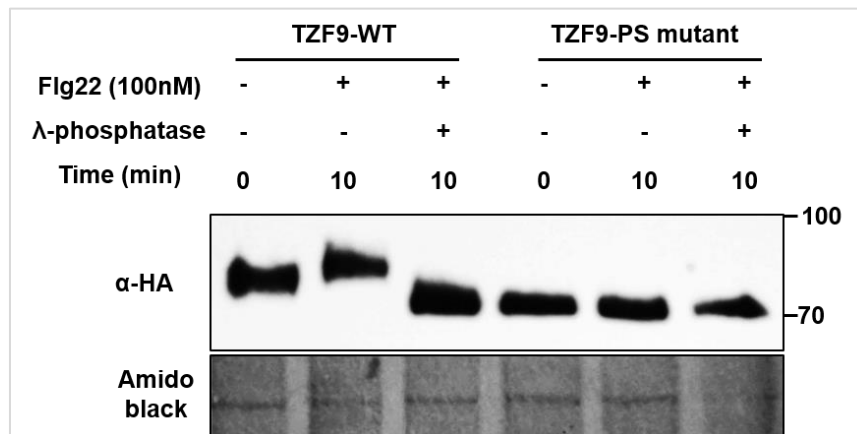


Fig. 12: Phospho-mobility shift of TZF9 after λ phosphatase treatment. Protoplasts expressing TZF9 WT-HA and TZF9 PS mut-HA were lysed and whole protein extracts were treated with flg22 and λ - phosphatase. Protein extracts were run on SDS-PAGE gel and blotted against α -HA antibody. TZF9-WT protein shows basal and further shift after flg22 treatment (10 min). However, no shift was observed in TZF9-WT upon λ phosphatase treatment.

3.1.5 TZF9 is phosphorylated by activation of MKK5-MPK3/6 pathway post flg22 elicitation

The flg22 elicitation, in general, could activate several kinases including CDPKs and other MAPKs in addition to specific MPK3/6 cascade. So it was to investigate that the mobility shift in TZF9 protein was specifically due to MPK3/6 phosphorylation (via MKK5-MPK3/6 module). To check this, TZF9-WT and TZF9-PS mut were co-expressed with a constitutively active version *Arabidopsis* MAP kinase kinase, MKK5^{DD} or an inactive version, MKK5^{KR} (Asai et al., 2002, Lassowkat et al., 2014). MKK5^{DD}, being upstream of MPK3/6 would activate MAPKs in the absence of flg22 elicitation and in turn, TZF9-WT would be phosphorylated in the protoplasts (Asai et al., 2002). As shown in **Fig. 13a**, TZF9-PS mut does not show any mobility shift but TZF9-WT, showed a mobility-shift when MKK5^{DD} (but not MKK5^{KR}) was co-expressed. This shift was comparable to that induced after flg22 elicitation. To reconfirm the mobility shift is due to phosphorylation, the protoplast extract expressing epitope tagged TZF9-WT and MKK5^{DD} was treated with λ phosphatase (**Fig. 13b**). λ -phosphatase treatment dephosphorylated TZF9-WT and the mobility shift was abrogated. For TZF9-PS mut version, MKK5^{DD} co-transfection did not lead to mobility shift consistent with the previous results (**Fig. 13a**). This proved that flg22-induced phospho-mobility shift in TZF9 is due to phosphorylation most likely via MKK5-MPK3/6 module.

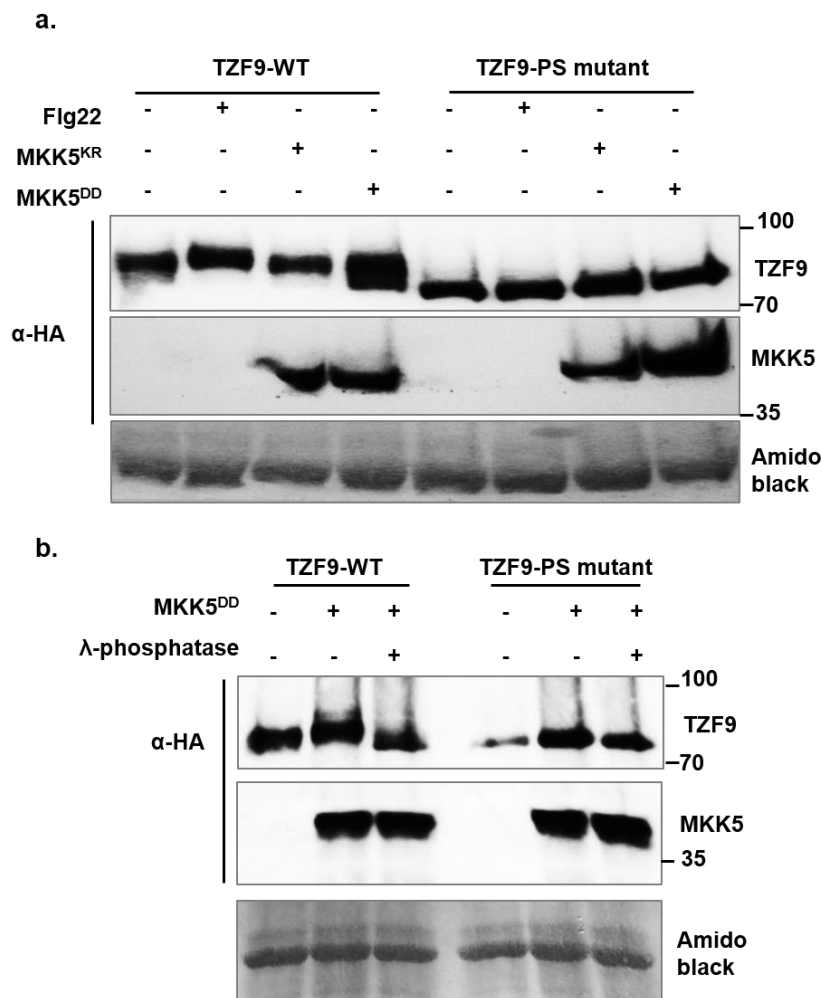


Fig. 13: Phospho-mobility-shift of TZF9 is due to MPK3/6 phosphorylation. (a) Protoplast expressing TZF9-WT-HA and HA tagged TZF9 PS mutant either alone or co-expressed with MKK5^{DD} or MKK5^{KR}. α-HA blot shows mobility shift of TZF9-HA when treated with flg22 or expressed with MKK5^{DD}. Middle panel of the blot shows HA-tagged MKK5^{DD} and HA-tagged MKK5^{KR} while lower panel shows the amido black staining of the membrane as loading control. (b) α-HA blot showing λ-phosphatase treatment abolished phospho-mobility shift in TZF9 (upper panel) and HA-tagged MKK5^{DD} and HA-tagged MKK5^{KR} (middle panel) and amido black staining of membrane (lower panel).

3.1.6 TZF9 interacts with MPK3 and MPK6

To further confirm the role of MPK3 and MPK6 in phosphorylating TZF9 during PTI, it was sought to investigate the interaction of individual MAPKs with TZF9 using BiFC (Bimolecular fluorescence complementation) assay in protoplasts. BiFC or Split YFP vectors (vector maps are shown in **Appendix Fig. A5**) used in this study were pUC-SPYCE (to express TZF9 in fusion with C-terminal fragment of YFP and HA) and pE-SPYNE (to express MAPKs in fusion with N-terminal fragment of YFP and myc). The reconstituted YFP signal in the cytoplasm was observed with both MPK3 and MPK6. This reflects that both MPK3 and MPK6 interact with TZF9-WT *in-vivo* (**Fig. 14**).

Since multiple mutations can cause conformational change in a protein. To rule out a possibility that MAPKs does not interact with TZF9 PS mutant due to conformational change, BiFC assay

was also performed. For this, TZ9-PS mut was co-expressed with MPK3 and -6. The reconstituted YFP signal is shown in **Fig. 14b**. This shows the phosphonull mutant version of TZF9 could also interact with MAPKs. [u7u](#)

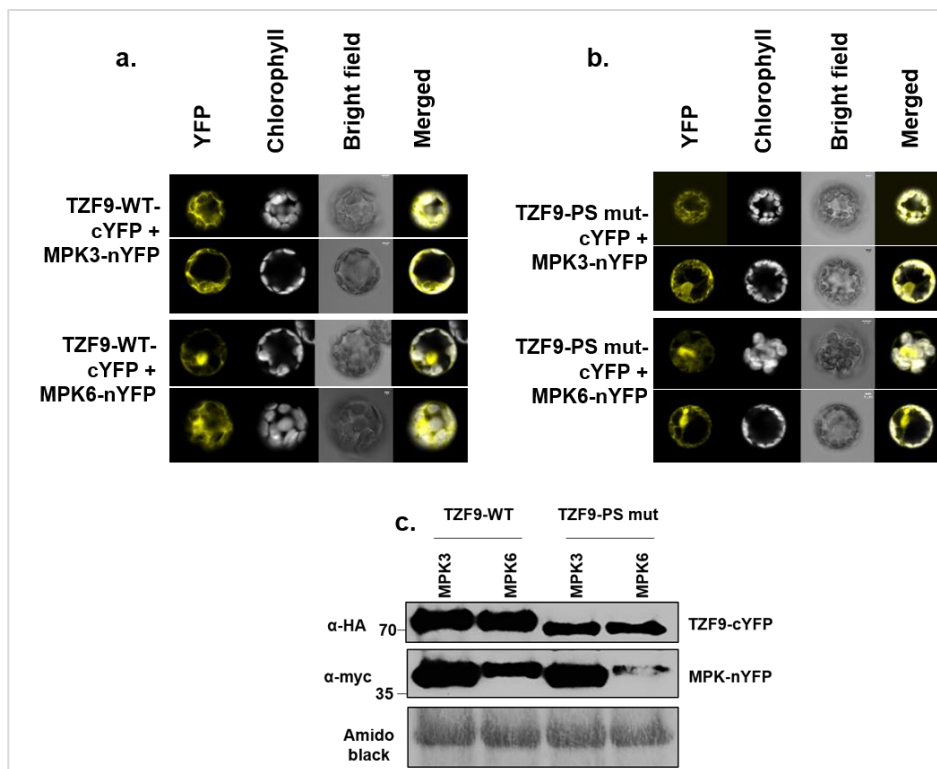


Fig. 14: TZF9 interacts with MPK3 and MPK6. BiFC assay showing *in-vivo* interaction of MPK3 and MPK6 with **(a)** TZF9 and **(b)** TZF9-PS mut. The indicated constructs were transfected into *Arabidopsis* protoplasts and expressed overnight, reconstituted YFP signals were observed under confocal microscope. In both the cases, reconstituted YFP signals (yellow signal) were seen via YFP channel of confocal microscope. Chlorophyll autofluorescence (white), bright field and merged images are shown in subsequent panels. (Scale Bar=5μM). **(c)** α-myc and anti-HA western blot showing integrity of the fusion protein, with amido black staining of the membrane to show equal protein loading.

Hence taken together with the previous *in-vitro* phosphorylation data (Maldonado-Bonilla et al., 2013), these findings are indicative of an *in-vivo* MAPK-mediated TZF9 phospho-modification after flg22 treatment. As MPK3 and MPK6 are activated by PAMPs, TZF9 as a MAPK substrate may contribute to the cellular signaling.

3.1.7 TZF9 phosphorylation by MAPKs alters its stability

Phosphorylation by MAPKs often affects the *in-planta* stability of their downstream target proteins (Sheikh et al., 2016). The next question addressed was whether MAPK phosphorylation alters the stability of TZF9. For this, plasmids harbouring HA tagged TZF9-WT and TZF9-PS mut were transfected into protoplast. After an overnight expression of proteins, the protoplasts were treated with 100 nM flg22 and 5 μM cycloheximide and harvested after different time-points. Cycloheximide, a translation inhibitor, stops the new synthesis of

protein so that the effect of flg22 on protein stability could be investigated. Phospho-mobility shift upon flg22 treatment and subsequent degradation was observed in TZF9-WT at later time points (**Fig. 15**). However, this effect was not observed in TZF9-PS mut where the protein levels remained fairly stable even after 150 min of flg22 treatment. At later time points (e.g. 150 min), TZF9-WT protein was observed to be *in-situ* de-phosphorylated by cellular phosphatases (**Fig. 15**). Taken together, it could be concluded that wild type TZF9 protein undergoes degradation after phosphorylation at MAP kinase targeted sites.

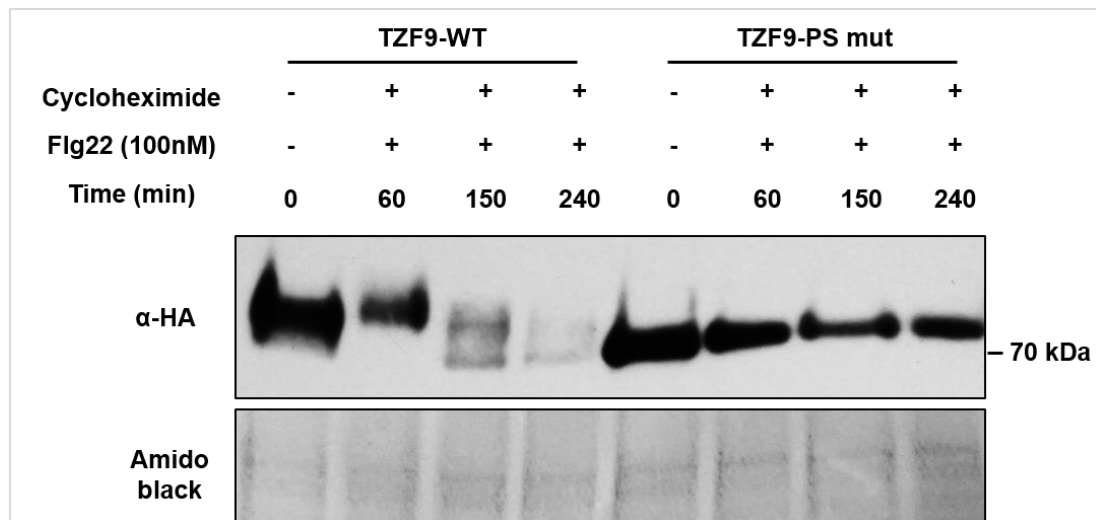


Fig. 15: Phospho-stability of TZF9 after flg22 treatment. Protoplasts expressing TZF9-WT-HA and TZF9-PS mut-HA were treated with cycloheximide and flg22 and harvested after the indicated time points. α -HA blot shows TZF9 protein levels at indicated time points.

3.1.8 TZF9 relocates upon flg22 treatment

As already mentioned that some of the MAPK substrates change their localization in response to PAMP elicitation. To check if TZF9 is altered in localization after flg22 elicitation, TZF9 was transiently expressed in fusion with GFP (*green fluorescent protein*) under moderate promoter, ubiquitin 10 (*pUbQ10::TZF9-GFP*) in protoplasts. TZF9 was observed to localize in foci like structures within the protoplasts (**Fig. 16**, shown by an arrow in enlarged image). The protoplasts were treated with water and multiple images were taken at vertical Z-planes in the time-series using confocal microscope. During the time-series, the foci like structures were constantly observed in Z-planes after water treatment (**Fig. 16a**). Interestingly, upon flg22 treatment, the foci like structures were constantly depleting and more cytoplasmic localization of the protein was observed (**Fig. 16b**).

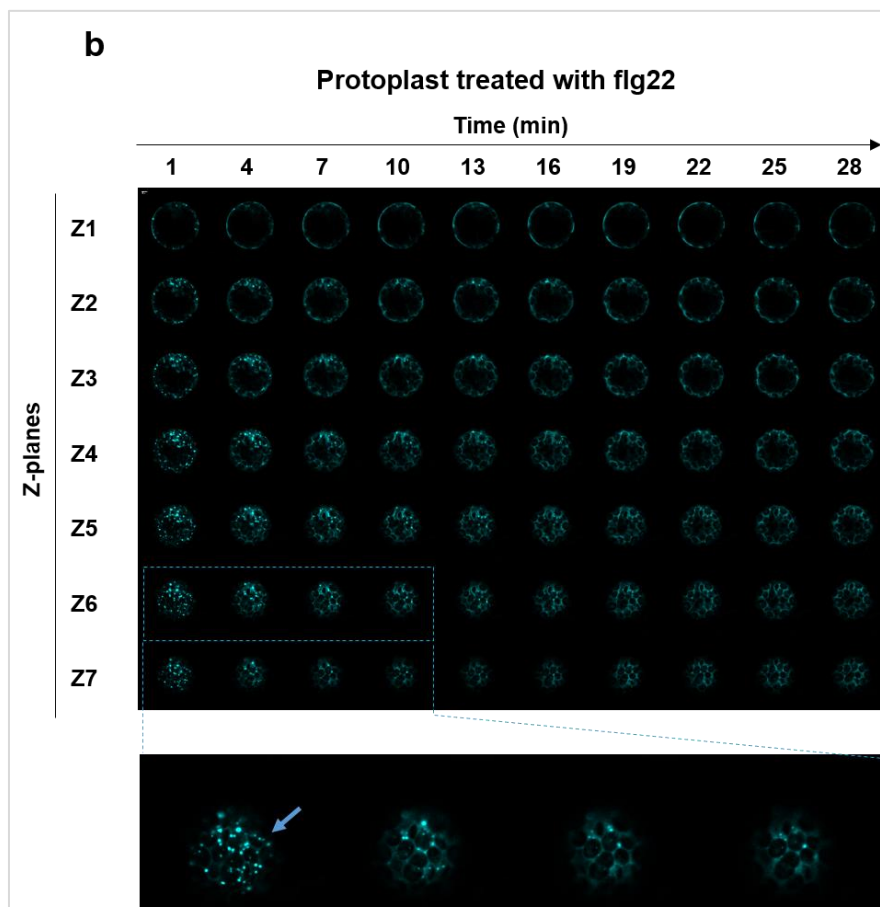
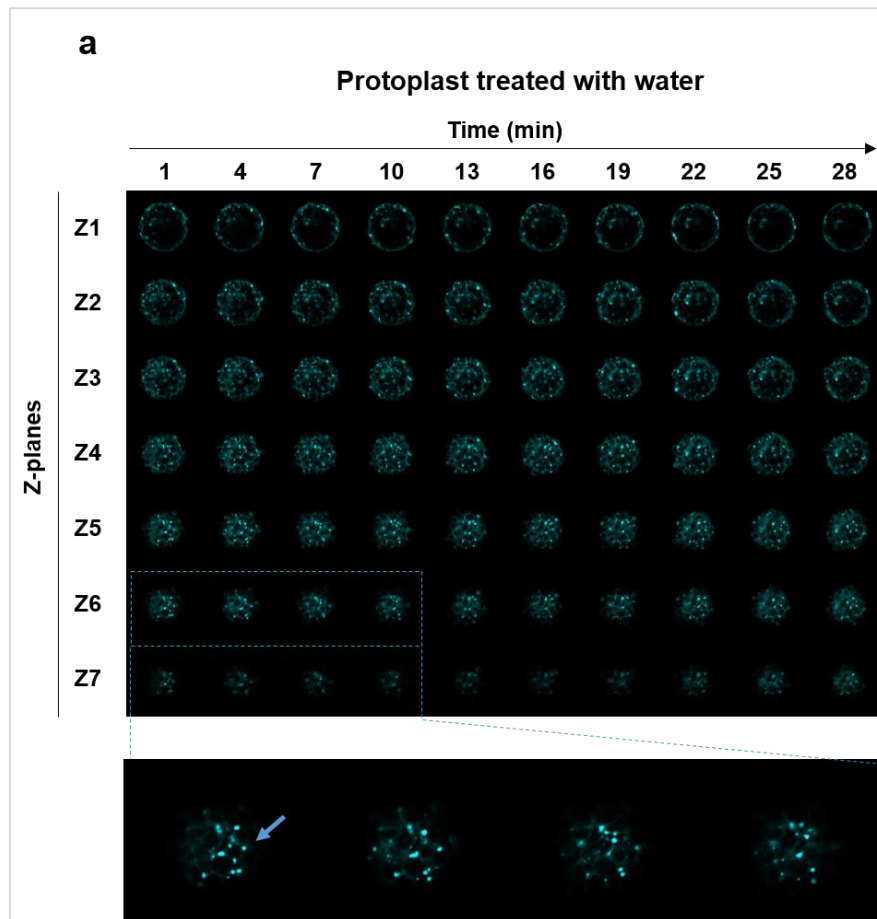


Fig. 16: Localization of TZF9 changes upon flg22 treatment. Representative photograph of TZF9 localized in cytoplasmic foci in protoplast. A single protoplast expressing TZF9-GFP was observed under confocal microscope, photographed in time-series after **(a)** water treatment and **(b)** flg22 treatment. 10 images (from 1 min to 28 min) were taken at seven Z-planes using Zeiss confocal microscope.

3.2 TZF9 localizes within Processing Bodies (PB).

As shown in **Fig. 16**, TZF9 was observed to be localized in cytoplasmic foci. These foci like structures were hypothesized to be PB, which are hubs for RNA processing. To ascertain that these cytoplasmic foci are PB, a co-localization study was performed using DCP1 and XRN4 as PB marker proteins. Both of the marker proteins are involved in mRNA degradation (Weber et al., 2008). For this, TZF9-GFP was transiently co-expressed with DCP1-tdTOMATO (**Fig. 17**, upper panel) and TZF9-RFP was co-expressed with XRN4-GFP (**Fig. 17**, lower panel). TZF9 was observed to co-localize with PB marker proteins (**Fig. 17**), suggesting that TZF9 may function in PB, a site for mRNA processing.

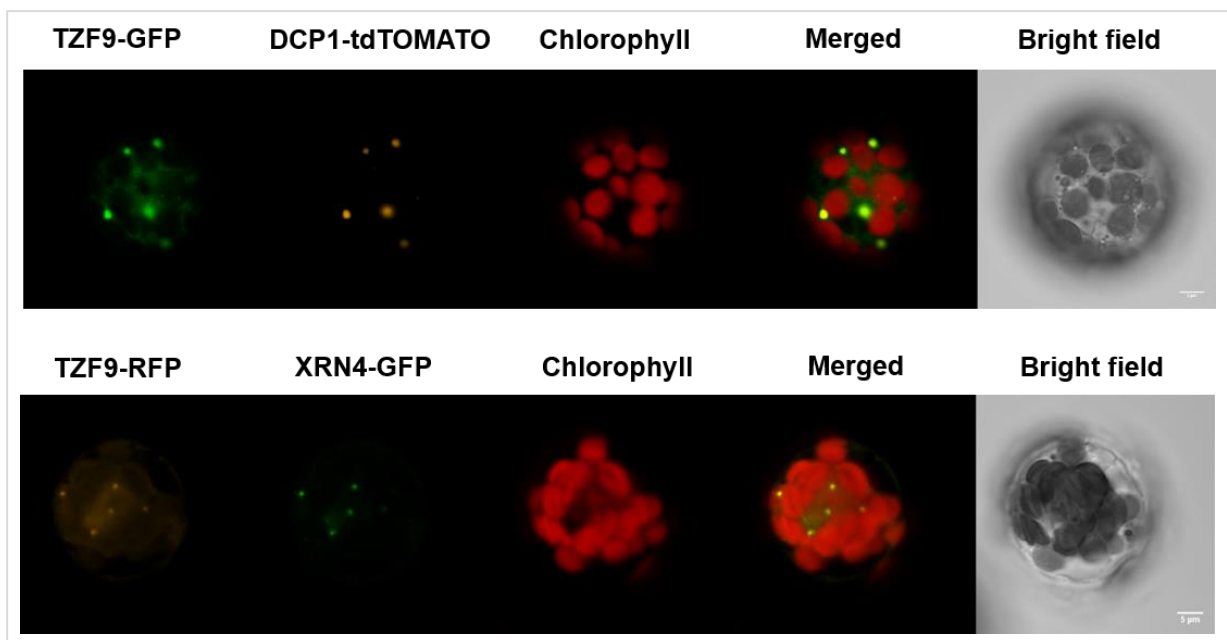


Fig. 17: Localization of TZF9 within PB. Representative photograph shows co-localization of TZF9 with markers of PB. In upper panels, mesophyll protoplast transfected with plasmids harbouring TZF9-GFP and DCP1-tdTOMATO. After overnight expression of genes, TZF9-GFP was observed through GFP channel (shown in green colour) and DCP1-tdTOMATO (shown as orange colour) was observed using RFP channel. In lower panel, TZF9-RFP construct was co-expressed with XRN4-GFP and subsequently observed under confocal microscope with red and green channels respectively. Autofluorescence from chlorophyll was shown in red colour (Scale Bar=5µM).

3.3 TZF9 interacts with RNA *in-vitro*

TZF9 localization in the PB suggests its possible involvement in post-transcriptional regulation processes. The mammalian homologous protein of plant TZFs, TTP is known to be involved in

such processes by targeting certain mRNAs but the biological RNA targets of plant TZFs are still unknown (Fenger-Gron et al., 2005). Nevertheless, TZFs are shown to be localized in the processing bodies. In addition, *Arabidopsis* TZF1 is shown to bind RNA *in-vitro* (Qu et al., 2014). Taken together, it was intriguing to check the RNA binding activity of TZF9.

3.3.1 TZF9 shows affinity to poly U and poly G ribohomopolymers

To get a hint if TZF9 binds to RNA, Electrophoretic Mobility Shift Assay (EMSA) was performed using 18 nucleotides long ribohomopolymers of adenine (rA), cytosine (rC), guanine (rG) and uracil (rU). Full-length protein and a zinc-finger deleted variant of TZF9 were used because zinc-finger is known to bind nucleotides in TZF family of proteins (Pomeranz et al., 2010b; Pomeranz et al., 2011). About 5 ng of purified recombinant proteins of TZF9-MBP-His10X and TZF9 Δ CCCH-MBP-His10X (zinc-finger deleted variant) were used for the assay (**Fig. 18a**). For a negative control, cell extract from non-transformed *E.coli* cells was purified in the same way. The purified proteins were incubated with radiolabelled-ribohomopolymers along with zinc-containing buffer and separated on a 5% native PAGE gel at low voltage.

Full-length (WT) TZF9 protein formed a smeary complex with two ribohomopolymers poly rU and poly rG (**Fig. 18b**). This smear might be formed due to binding of TZF9 to multiple sites of poly rU / poly rG or due to dissociation. In addition, some degradation of the unbound poly rC probe with the (WT) TZF9-MBP-His10x may indicate an RNase activities. The possible binding or degradation of RNAs was observed only with full length (WT) protein but not with the zinc-finger-deleted variant of TZF9, suggesting that the CCCH-zinc-finger domain is required for its RNA binding and/or degradation activity (**Fig. 18b**).

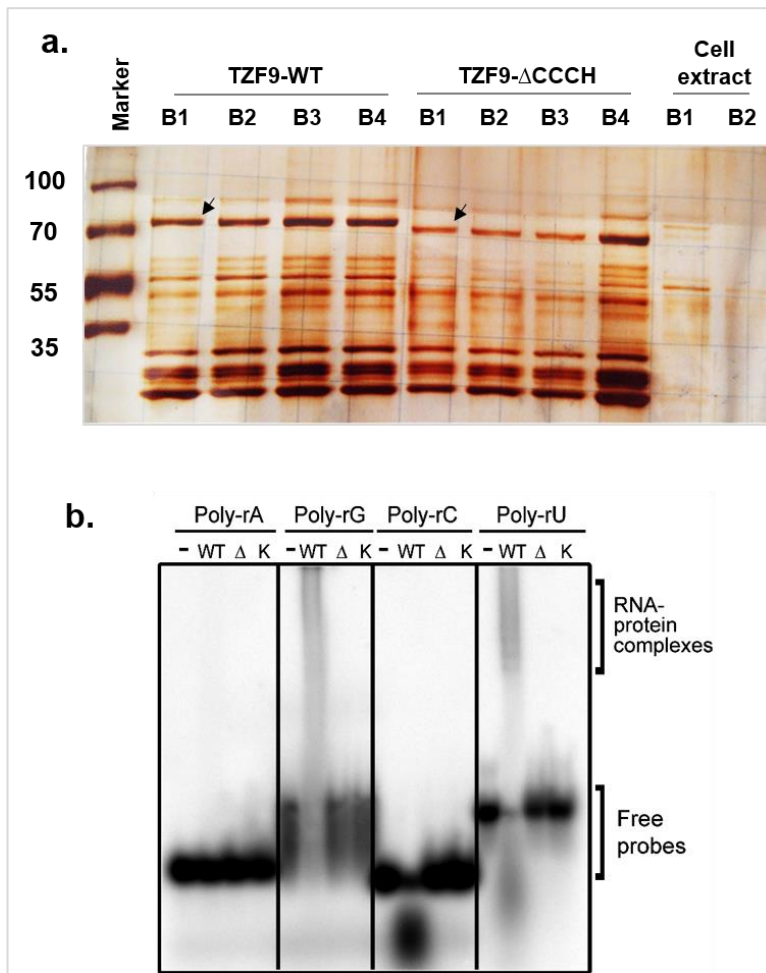


Fig. 18: TZF9 interacts with specific ribohomopolymers in EMSA assay. **(a)** Silver stain of purified proteins from *E. coli* KRX cells. Four batches (B1, B2, B3, B4) of bacterial culture expressing TZF9-MBP-His10x (referred as WT) and TZF9- Δ CCCH-MBP-His10x (abbreviated as Δ) and two batches (B1, B2) of non-transformed cells as controls (K) were used to bulk-purify the proteins. Arrows mark the expected sizes of the purified proteins. **(b)** Recombinant TZF9-WT (WT) binds poly rU and poly rG homopolymers *in-vitro*. P^{32} -labeled ribohomopolymers were incubated without (-) or with approximately 5 ng of purified proteins (WT, Δ and K) and separated on gel. The smeary signals at higher molecular weight correspond to complex(es) between wild-type (WT) TZF9-MBP-His10x and ribohomopolymers of uracil (poly rU) and guanine (poly rG). Free unbound probes are shown at the bottom of the gel.

3.3.2 TZF9 binds specifically to pentaprobe 2 among other RNA sequences

The next objective was to decipher the particular RNA sequences which are primary *in-vitro* targets of TZF9. As mentioned earlier, the RNA targets of plant TZFs are still unknown, so it was decided to test 12 RNA probes with randomized sequences called pentaprobos (PP) (Bendak et al., 2012). Since most of the nucleotide binding proteins require only 5-6 nt-motif to bind, the number of possible combination of 4 bases to test would be 4^5 or 1024. PP are designed to contain all 1024 possible combinations of 5-mer sequences. PPs were computationally created in an overlapping manner to shorten the length to 100 bp in 12 probes. These were named as PP1 to PP12. In short, PPs are 100 nt long overlapping RNA sequences that cover all possible combinations of potential protein binding 5-nt motifs (PP sequence, **Appendix Fig. A6**).

To test TZF9 binding to pentaprobos, RNA-EMSA was used as described earlier. P^{32} radiolabelled pentaprobos were incubated with (+) and without (-) TZF9 protein and run on a

native PAGE gel. The multiple signals in upper part of the gel might be due to the secondary structure of RNA which is reported earlier (Bendak et al., 2012). Comparing the two lanes (- and +) of each pentaprobe, it was observed that TZF9 shows binding to only one pentaprobe, namely pentaprobe 2. The binding was consistently observed in three independent experiments (**Fig. 19**).

Our independent RNA-EMSA experiments showed that TZF9 is indeed an RNA binding protein and it potentially binds to specific RNA sequence(s). This correlates with the hypothesis that TZF9 may target specific RNA(s) possibly in the PB to modulate plant defense responses.

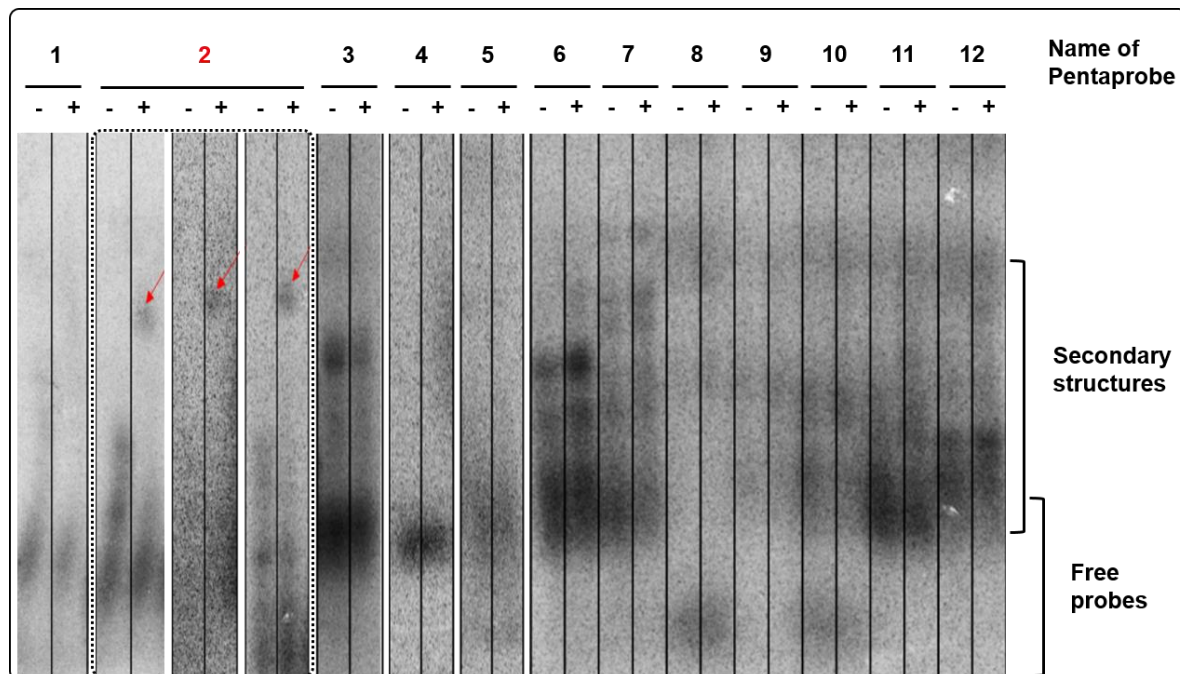


Fig. 19: Binding assay of TZF9 with pentaprobos. Autoradiograph of the 5% native PAGE gel showing RNA pentaprobos with TZF9 protein (+ lane) and without protein (- lane). Pentaprobe 2-TZF9 complex is shown by red arrows. Other probes formed secondary RNA structure smears in the upper part of the gel in the presence or absence of protein. The RNA-binding assay with Pentaprobe 2 was repeated three times with similar results. The sequence of individual pentaprobos is given in **Appendix Fig. A6**.

3.4 TZF9 interacts with a calmodulin binding protein annotated as a putative RNA ligase

After establishing the RNA binding capability of TZF9, it was sought to study the protein interactions of TZF9. Earlier, Y2H analysis revealed that TZF9 interacts with a protein annotated as a putative RNA ligase (At5g40190) (Arabidopsis Interactome Mapping 2011). This putative RNA ligase was also identified as a calmodulin (CaM)-binding protein in a protein-protein interaction screen of auxin-treated expression library with CaMs (Reddy et al., 2002). However, it has not been functionally characterized. Another study showed that this putative RNA ligase belongs to 2', 3' cyclic nucleotide phosphodiesterase superfamily (Mazumder, et

al., 2002). Based on this information, the interaction between TZF9 and putative RNA ligase was further investigated in detail.

3.4.1.1 Putative RNA ligase binds to both Apo- and Ca²⁺ calmodulin *in vitro*

Calmodulin proteins (CaM) are calcium sensor proteins and are known to play crucial role in cellular signaling. The CaM in the native form is called apo-CaM whereas upon binding to Ca²⁺, CaM is allosterically altered that may or may not change its function. In animals, the apo- or Ca²⁺-bound CaM may have the same or different substrate specificity (based on the physiological function to be executed). However, this specificity is poorly understood in plants. Since Ca²⁺ signaling is one of early PTI response, it prompted us to check whether putative RNA ligase binds to CaM in the presence and/or absence of Ca²⁺. To test this, His-tagged putative RNA ligase was expressed in *E.coli*, purified with Ni-NTA beads and eluted in native form (**Fig. 20a**). The protein extract was incubated with the CaM-agarose beads (Sigma) with buffer containing either CaCl₂ or EGTA (chelator of calcium ions). The beads were washed thoroughly, protein was eluted, run on SDS-PAGE gel and blotted against anti-His antibody. Putative RNA ligase was detected in both the cases suggesting that CaM binding to putative RNA ligase might not require calcium *in-vitro* (**Fig. 20b**).

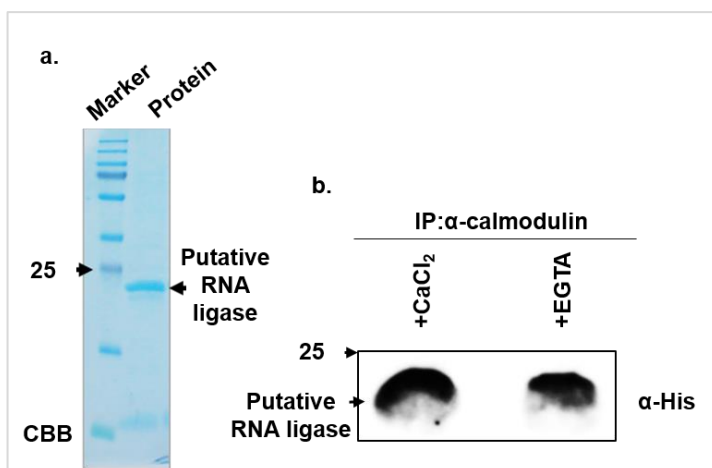


Fig. 20: Putative RNA ligase, is a calmodulin binding protein. **(a)** Coomassie staining of the SDS-PAGE gel showing recombinant expression and purification of putative RNA ligase. α -His blot showing Putative RNA ligase immunoprecipitated with calmodulin in the presence of calcium (CaCl₂) or absence of calcium (EGTA) from bacterial extract. **(b)** Putative RNA ligase detected at respective molecular weight of 20.6 kDa using anti-His antibody.

3.4.2 Validation of interaction between TZF9 and putative RNA ligase by Co-immunoprecipitation (CoIP)

A CoIP experiment was performed to validate the interaction between TZF9 and putative RNA ligase. For this, double (YFP and HA) tagged TZF9 was transiently co-expressed with HA tagged putative RNA ligase in protoplast. The proteins were allowed to express overnight and the protein extraction was performed followed by immunoprecipitation of TZF9 with GFP-trap® agarose beads (Chromotek GmbH). GFP-trap beads are very efficient to pull down all GFP

variants like YFP (binding capacity: 4µg of protein/10µl). After pull-down, as per recommended protocol, the beads-protein complex was denatured and loaded on a 10% SDS-PAGE gel, blotted against anti-HA to detect both the proteins in single detection step (**Fig. 21a** and **b**)

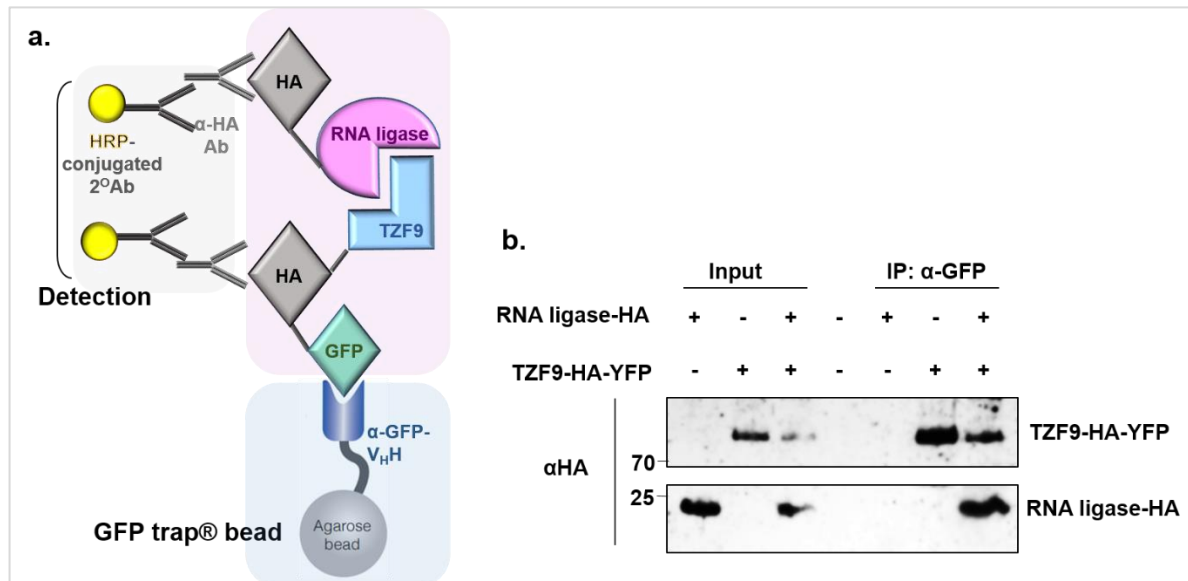


Fig. 21: TZF9 binds to putative RNA ligase *in-vitro*. **(a)** Methodology employed for single-step detection of interacting partners using CoIP assay. TZF9-HA-YFP and RNA ligase-HA were transiently expressed in protoplasts and proteins were immunoprecipitated with GFP trap beads. The interacting partner was co-immunoprecipitated and detected using anti-HA antibody. **(b)** CoIP showing interaction of TZF9 with putative RNA ligase. IP was performed using GFP trap beads and immunoblotted with anti-HA antibody.

3.4.3 Ankyrin domain of TZF9 is required for interaction with putative RNA ligase

TZF9 has some conserved domains (**Appendix Fig. A1**). As different motifs or domains of the proteins are involved in mediating protein-protein interactions, next it was sought to investigate the role of TZF9 motifs/domains in facilitating the interaction with RNA ligase. For this, full length TZF9 (TZF9-WT), CCCH-motif deleted version (TZF9 Δ CCCH), ankyrin-motif deleted version (TZF9 Δ ANK), and MAPK phosphosite-mutant version of TZF9 (TZF9-PS mut) were used for CoIP assays. TZF9 Δ CCCH protein, which was already shown being unable to bind RNA in EMSA assay (**Fig. 18b**) was used to validate whether the interaction is dependent on the RNA binding property of TZF9. Ankyrin domain is a conserved domain and is known to mediate protein-protein interactions (Li et al., 2006). TZF9-PS mut was used to validate whether the interactions are regulated by or related to MAPK phosphorylation of TZF9. These constructs were individually co-expressed with putative RNA ligase in *Arabidopsis* protoplasts. Aforementioned CoIP method and α -HA immunoblotting strategy was used to detect proteins. In this experimental set-up, putative RNA ligase protein could be pulled down in all the cases except with ANK-deleted motif version of TZF9. This data suggested that ankyrin motif of TZF9 is required for its interaction with putative RNA ligase (**Fig. 22**).

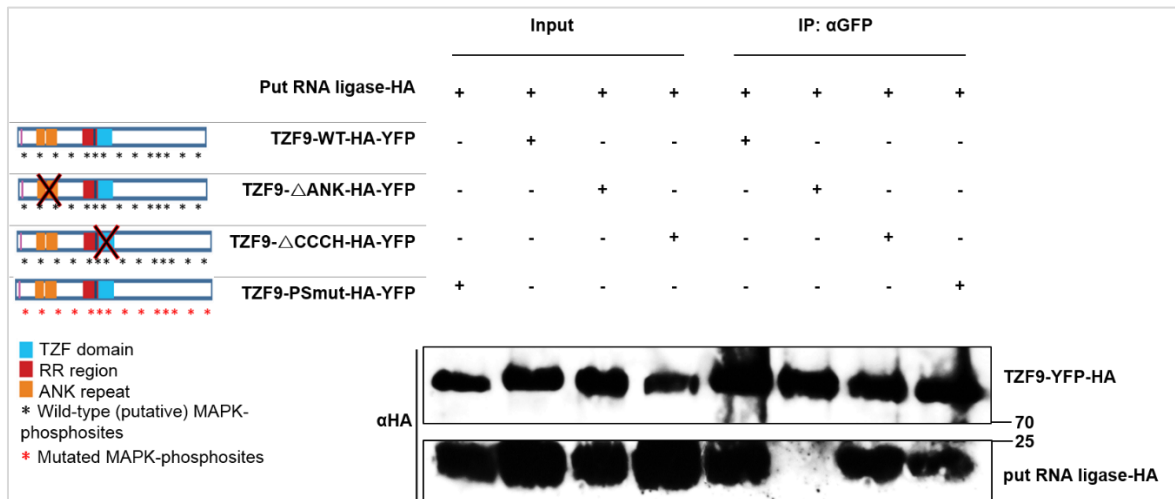


Fig. 22: Ankyrin domain is required for TZF9 and Putative RNA ligase interaction. The indicated constructs were co-expressed in protoplasts and GFP trap beads were used to pull down TZF9 variants. α-HA blot was used to detect putative RNA ligase before (Input) and after IP (lower panel). In the upper panel, TZF9 variants were detected using α-HA blot before and after IP.

3.4.4 TZF9 interacts with putative RNA ligase predominantly in cell cytoplasm

The next objective was to check the site of the interaction between TZF9 and putative RNA ligase. This was performed by using a BiFC assay where putative RNA ligase and TZF9 were fused to N-terminal (pE-SPYNE) and C-terminal (pUC-SPYCE) of YFP respectively and expressed overnight in protoplast. The protoplasts were observed with LSM710 confocal microscope (Zeiss) using appropriate filters. It was observed that the interaction mainly takes place in cytoplasm and further confirms their interaction (**Fig. 23**).

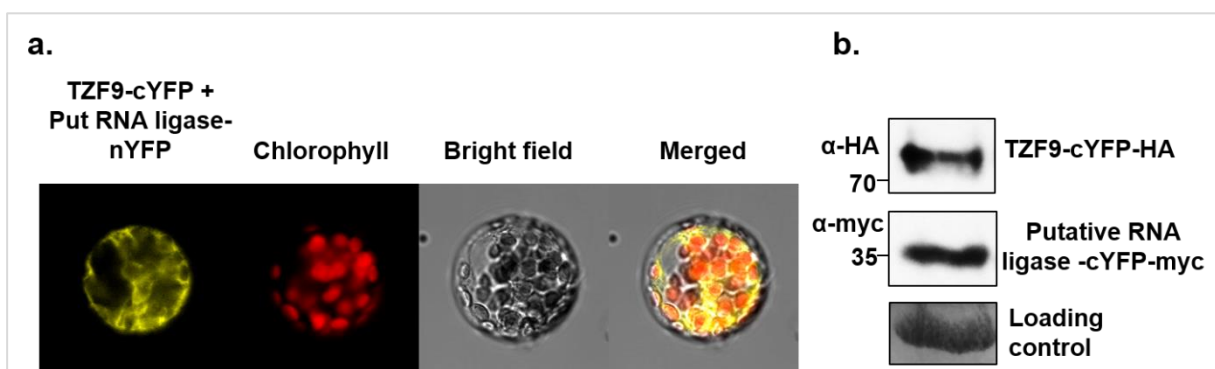


Fig. 23: BiFC assay showing localization of the interaction between TZF9 and putative RNA ligase. **(a)** TZF9-cYFP and Putative RNA ligase-nYFP were expressed in protoplasts and the fluorescent signals were observed with confocal microscope. Reconstituted YFP signal was observed using YFP channel of the microscope. Chlorophyll autofluorescence is shown in red, protoplast (under bright field) and merged images are also shown (scale bar=5μM). **(b)** α-HA and α-myc blots shows expression of both the proteins in protoplasts.

3.4.5 Putative RNA ligase is localized in cytoplasm

For localization study, RFP-fused putative RNA ligase was co-expressed with the PB marker protein, XRN4, in the protoplast and observed under LSM710 confocal microscope (Zeiss) after overnight expression under *UbQ10* promoter. Putative RNA ligase was mostly observed to be localized in the cytoplasm (**Fig. 24**). Interestingly no PB localization of putative RNA ligase was observed, however the cytoplasmic localization is in agreement with the observations in **Fig. 23**. These data show that putative RNA ligase is mainly a cytoplasmic protein.

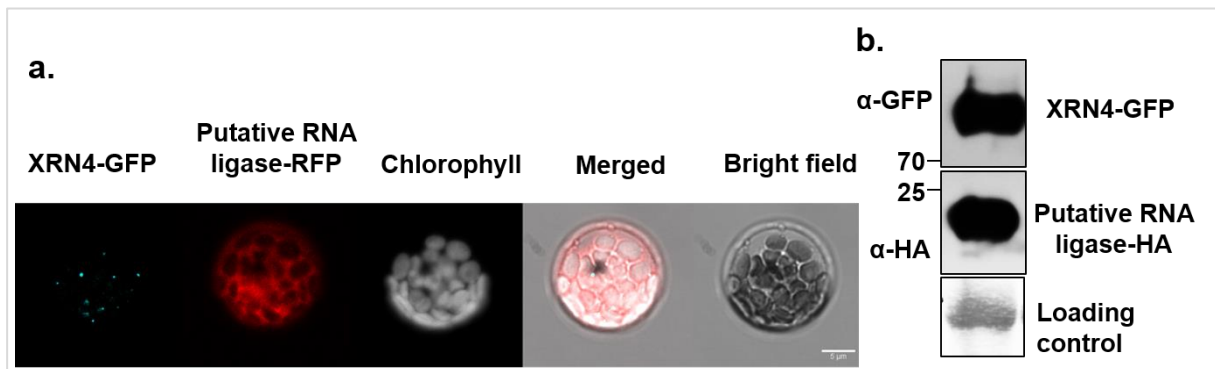


Fig. 24: Localization of putative RNA ligase. **(a)** Images taken with confocal microscope showing RFP-tagged putative RNA ligase using RFP channel (red) and GFP-tagged PB marker XRN4, observed in GFP channel (cyan). Chlorophyll autofluorescence (white), merged and bright field images are also shown (Scale Bar=5μM). **(b)** Protein expression is shown by respective western blots.

3.5 TZF9 and plant immunity

3.5.1 Attenuated defense response in *tzf9* knockout line: ROS assay

To study the possible role of TZF9 in plant immunity, a reverse genetics approach was pursued. A knock out *tzf9* T-DNA insertion mutant was characterized by performing multiple assays (Maldonado-Bonilla et al., 2014). One of the hallmarks of early defense response in plants is the production of reactive oxygen species (ROS), also known as an oxidative burst. Typically, in *Arabidopsis* plants oxidative burst attains a peak around 15 min post flg22 elicitation. Luminol-based detection of ROS (Fig. 25a) was used to measure ROS. ROS oxidizes luminol and the emitted light is measured in relative luminescence units (RLUs) via a luminometer (Luminoskan™, ThermoFisher). For the assay, three different genotypes, wild type (Col-0), knockout line (*tzf9*) and a complemented line (*tzf9-gTZF9*) were used. *tzf9-gTZF9* line was generated by complementing *tzf9* mutant with a genomic fragment (~4230 bp) of the wild-type *TZF9* gene. The leaf-discs (diameter=5mm) from the three aforementioned plants were treated with 50 nM flg22 and RLU was measured. The *tzf9* mutant showed significantly lower accumulation of ROS than Col-0 (Fig. 25b). However, an intermediate accumulation of ROS was observed in the complemented line. It is possible that only a partial complementation of the gene was achieved in the *tzf9-gTZF9* line.

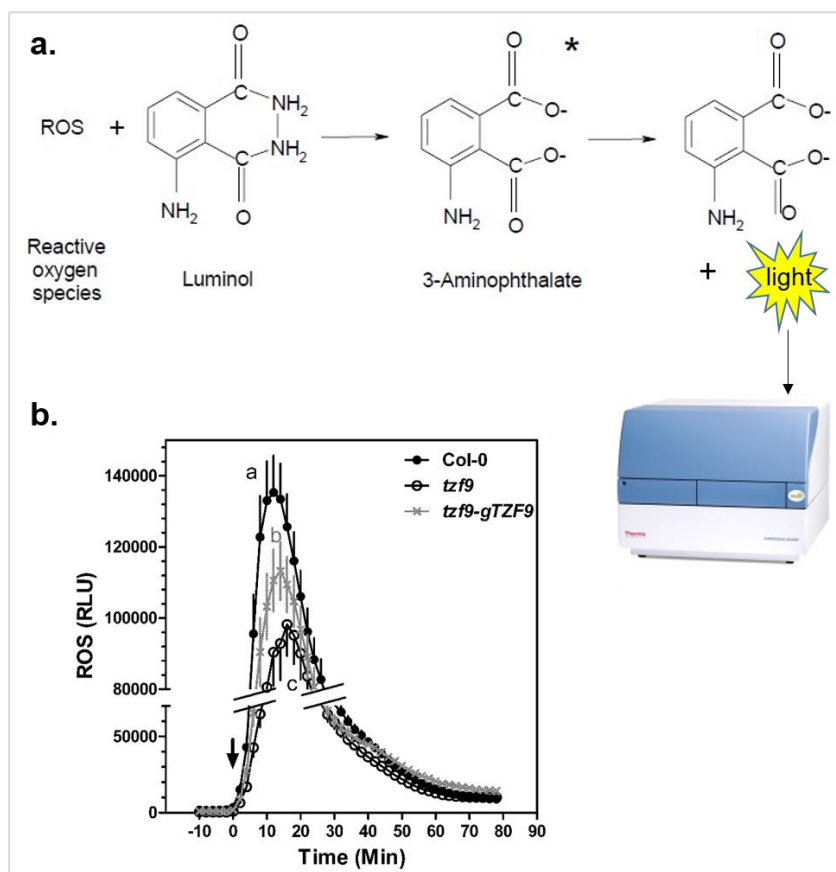


Fig. 25: Flg22-induced ROS accumulation is attenuated in *tzf9*. **(a)** Principle behind luminol based ROS detection in *Arabidopsis* leaf discs. **(b)** Detection of ROS in leaf-discs from Col-0, *tzf9* and the complemented line (*tzf9-gTZF9*). The basal ROS levels were first measured for 10 min before addition of 50 nM flg22 (marked with an arrow). The data is presented as mean $RLU \pm SE$ ($n=32$ leaf discs). Statistics significance was assessed with two-way ANOVA (with a statistically distinct group marked with different letters, a, b and c).

3.5.2 Omics studies to characterize TZF9

3.5.2.1 Transcriptome: Profiling of Total mRNA

The role of TZF9 in regulating the early plant defense responses has been demonstrated, however the molecular mechanism of this regulation is not known. So, a comparative global gene expression analysis between wild-type (wt) Col-0 plants and *tzf9* was performed. For this, hybridization-based microarray was used to study the expression profile in Col-0 and *tzf9* plants before and after PAMP elicitation. To compare flg22-mediated response in early transcriptional reprogramming in both the genotypes, leaves were infiltrated with 1 μ M flg22 and harvested after 1 hour. As a control, non-infiltrated leaves were used (**Fig. 26**).

After harvesting the samples, total RNA was extracted and cDNA was synthesized. cDNA was labelled and the hybridization was performed on commercially available chip (Affymetrix1.1 ST exon array). The chip compatible GeneAtlas® system (instrument and software) was kindly provided in-house within the department of Prof. Tissier. Exported microarray readout was processed by our collaboration partner, Dr. Benedikt Athmer (SZB, IPB). Briefly, hybridization data were pre-processed by the R package XPS. Raw data were normalized by Robust Multi-Array Average Expression Measure (RMA), which include probe-set summarization and quantile normalization. The dataset was filtered for unexpressed features by detection above background calls (DABG). Genes were retained if all signals of at least one replicate group were detected in either of the two genotypes. The hybridization signal was detected for 12351 genes out of 24000 genes on the chip. Linear models were fitted for each feature using LIMMA (Ritchie et al., 2015) and p-values were adjusted by the false discovery rate procedure proposed by Benjamini-Hochberg (Benjamini and Hochberg, 1995)

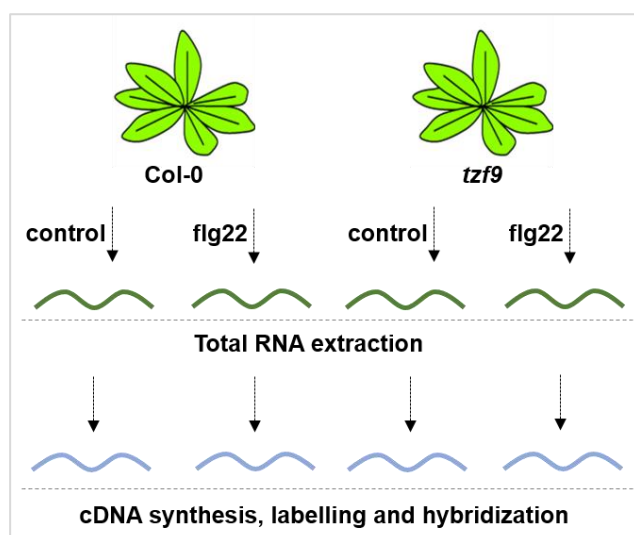


Fig. 26: A schematic workflow of transcriptomic experiment. Leaves of Col-0 and *tzf9* mutant were infiltrated with flg22 and harvested after 1 hour. Total RNA was extracted from pulverized material, cDNA was synthesized, labelled and hybridization was performed on the Affymetrix chip. Triplicate samples were used in the experiment.

3.5.2.1.1 Validation of genes identified in microarray

Before the in-depth analysis of microarray data, it was important to validate the microarray data with quantitative real time PCR (qRT-PCR). For this, a new batch of Col-0 and *tzf9* plants were grown in the same condition, treated with flg22 and harvested after 1 hour. Total mRNA were extracted and cDNA were prepared for qRT-PCR. The expression levels of six selected genes *BIK1* (AT2G39660), *IOS1* (AT1G51800), *PBS1* (AT5G13160), *FRK1* (AT2G19190), *WRKY22* (AT4G01250), and *Chitinase* (AT2G43620) were monitored. These include RLCKs, transcription factor and are involved in defense signaling (Yeh et al., 2016, Asai et al., 2002, Mohr et al., 2006, Kloth et al., 2015, Sun et al., 2017). The transcript levels normalized to the reference gene *PP2A* (AT1G69960) is shown in **Fig. 27a**. A heat map based on the expression level of these genes in microarray (log fold values) is shown for reference in **Fig. 27b**. Overall, a good correlation was observed between the two datasets (microarray and qRT-PCR) suggesting reliable microarray data. Expression of RLCKs like, *BIK1*, *IOS1*, were induced by flg22 in Col-0 and *tzf9* but relative level of expression were significantly different in *tzf9* whereas expression of another RLCK, *PBS1* was not induced by flg22 (as shown in microarray and qRT-PCR). Interestingly, defence related gene *FRK1* was induced by flg22 in Col-0 but not in *tzf9*. Other defense related genes *Chitinase* and *WRKY22* were significantly upregulated in both Col-0 and *tzf9* upon flg22-treatment. The relative expression of *Chitinase* in Col-0 was higher than in *tzf9* as shown by qRT-PCR. These data suggested *TZF9* might regulate the expression some of the genes which were involved in early defense signaling as well as some of the other defense related genes.

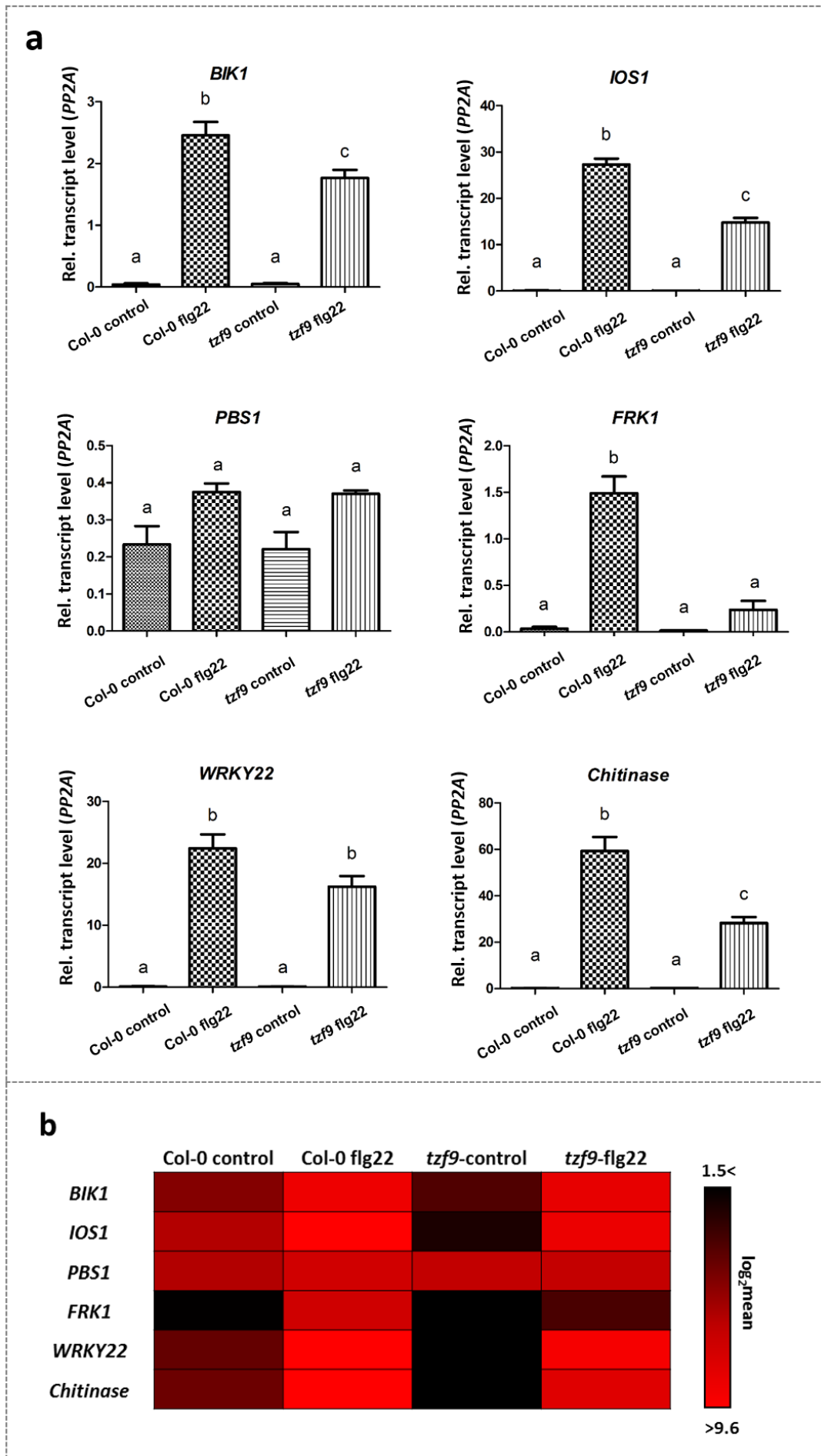


Fig. 27: Validation of differentially expressed genes identified in microarray. **(a)** Quantitative real time PCR of six selected genes: *BIK1* (AT2G39660), *IOS1* (AT1G51800), *PBS1* (AT5G13160), *FRK1* (AT2G19190), *WRKY22* (AT4G01250), and *Chitinase* (AT2G43620). The data represents an average of triplicates and the error bar indicate the standard error of mean. Statistical significance was analysed by one way ANOVA with Bonferroni's Multiple Comparison Test (P value<0.05). **(b)** The expression levels of the above selected genes in the microarray are shown as a heat map.

3.5.2.1.2 Analysis of transcriptome

Having known that the microarray data is reliable, analysis of transcriptome data was done. Overall, the aim was to analyse differentially expressed genes (DEGs) as three representative sets, set A, B and C. Set A represents DEG (flg22 up- or down- regulated genes) in wild type (wt_flg22 vs. wt_ctrl), set B represents DEG in *tzf9* (*tzf9*_flg22 vs. *tzf9*_ctrl) and set C represents DEG in two genotypes without flg22 treatment (*tzf9*_ctrl vs. wt_ctrl). DEGs were identified using a significance threshold of 0.05 and a log₂ fold-change of ± 1 . The analysed data from the already mentioned 3 sets is shown as a Venn diagram where the number of upregulated genes are depicted in red text and the downregulated genes in green text (**Fig. 28**). Among the 2103 downregulated genes, 792 (756+36) genes were commonly downregulated upon flg22 treatment in wt and *tzf9* mutant. 632 (581+51) and 610 (607+3) unique genes were downregulated in wt and *tzf9*, respectively, upon flg22 elicitation. Out of 2685 upregulated genes, 1161 (1102+59) genes were commonly upregulated in wt and *tzf9* upon flg22 elicitation. 1173 (1122+51) and 127 (123+4) unique genes were upregulated in wt and *tzf9* respectively. Interestingly, the number of flg22 responsive unique genes which are upregulated in wt was 1173 (1122+51). This is about 45.5% genes of all the flg22 inducible genes {1122/ (1122+1102+130+51+59+4)}. In contrast, in the *tzf9* mutant this is about 5.2%. In other words, about 45.5% of flg22-inducible genes (in wt) require TZF9 to be upregulated. As already described that TZF9 is involved in early PAMP signaling, for example, ROS production or MAPK activation, it was interesting to investigate the function of DEGs in the non-elicited state (set C, *tzf9*-ctrl vs. wt-ctrl).

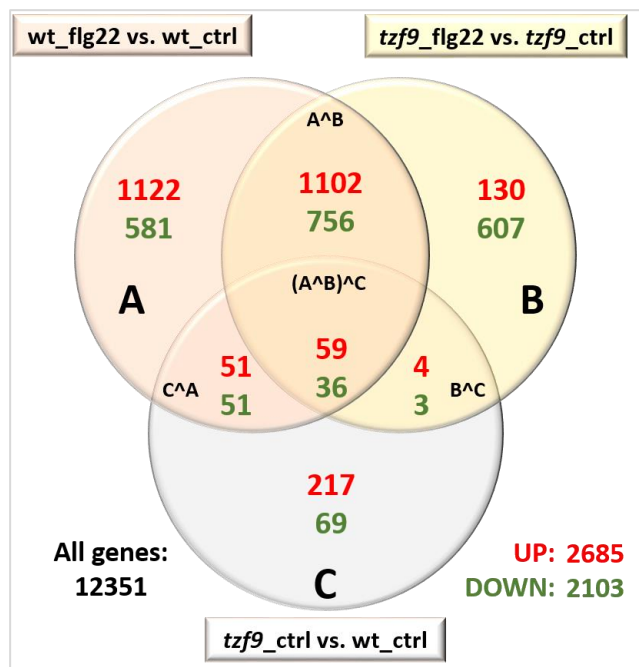


Fig. 28: Venn diagram showing number of differentially expressed genes (DEGs) in total mRNA pool in the indicated genotypes and treatments. DEGs upon flg22 in wt (set A) is given on the left side. DEGs upon flg22 in *tzf9* (set B) is given on the right side and DEGs in *tzf9* /wt (set C) is given at the bottom. The red colour indicates the upregulated while green shows the downregulated genes. The full gene-list attached as a soft copy in Appendix II.

3.5.2.1.3 Enrichment of stress/stimuli responsive genes in the *tzf9* mutant

To analyse the up- and downregulated genes in set C (*tzf9*_ctrl vs. wt_ctrl, **Fig. 27**), gene ontology enrichment (biological function) analysis was performed with AgriGO-analytical tool (bioinfo.cau.edu.cn/agriGO/). This analysis compared input list against background or whole genome as a reference list (from TAIR10). The processed data is exported as table indicating percentage of genes with respective p-values. A bar-plot (**Fig. 29a** and **b**) shows the percentage of genes (in x-axis) which is plotted against selected GO annotation or pathway (y-axis, left side). A significant population of up as well as downregulated genes in *tzf9* were categorized under stress/stimuli responsive genes. An extended table with significant p-value is shown in **Appendix Table A6, A7**. The full table is attached as a soft copy in **Appendix II**.

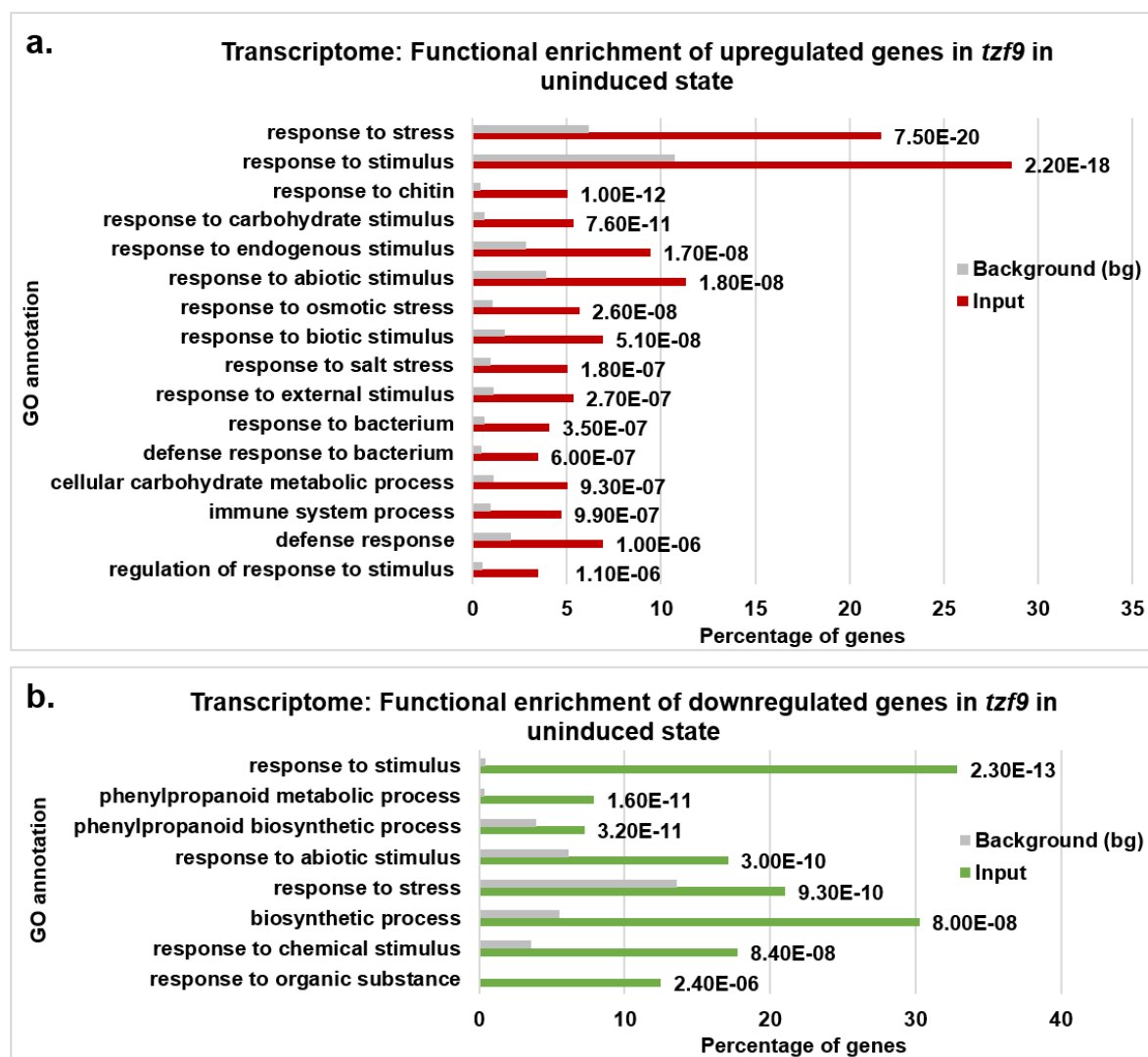


Fig.29: Differentially regulated genes in *tzf9* in uninduced state are enriched under stress/stimuli responsive. **(a)** Categorization of upregulated genes is shown in red bars against background (gray bar). **(b)** Categorization of downregulated genes is shown in green bar against background (gray bar). P-values for respective annotations are given in the right side of the bar. Analysis was performed using AgriGO analysis tool (bioinfo.cau.edu.cn/agriGO/).

Some representatives of stress/stimuli responsive genes are given in the following **Appendix Table A6.1** (upregulated genes) and **Appendix Table A7.1** (downregulated genes). These differentially expressed genes in *tzf9* are not functionally specific but diverse which included WKRY transcription factors, components of protein degradation machineries, kinases, RNA binding proteins. Some of them are known to play important roles during cellular signaling and hence their deregulation in *tzf9* might potentially explain the overall defense-related phenotype.

3.5.2.2 Translatome: profiling of ribosome-associated mRNA

As transcriptome does not always correlate with the actual translation process, it was interesting to get a profile of mRNAs which are undergoing translation (or translatome). The method employed for translatome analysis is outlined in **Fig. 30**. For this, ribosome associated

mRNAs (actively translating mRNAs) were isolated by immunopurification of ribosomes from transgenic *Arabidopsis* lines expressing FLAG-tagged ribosomal protein L-18 (RPL18) under the control of a *CaMV 35S* promoter (Mustroph et al., 2009). This *p35S::RPL18* transgenic line was crossed with the *tzf9* knockout line and homozygous lines were selected in the F2 generation. For microarray study, the *p35S::RPL18* and *p35S::RPL18/tzf9* lines were treated with flg22 and harvested after 1 hour. In an RNase free environment, polysomes from leaves were extracted in polysome extraction buffer (PEB). Ribosomes (or polysomes) were immunoprecipitated with anti-FLAG beads. RNA was extracted from immunoprecipitated ribosomes, purified and RNA quality was checked in Qiaxcel machine (Qiagen).

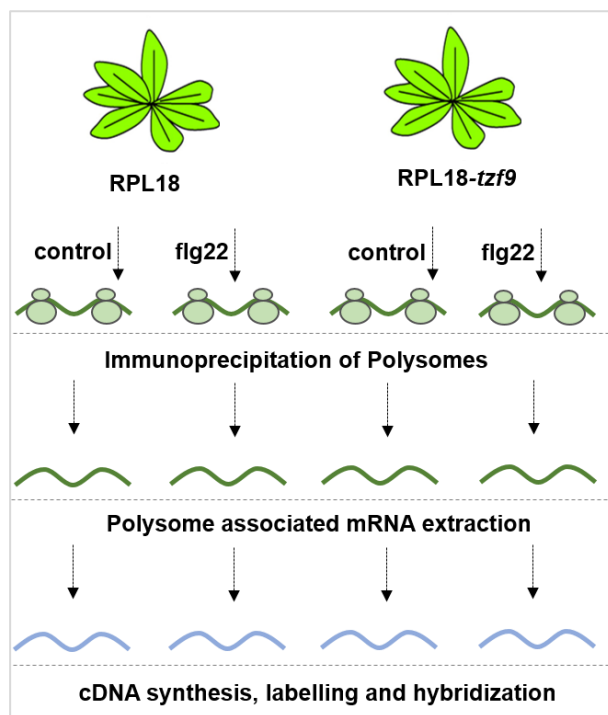


Fig. 30: A schematic workflow of translome profiling of TZF9. Leaves of *p35S::RPL18* and *p35S::RPL18/tzf9* lines were infiltrated with flg22 and harvested after 1 hour. Non infiltrated leaves served as uninduced control. Polysomes were extracted and immunoprecipitated with anti-FLAG M2 agarose resins (Sigma). RNA associated with polysomes was extracted in all four indicated conditions. After cDNA synthesis and labelling, hybridization was performed on the chip (Affymetrix1.1 ST exon array). Triplicate samples were used in the experiment.

As shown in **Fig. 31a**, this RNA did not contain ribosomal RNA from chloroplast or mitochondria unlike total RNA on gel. 150 ng of RNA was used to synthesize cDNAs and microarray was performed and data was analysed using the previously described criterion for transcriptome analysis, DEGs were represented in a Venn diagram (**Fig. 31b**). As indicated in set C, the number of up- and downregulated genes in *tzf9* as compared to Col-0 in the uninduced state were 592 (348+108+136) and 354 (125+207+22), respectively. An enrichment of stress and stimuli responsiveness genes was observed for genes upregulated in the *tzf9* background (**Appendix Table A8, A9**). Flg22 induced and suppressed genes in Col-0 were 1990 (322+1424+136+108) and 1567 (421+917+22+207), respectively, whereas flg22 induced and suppressed genes in *tzf9* were 2107 (1424+547+136) and 2302 (1363+917+22), respectively. The full gene-list attached as a soft copy in **Appendix II**.

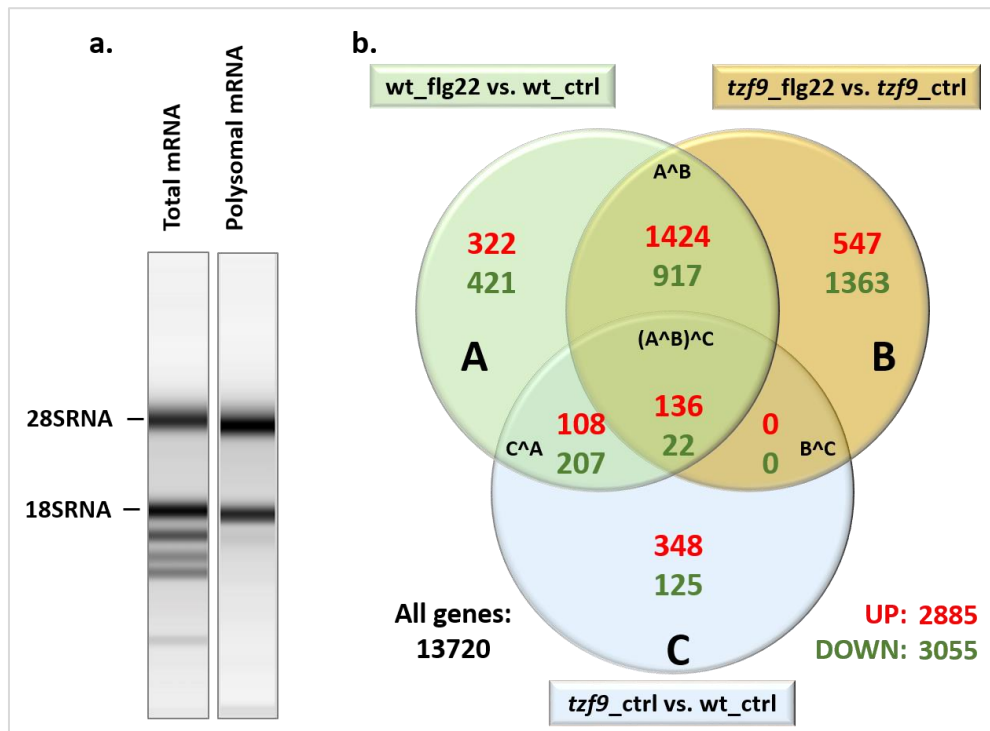


Fig. 31: (a) Visualization of ribosomal bands from total RNA samples and ribosome-associated RNA samples. Ribosome associated RNA was extracted from immunoprecipitated polysomes by pulling down RPL18 protein of polysomes. **(b)** Venn diagram of DEGs in polysomal RNA in wt and *tzf9*. DEGs upon flg22 in wt (set A) is given in the left side. DEGs upon flg22 in *tzf9* (set B) is given in the right side and DEGs in *tzf9*/wt (set C) is given in the bottom. The red fonts indicate the upregulated while green shows the downregulated genes.

3.5.2.2.1 Analysis of polysome associated mRNA population in *tzf9* and wt plants shows enrichment of stress/stimuli responsive genes in the *tzf9* mutant under uninduced condition.

After showing the GO enrichment of DEGs in *tzf9* transcriptome in uninduced state in **Fig. 29**, the next GO enrichment analysis was performed for polysome associated mRNA and DEGs in set C were analysed (*tzf9*_ctrl vs. wt_ctrl). Again, this analysis was performed using AgriGO analytical tool. Upregulated genes were significantly enriched in stimuli/stress category (**Fig. 32a, Table A8.1**). While downregulated genes were also enriched in stress/stimuli responsive genes, the most significant enrichment were for other processes such as translation or ribonucleoprotein complex biogenesis (**Fig. 32b, Table A9.1**). These analyses reflect that while TZF9 might be involved in stress-related processes, it might also function in translational or post-transcriptional related process.

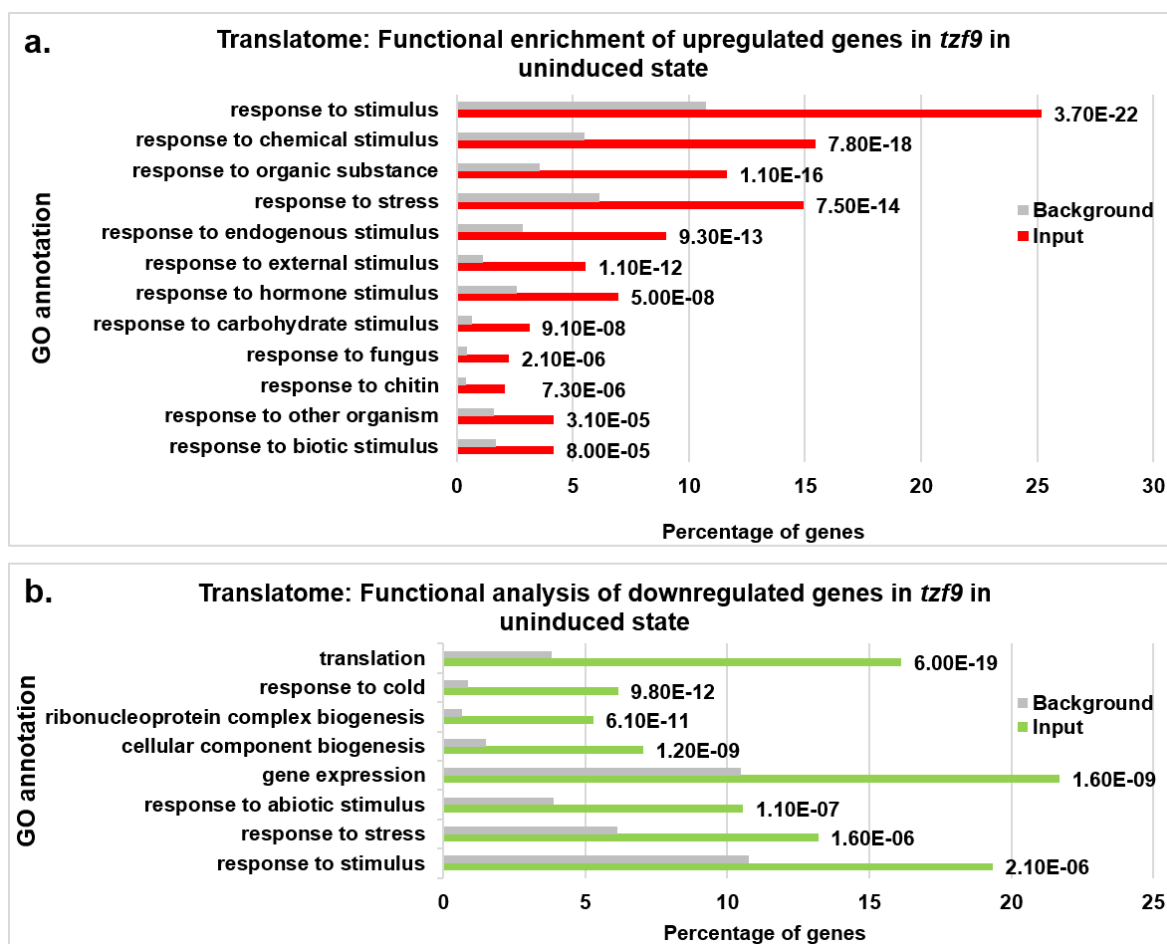


Fig. 32: Translatome analysis of differentially regulated genes in *tzf9* in uninduced state. **(a)** Enrichment of upregulated genes under stress/stimuli responsive category shown in red bar against background (gray bar). **(b)** Enrichment of downregulated genes are under stress/stimuli responsive and translational category (green bar) against background (gray bar). P value for respective annotations are given in the right side of the bar. Analysis was performed using AgriGO tool box (bioinfo.cau.edu.cn/agriGO/) and the full table is attached as a soft copy in **Appendix II**.

3.5.2.3 Description of DEGs from transcriptome and translatome data

From the data, it was obvious that *tzf9* mutant showed enrichment of stress/stimuli responsive genes in uninduced state, both in total mRNA and polysomal mRNA fractions (**Fig. 29** and **32**), so it was interesting to compare DEGs from transcriptome and translatome data. The DEGs in the three sets (**Fig. a, b and c**) are depicted as heat maps (**Fig. a', b' c'**). The total cumulative number of DEGs in *tzf9* as compared to Col-0 in uninduced state was 1356. Upon flg22, the cumulative number of DEGs in the wt and *tzf9* were 5132 and 5142, respectively. It is interesting to note that in all the three comparisons, the DEGs showed marked differences in transcriptome and translatome profiles (**Fig 33**).

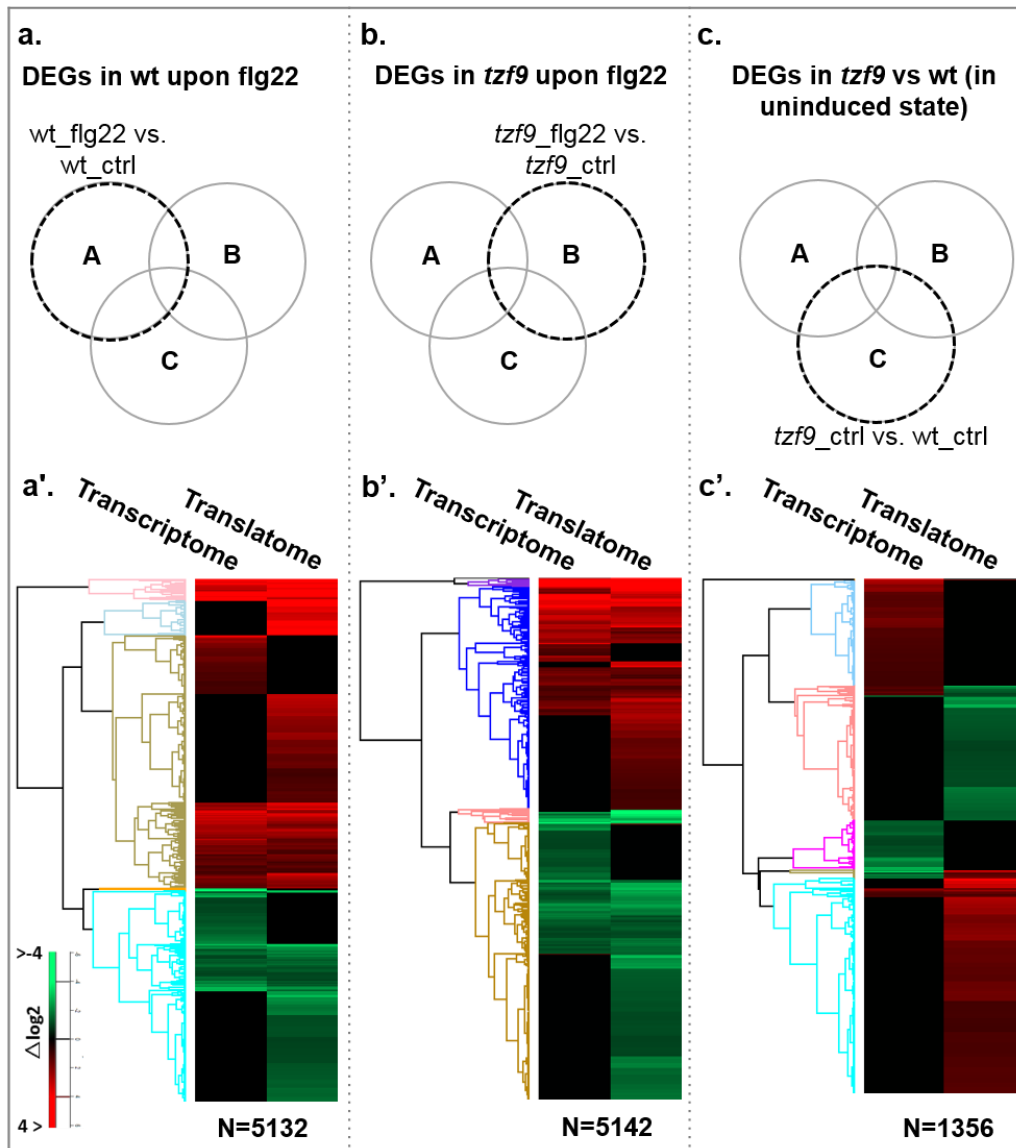


Fig. 33: Distinction between transcriptome and translome profiles in wt and *tzf9* before and after PAMP elicitation. Heat map showing DEGs in (a') wt upon flg22, (b') *tzf9* upon flg22 and (c') between the two genotypes in uninduced state. Corresponding set (as represented in Fig. 28 and 31b) is shown in Venn diagrams. Heat map was generated using the program Perseus (Tyanova et al., 2016). Relative changes of mRNAs were depicted as log₂ ratios after performing microarray analysis of total RNA. All mRNAs with significant induction (log₂ ratio ≥ 1 and p-value, 0.05) were applied to clustering using Perseus. Clustering was based on k-means method according to Euclidean distance. Columns represent transcriptome/translatome and rows represent individual genes.

The heat maps shown above are obviously very complex given the partial uncoupling between total cellular transcript levels and the profiles of translated mRNAs. To facilitate interpretation of these results, selected subsets of genes are schematically color-coded (Fig. 34a) as follows: Many genes are differentially expressed in the transcriptome but not in the translome, these genes are classified as changes only in the transcriptome and highlighted in blue (●) beside the heat map. On the other hand, DEGs in the translome but not in the transcriptome are classified as “translatome only” changes and highlighted in yellow (●). In addition to these, there are many genes showing upregulation in transcriptome but are downregulated in the

translatome (or vice-versa) profiles and are categorized as “antidirectional changes” (shown in red ●). Also, genes that are upregulated (or vice-versa, downregulated) in both transcriptome and translatome are categorized as “homodirectional changes” (marked in green, ●).

In concordance with the variation of the transcriptome and translatome data sets, the DEGs were represented as “coupling” and “uncoupling” between transcription and “translationability” of the mRNAs (Fig. 34b). The homodirectional DEGs are coupled (●) while the uncoupled DEGs could of three types, antidirectional (●), transcriptome only (●), and translatome only (●) changes. These analyses were performed in the three aforementioned sets, *wt_flg22* vs *wt_ctrl*, *tzf9_flg22* vs *tzf9_ctrl* and *tzf9_ctrl* vs *wt_ctrl*.

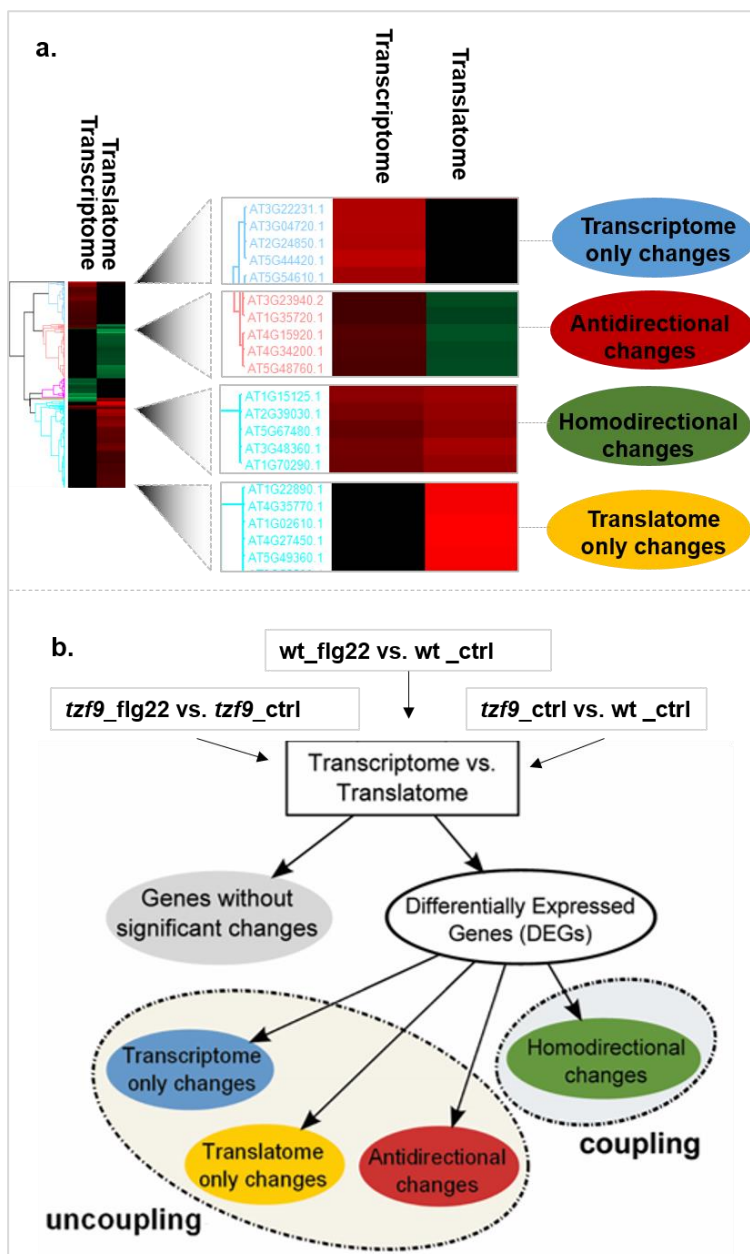


Fig. 34: Variation in transcriptome and translatome data. **(a)** Schematic view of subsets of up- and down-regulated genes in transcriptome and translatome in *tzf9* vs *wt* (under untreated control condition) showing four types of variable changes. **(b)** Flow chart of differential expression analysis between transcription and translatome after *flg22* treatment in *wt* and *tzf9* mutant, also between the genotypes in control condition and representation of coupling and uncoupling of DEGs (Tebaldi et al., 2012).

3.5.2.4 Analysis of DEGs shows high degree of uncoupling between transcriptome vs. translome profiles

After compiling the transcriptomic and translome data in the heat map, DEGs from the above categorized coupling and uncoupling data sets were presented as a Venn diagram using an online tool (<http://bioinfogp.cnb.csic.es/tools/venny/index.html>). As shown in **Fig. 36 -a, -b** and **-c**, Venn diagram of the DEGs was plotted using the following four criteria:

Upregulated in transcriptome (cyan eclipse, ○),

Downregulated in transcriptome (○),

Upregulated in translome (○),

Downregulated in translome (○)

Among the total of 5132 DEGs upon flg22 elicitation in wt leaves (**Fig. 35a**, the number of differentially regulated genes in the “transcriptome only” or “translome only” categories were 1566 (822+744) and 1374 (487+887), respectively. The number of genes regulated in an antidiagonal way were 4 (2+2), whereas the number of genes regulated in homodirectional manner were 2188 (1510+678).

Using the same criteria, DEGs were shown in *tzf9* mutant leaves in a separate Venn diagram using the same colour code (**Fig. 35b**). Out of 5142 DEGs, the number of differentially regulated genes in the transcriptome and translome only category were 734 (179+555) and 2445 (985+1460), respectively. The number of genes regulated in an antidiagonal way were 7 (6+1), whereas that of homodirectional genes were 1956 (1115+841).

A third Venn diagram (**Fig. 35c**) shows the DEGs in *tzf9* mutant vs. wild-type under untreated/control conditions where the number of DEGs were 1356. In this set, the number of differentially regulated genes in the transcriptome and translome only category were 410 (279+131) and 866 (543+323), respectively. The number of genes regulated in an antidiagonal way were 49 (23+26), whereas the number of genes regulated in homodirectional manner were 31 (26+5). For a better understanding of the overall data, the categories of DEGs in each dataset were represented as percent bar plots (**Fig. 35 a'-c'**, which retains the same colour codes used in **Fig. 35 a-c**).

As shown in **Fig. 35c'**, DEGs in *tzf9* vs wt in untreated state showed 30% genes {410/1356} to be significantly changed in transcriptome only and 64% genes {866/1356} to be significantly changed in translome only. Interestingly, the antidiagonal genes constitute 4% but there were only 2% of the genes showing homodirectional (coupled) change. In other words, the overall uncoupled genes in this set were 98%. Upon flg22 treatment, homodirectional expression tended to higher percentages (43% in wild-type and 38% in *tzf9*). This is expected together with the antidiagonal expression of DEGs lowered to ~0% in both the cases. The distribution of uncoupled DEGs in wt and *tzf9* after flg22 treatment is of particular interest. For

example, DEGs which are significantly changed post flg22 treatment specifically in translome were 27% and 31% in wt and *tzf9*, respectively. Besides, transcriptome specific DEGs were 31% and 14% in wt and *tzf9*. This hints that flg22 induced gene regulation in wt and *tzf9* is different at transcriptional and translational levels. In other words, TZF9 might regulate the mRNA pool upon flg22 elicitation at post-transcriptional level.

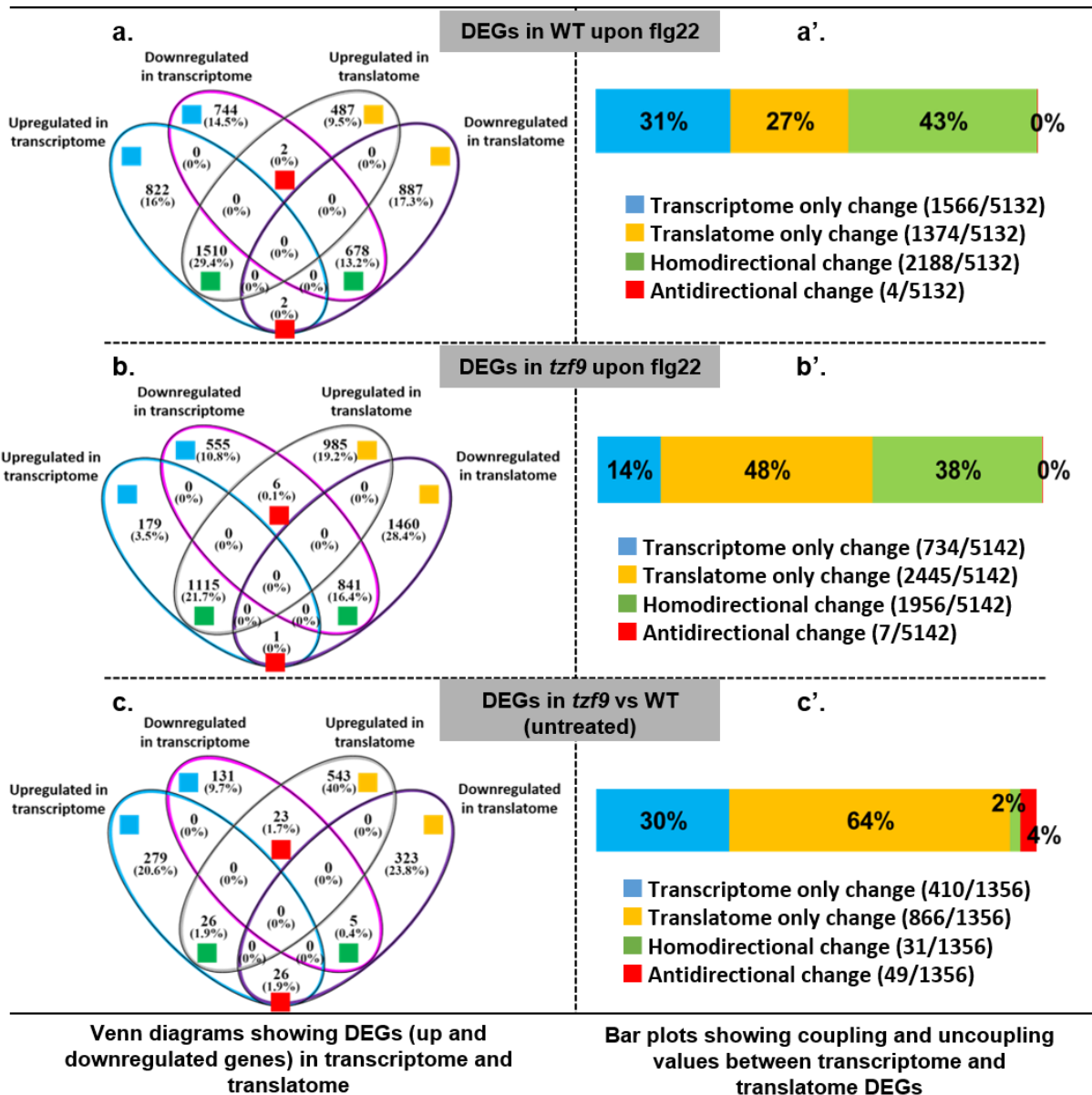


Fig. 35: Venn diagrams showing the number of coupling and uncoupling of DEGs between transcriptome and translome in (a) wt after flg22, (b) *tzf9* after flg22 and (c) *tzf9* as compared to wt in control condition. (a', b', c') The coupling and uncoupling percentages of the DEGs in transcriptome and translome in the given three sets is shown as bar charts.

4 Discussion

4.1 TZF9 is a MAPK substrate

Post-translational modifications increase the functional diversity in the proteome. The post-translational modification undertaken by MAPK pathways is phosphorylation. Four *Arabidopsis* MAPKs, MPK3, -4, -6, -11 are known to be involved in PAMP-triggered immunity by phosphorylating various downstream substrates upon elicitation (Meng and Zhang 2013).

TZF9 was identified and validated as an MPK3 and MPK6 substrate (Feilner et al., 2005; Maldonado-Bonilla et al., 2014). It is shown in this study that TZF9 is phosphorylated by MAPKs upon flg22 elicitation (**Fig. 12** and **Fig. 13**). Also, *in-vivo* phosphorylation of TZF9 correlates with increased degradation (**Fig. 15**), which might be important in the context of protein-turnover. Some of the PTI-responsive MAPK substrates that positively regulate immunity are stabilized after MAPK phosphorylation (Li et al., 2012). However, there are also reports where MAPK phosphorylation leads to the degradation of substrates which positively regulate immunity. For example, WRKY46, an MPK3 substrate and a positive regulator of immunity, degrades faster than phosphonull mutant protein (Sheikh et al., 2016). Another example is MVQ1, an MPK6 substrate, which negatively regulates immunity. Phosphomutated MVQ1 was shown to be more stable than the wild-type protein (Pecher et al., 2014). A closely related CCCH-TZF, TZF7, is also known to be phosphorylated by MPK3/6 (Feilner et al., 2005; Lassowskat et al., 2014); however, the effect of phosphorylation is not clear. Another closely related TZF, TZF10 was reported to be *in-vitro* phosphorylated by a calcium-dependent protein kinase (CPK3) (Kanchiswamy et al., 2010), although CPK3 is not yet known to be activated by flg22 (Boudsocq et al., 2010). This raised the possibility that TZF9 could be phosphorylated by other flg22-responsive kinases. However, when *MKK5^{DD}* was co-expressed with TZF9, the observed phosphoshift was comparable to that caused by flg22 elicitation. (**Fig. 13**). Based on these indications, it is more likely that TZF9 is phosphorylated via MKK5-MPK3/6 module after flg22 elicitation. However, it is not completely excluded that there may be other PTI-inducible kinases that can potentially phosphorylate TZF9.

Interestingly, phosphorylated TZF9 eventually reverted back to a dephosphorylated state 150 min post flg22 elicitation (**Fig. 15**), presumably through phosphatases that are activated in the course of flg22 treatment. This indicates that phosphorylation needs to be tightly controlled *in-vivo*. It could also mean that the function of TZF9 requires phosphorylation at a definite site at particular time points.

Overall, the current study successfully shows that TZF9 is a substrate of PTI-induced MAPK3/6 and phosphorylation of TZF9 alters its stability (**Fig. 15**). Nevertheless, phosphorylation at different phospho-sites might affect the protein differently and therefore, it will be important to identify the MAPK-targeted sites within TZF9.

4.2 Phosphosite mapping of TZF9: Challenges and prospects

TZF9 contains 14 putative MAPK phosphorylation sites and identifying the MAPK-targeted sites proved to be challenging in this study since not all sites are covered by mass spectrometry. Two alternative methods are ongoing in our laboratory but require further optimization and repetition.

First, an *in-vitro* method involving spot-synthesis of peptides on a membrane support was used to detect the phosphosites in TZF9. 17-amino acid-long peptides encompassing the 14 putative TZF9 phosphosites were synthesized onto a nitrocellulose membrane (Hilpert et al., 2007). The membrane was subjected to radioactive kinase assay using pre-activated MPK3 and MPK6. The idea behind this method is to rely on the ability of kinases to differentiate its phosphorylation site at the peptide level (Frank 2002). The target peptides were synthesized in duplicates. The blot included negative control where Ser or Thr was changed into ala. In this experiment, T⁶⁰, S¹⁴¹, S³²³, S³⁶², S⁴⁷² could be shown to be phosphorylated by MPK3 but no site was phosphorylated by MPK6. Interestingly, the mass spectrometry data shows that some sites to be phosphorylated by MPK6 but not MPK3. It is possible that putative phosphosite in the individual peptide was not appropriately oriented in the blot for MAPK interaction and phosphorylation, also the optimal physiological conditions for the phosphorylation may not be present. However, this assay could be optimized and repeated to check for the phosphorylation mediated by MPK6.

A **second** approach was using a phosphomutant version of TZF9 containing only one of the 14 putative phosphosites. These clones are generated by reintroducing a single phosphosite into the complete TZF9 phosphonull mutant version. These constructs, in future, can be transformed into protoplasts, which can be treated with flg22. The mobility-shift can then be checked in Phos-tagTM SDS-PAGE gel (Kinoshita et al., 2006). Phos-tagTM binds phosphorylated residues and Phos-tagTM-PAGE gel is used to separate phosphorylated from non-phosphorylated proteins. Using this method, the *in-vivo* phosphorylation site of TZF9 can be studied individually. After confirming the phosphorylation site by this method, those variants can be tested for phosphorylation by MPK3 or MPK6 via *in-vitro* kinase assay.

In this study, a phosphonull version of TZF9 proved to be more stable than the wt protein. This indicates that phosphorylation affects the degradation/stability of the protein. However, phosphorylation at distinct sites might differentially alter the effect on the stability of TZF9. So, after mapping the phosphosites, the stability experiment can be re-evaluated. Effect of the individual kinase can also be studied. For this, TZF9 carrying mutation at a specific site can be transformed in *mpk3* and *mpk6* knockout background to study the biological relevance of phosphorylation mediated by MPK6 and MPK3. Overall, the MAPK-targeted phosphorylation sites can be conclusively identified in near future using aforementioned techniques, afterwards, their biological relevance can be deciphered.

4.3 Localization studies suggest the dynamic nature of TZF9

One interesting outcome of this study is that TZF9 shows diverse sub-cellular localization. TZF9 co-localized with the PB marker proteins, DCP1 and XRN4 (**Fig. 17**). DCP1 assists in mRNA decapping and XRN4 is involved in 5' to 3' degradation of decapped mRNAs. Loss of XRN4-mediated exoribonuclease activity may result in accumulation of uncapped mRNAs in PB (Weber et al., 2008). Another study suggests that the accumulation of uncapped intermediates potentially involved in short interfering (siRNA) biogenesis is prevented by XRN4 (Gregory et al., 2008). Thus, co-localization with these PB components suggests TZF9 is potentially involved in mRNA processing.

The BiFC study showed that TZF9 interaction with MAPKs and putative RNA ligase occurs in the cytoplasm (**Fig. 14 and 23**). This suggests that the cytoplasmic distribution of TZF9 might be due to tethering to other cytosolic proteins, perhaps MAPKs. It is intriguing that different interacting partners could tether TZF9 into different compartments in the cell. Interestingly, phosphonull version of TZF9 also interacts with MAPKs (**Fig. 14**). This indicates that the phosphorylation is not a requisite for TZF9-MAPK interaction. Also, localization of TZF9-PS mutant in the cytoplasm and the PB (**Appendix Fig. A9**) shows that phosphorylation state is not a determinant for the protein to localize within or outside of PB. However, these experiments need to be performed using the phosphomimic version of TZF9. It is also possible that TZF9 localization is spatiotemporally regulated pre- and post- elicitation in plants and could be different than transient assays performed using mesophyll cells. Thus, it would be important to confirm the dynamics of TZF9 localization in stable transgenic lines. In any case, when transiently expressed, TZF9 localization in the cytoplasmic foci is altered upon flg22 treatment as compared to the water treatment (**Fig. 16**). By contrast, PAT1 relocalizes to PB after MAPK phosphorylation (Roux et al., 2015). It is possible that flg22 elicitation triggers the shift of TZF9 from PB to the cytoplasm to mediate defense-related functions (such as interaction with MAPKs) other than PB-related function. Overall, the dynamic localization of TZF9 suggests at least two functional aspect of TZF9; one, its role in defense and second, mRNA processing.

PB are very dynamic structures and formation of PB is dependent on the availability of targeted mRNAs. Both in plants and mammalian cells, treatment with cycloheximide (antibiotics that inhibits translational elongation) inhibit the assembly of PB (Weber et al., 2008; Kedersha et al., 2005). Localization studies with *Arabidopsis* TZF1 in protoplast transient assays showed that cycloheximide treatment reduced the number of PB but some foci (indicated as non-PB/SG identity) were insensitive to cycloheximide. Also, the localization of cytoplasmic foci associated with TZF9 is shown to be dynamic and dependent on mRNA availability. For example, treatment with transcriptional inhibitor, actinomycin D (ActD) showed suppressed localization of TZF9 in foci and (re)localization to the nucleus (Maldonado-Bonilla et al., 2014). Leptomycin B, an antibiotic that inhibits exportin1 protein required for nuclear export of other proteins,

disrupted PB localization of TZF9. Taken together, localization of TZF9 in PB relies on mRNA availability to localize in foci.

The subcellular localization of other TZFs has been shown to be diverse. For example, studies showed the AtTZF1, AtTZF11 and GhZFP1 (Cotton Zinc-finger Protein 1) proteins localize solely in nuclei (Han et al., 2014; Sun et al., 2007; Guo et al., 2009). TZF1, in another study, was shown to be shuttling between nucleus and cytoplasm (Pomeranz et al., 2010b). TZF2 and -3 were found in the cytoplasm when expressed in the epidermal cell of *Nicotiana* (Lee et al., 2012). TZF4 and OsTZF2 localized to nuclei in root cells of *Arabidopsis* and rice, respectively (Kim et al., 2008; Kong et al., 2006). In other studies, TZF4,-5,-6 and -11 were also reported to be localized in the nucleus (Blanvillain et al., 2011; Bogamuwa and Jang 2013). Sequence analysis of CCCH-TZF proteins from several plants like *Arabidopsis*, Rice, Maize, Medicago, Poplar, and Soybean revealed that majority of them have NES (nuclear export signal) and all of them have NLS (nuclear localization signal) sequences (Bogamuwa and Jang 2014). TZF9 was only occasionally found to be localized to the nucleus (Maldonado-Bonilla et al., 2014). Interestingly, when transiently expressed in protoplasts, all the 11 closely related proteins (of subfamily IX) and OsTZF1 were reported to be localized in cytoplasmic foci (Pomeranz et al., 2010a; Jang 2016; Jan et al., 2013). It is important to mention that these cytoplasmic foci, identified as PB (processing bodies) are distinct from heat stress granules (Weber et al., 2008). Overall, these studies reveals that CCCH-TZFs are diverse in localization. In addition to that, most of them (including TZF9) localize in PB - a hub for mRNA processing.

4.4 TZF9 binds to specific RNA sequences:

Besides localizing to PB, this study revealed that TZF9 could bind to poly (rU) and poly (rG) probes in RNA-EMSA assay (**Fig. 18**). The RNA-complex were observed as smears, which might be due to weak binding to these sequences. Another reason is potential RNase activity of TZF9, which was observed when incubated with the poly (rC) probe. *Arabidopsis* TZF2 and 3 are already known to have RNase activity *in-vitro* (Lee et al., 2012). TZF2 and-3 were shown to target 3'UTR of mRNAs and degrade them but their sequence specificity was not determined (Lee et al., 2012). This study further demonstrated that TZF9 binds to pentaprobe2, where the protein-RNA complex is not smeary but discrete. The nucleotide composition of pentaprobe2 is U=43, C=18, G=16, A=13 (sequences of all the 12 pentaprobases are given in **Appendix Fig. A6**). This is in concordance with the ribohomopolymers-TZF9 EMSA assay, which showed smeary binding of TZF9 to poly-U or-G sequences and RNase activity with C rich sequence. Additionally, a SELEX (systemic evolution of ligands by exponential enrichment) assay was used to determine the target sequence of TZF9 (Martina Brode, Master thesis). Briefly, the method involves multiple rounds of protein-RNA binding to select for a high-affinity target sequence from a pool of *in-vitro* transcribed RNAs with randomized sequences. After each

round of RNA binding, cDNA was synthesized using reverse transcriptase, PCR-amplified, cloned, and sequenced. It was performed over several rounds, resulting in enrichment of high-affinity RNAs in each round (**Appendix Fig. A10**). The consensus sequences deduced from SELEX experiment are shown in **Table 7** with their respective frequencies of occurrence. Taken together, TZF9 was identified as an RNA binding protein based on separate *in-vitro* experiments.

Table 7: Deduced short sequences identified in SELEX with their respective frequencies

Frequencies	Sequences
9x	5'-TAAA-3'
7x	5'-TTTG-3'
6x	5'-GAGC-3'
4x	5'-ACTTTGA-3'
4x	5'-GCGTT-3'
4x	5'-GGCGG-3'

Related CCCH-TZFs are known to bind specific RNA sequences. For example, mammalian TTP, a homolog of plant CCCH-TZFs, binds so-called class II AU rich elements (AREs) with the consensus sequence of UUAUUUAUU (Blackshear et al., 2003). TTP binds AREs via the TZF domain and RNA binding is abrogated by single mutations at any of eight cysteines or histidines in the TZF domain of TTP (Lai et al., 2000). TZF1 was shown to bind AREs at the 3'UTR and promote degradation of certain genes (Qu et al., 2014). However, AREs in plants are different in the consensus sequence to the AREs targeted by mammalian TTP. In contrast, TZF1 also shows weak affinity to consensus AREs bound by TTP. Also, rice TZF1 has been shown to bind ribohomopolymers of U and ARE-like motifs (Jan et al., 2013). These shreds of evidence demonstrate a broad range of RNA sequences being targeted by TZFs. A number of studies in plants show other CCCH-type zinc-finger proteins interact with RNA as well. For example, HUA1, a CCCH type TZF nuclear protein containing six tandemly repeated zinc-finger domains also binds RNA *in-vitro* (Cheng et al., 2003). Another CCCH-zinc-finger protein, C3H14 is known to bind mRNAs and is involved in cell elongation (Kim et al., 2014). However, the mechanistic action(s) of CCCH-TZFs in post-transcriptional processes is/are largely unknown in plants.

Furthermore, the CCCH-motif is required for binding to ribohomopolymers (**Fig. 18**). Also, zinc-finger deletion rendered TZF9 localization to the cytoplasm, rather than PB (Maldonado-Bonilla et al., 2014). It has already been reported that zinc-finger and ankyrin domains of TZF1 are important for RNA binding (Qu et al., 2014). The binding is zinc-dependent, reflecting the integrity of the ZF domain is also important.

It is important to mention that most of CCCH TZFs bind RNAs but DNA binding CCCH-type zinc-finger proteins are also known. For example, *Arabidopsis* PEI1 is an embryo-specific

transcriptional factor that plays a role in embryogenesis (Li and Thomas 1998). OsTZF9 (OsGZF1) was shown to bind promoter region of *GluB-1* (one of the glutelin genes in rice) in yeast one-hybrid assay and later confirmed by EMSA. OsTZF9 was shown to downregulate the expression of *GluB-1* and thus OsTZF9 was proposed to a transcriptional repressor (Chen et al., 2014). AtTZF7, a close homolog to TZF9 was shown to be a transcription factor (Blanvillain et al., 2011). However, other TZFs, AtTZF1 and OsTZF1 can bind DNA but have not been shown to be an activator or a repressor (Jan et al., 2013; Pomeranz et al., 2010b). Interestingly, AtTZF1, which shuttles between cytoplasm and nucleus, was shown to bind both DNA and RNA. As TZF9 also occasionally localizes to nucleus, its ability to bind DNA cannot be ruled out. However, based on the pieces of evidence found so far, the most accepted mechanism of TZF9 is the mRNA binding and possibly the PB-mediated post-transcriptional regulation.

4.5 TZF9 interaction with putative RNA ligase

TZF9 was shown to interact with putative RNA ligase (At5G40190) (**Fig.21 and 23**). The ankyrin (ANK) domain of TZF9 is required for their interaction (**Fig. 22**). Putative RNA ligase is poorly characterized as its *in-vivo* function remains obscure. The structural analysis of the putative RNA ligase and its homolog (At3G28140) suggested that they are atypical members of a phosphodiesterase superfamily characterized by two conserved histidines in its catalytic center (Mazumder et al., 2002). The members of this superfamily are 2', 3' cyclic nucleotide phosphodiesterase that catalyzes splicing of tRNA introns in eukaryotes. However, the putative RNA ligase and its paralogous protein are two plant-specific members of this family that lacks one of the conserved histidines. This suggests these proteins might possess an alternative activity. Being an interactor of TZF9, they may be involved in mRNA metabolism.

Interestingly, putative RNA ligase was shown to interact with another MPK3 and -6 substrate, TZF7 in BiFC assays (**Appendix Fig. A7**). It indicates that PTI-induced MAPKs might play a central role in the regulation of TZFs-RNA ligase function. However, no significant defense-related phenotype could be associated with putative RNA ligase knockout mutant after performing MAPK activation assays, root growth inhibition assays and ROS assays (data not shown). It may be because of the homologous protein (At3G28140), which share 81% identity with putative RNA ligase. This homologous protein is also a calmodulin binding protein (Reddy et al., 2002) and interacted with TZF9 in BiFC assays (**Appendix Fig. A8**). There is possibly functional redundancy between the two proteins (At5G40190 and At3G28140) *in-planta*. Another CCCH protein AtCPSF30 (cleavage and polyadenylation specificity factor) is an RNA binding protein that interacts with calmodulin (CaM). In this case, CaM inhibits the RNA binding of AtCPSF30 in a Ca²⁺ dependent manner (Delaney et al., 2006). In this study, it has been shown that the putative RNA ligase binds calmodulin in the presence/absence of Ca²⁺.

Critically, our experiment could be repeated using a negative and a positive control to exclude any technical error. Also, it would be interesting to compare the *in-vitro* binding affinity of TZF9 to ribohomopolymers or pentaprobins in the presence or absence of the putative RNA ligase (which is a calmodulin binding protein). A CaM-like protein from *Nicotiana* (NbCaM) is also known to interact with zinc-finger protein, SGS3 (Suppressor of Gene Silencing 3) (Li et al., 2017). SGS3 is a plant-specific RNA binding protein, which is involved in post-transcriptional gene silencing. It functions together with RNA-dependent RNA polymerase (RDR6) as a chaperone protein. These two proteins co-localize in certain cytoplasmic granules called SGS3/RDR6 bodies. Overall, it would be interesting to study the role of putative RNA ligase in TZF9-mediated post-transcriptional regulation, also, whether or not calmodulin and/or Ca²⁺ plays a role in this scenario.

TZFs have been shown to interact with stress-related proteins. For example, *Arabidopsis* seed specific TZFs, TZF5, 4, 6 are known to interact with two stress-responsive proteins, MARD1 (Mediator of ABA-Regulated Dormancy 1) and RD21A (Responsive to Dehydration 21A) in PB and SG (Bogamuwa and Jang 2016). This, in particular, is interesting because TZF9 also interacts with stress-responsive proteins, MPK3 and MPK6 in our study. Interestingly, these TZFs (TZF 4, 5 and 6) do not contain Ankyrin repeat. This further depicts the broad range of interaction patterns and possible diverse mode of action of TZF proteins. Also, GhZFP1, which is a homolog of TZF4 and 5 in *Arabidopsis*, was shown to interact with PR-5 (pathogenesis-related protein 5) and RD21A (Guo et al., 2009). Although PR-5 and RD21A are also not fully characterized but their interaction with GhZFP1 was able to enhance biotic and abiotic resistance, respectively (Guo et al., 2009) The interaction of GhZFP1 with RD21A and PR5 takes place in the cytoplasm and nucleus when transiently expressed in *Nicotiana* (Guo et al., 2009) and their interaction is mediated by the TZF motif and the N-terminal region. Also, putative RNA ligase is mainly a cytoplasmic protein and interacts with TZF9 in the cytoplasm and occasionally in the nucleus. This also supports the hypothesis that TZFs might have different functions in different cellular compartments.

Mammalian TZF protein TTP is believed to be a part of the mRNA decapping complex in PB (Brooks and Blackshear 2013). However, TTP was also co-immunoprecipitated and co-localized with other proteins that reside outside PB (Brooks and Blackshear 2013). This is possible because the interacting domain of TTP is claimed to be different with different proteins. For example, TTP interacts with a cytoplasmic protein hCIN85 (human Cbl-interacting protein85) via its carboxyl terminus and with a nuclear protein PABP8 via its TZF domain (Kedar et al., 2010; Su et al., 2012). Although TTP is thought to function in a complex but a clear evidence which could show a direct interaction in most of the cases is still lacking. This knowledge, however, is difficult to extrapolate into plant systems as the sequence homology between TTP and plant-TZFs is limited except for the common TZF domain. *Arabidopsis* TZFs

could not directly interact with any PB marker protein in yeast two-hybrid analysis (Bogamuwa and Jang 2016). Also, in this study TZF9 failed to interact with selective PB proteins like DCP1, DCP2, XRN4, AGO1 in a split-YFP analysis. Actually a number of studies suggest that plant TZFs are localized in the PB, though none of them have been reported to be interacting with any PB marker (Jang 2016). Taken together it is hypothesised that TZF9 could interact with specific proteins (like put. RNA ligase) to regulate RNA metabolism and immunity, however more studies are required to establish the role of these interesting interactions *in-planta*.

4.6 Global gene expression changes regulated by TZF9: omics approach

The original 'central dogma' of molecular biology proposes the flow of genetic information decoding from DNA to mRNA to protein. In this scenario, the abundance of proteins (produced through translation) is determined by the abundance of mRNA (formed in the preceding transcription step). However, the high degree of uncoupling between transcription and translation suggests mRNAs undergo transcriptional control and overall regulation of gene expression in the biological system is very complex and poorly understood. At the same time, it also indicates that regulation at the post-transcriptional level plays a major role in the overall gene expression.

Despite the high level of uncoupling between the transcriptomic and translatomic data (**Fig 35c and 35c'**), GO analyses of each data-set revealed many defense/stimuli genes being downregulated in the *tzf9* mutant in its uninduced state (**Appendix Table A7 and A9**). The *tzf9* mutant exhibited attenuated early and late defense responses (Maldonado-Bonilla et al., 2014). One of the early response in the *tzf9* mutant is reduced ROS accumulation (**Fig 25b**). As many important regulators of cellular signaling (such as, transcription factors, RNA binding proteins, components involved in protein degradation, receptors kinases) are downregulated in *tzf9* mutant (**Appendix Table 7.1, 9.1**), it is tempting to hypothesize that TZF9 might directly or indirectly regulate the expression of the component(s) involved in early signaling.

It is challenging to identify the direct target of TZF9 on the basis of these experiments though. It would, however, be interesting to perform the mRNA sequence analysis of those differentially regulated genes and to analyse whether these have a sequence similarity with pentaprobe 2 sequence or sequence identified in SELEX. This might provide a hint for the biological target of TZF9.

The GO analysis of downregulated genes in *tzf9* mutant indicated TZF9 is required for the expression of defense-related genes. However, many stress and stimuli-responsive genes are upregulated as well (**Appendix Table A6 and A8**). This suggests that TZF9 might help in the fine-tuning of defense by mediating upregulation of some genes while downregulating some other genes at the same time. As *tzf9* shows attenuated defense response, overall, TZF9 might be a positive regulator of PTI.

4.7 TZF9 as possible post-transcriptional regulator of gene expression

TZF9 binds RNA *in-vitro* and localizes in PB. Since PB proteins are known to regulate mRNA processing and storage, it is highly plausible that TZF9 acts as a post-transcriptional gene regulator by mediating RNA stability and decay in PB. This hypothesis was supported by our comparative omics analysis between wt and *tzf9*. It was shown that upon flg22 elicitation, homodirectional changes were ~40% in both the wt and *tzf9* mutant lines (**Fig. 35 a', b'**). This means that the overall differentially expressed unique genes (**Fig. 36 a', b'**, transcriptome +translatome +antidirectional) were about 60% in wt and *tzf9* mutants. In the wt genotype, this 60% is split roughly halfway into 31% of “transcriptome only” and 27% of “translatome only” categories. Considering this as 'wild-type scenario', in the *tzf9* mutant, there is a shift from 27% to 48% of the “translatome only” changes (upon flg22 elicitation) (**Fig. 36**). These numbers indicate a translational bias and suggest that TZF9 can affect the overall mRNA population that actively undergoes translation, another hint of involvement of TZF9 in post-transcriptional regulation.

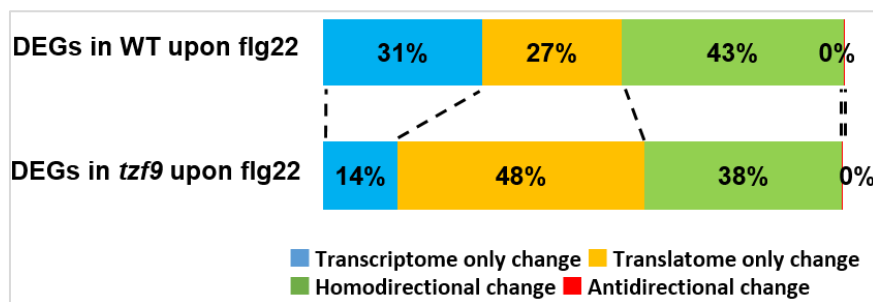


Fig. 36: Comparison of flg22-mediated changes in *tzf9* and wt. A high fraction of genes are differentially regulated at translational level in *tzf9* as compared to wt.

TTP is one of the best studied post-transcriptional regulators in mammals which binds AU-rich elements (AREs). TTP undergoes several post-translational modifications, like phosphorylation or ubiquitination that might affect its property. TTP is phosphorylated by p38 MAPK and MK2 (a downstream target of p38 MAPK) (Chrestensen et al., 2004). The MK2 phosphorylation was thought to regulate TTP binding to mRNAs (Hitti et al., 2006) but later work showed that phosphorylation of TTP does not affect its binding to mRNA but recruitment of deadenylation machinery and therefore, mRNA decay (Clement et al., 2011). The current understanding of phosphorylation of TTP and the effect of phosphorylation on TTP is still unclear. So it is also plausible that TZF9 binding to RNA is dependent on phosphorylation and possibly MAPK cascade might play an important role in the post-transcriptional regulation. As various plant PB marker proteins are also known to be MAPK substrates (Xu and Chua, 2012; Lassowskat et al., 2014), this indicates that MAPKs might regulate the gene expression at the post-transcriptional level by regulating the PB proteins involved in RNA processing. For example, MAPK-mediated phosphorylation of DCP1 affects its stability and MAPK-mediated

phosphorylation in PAT1 affects its localization. Also, *Arabidopsis* CCCH-type tandem Zn-finger proteins (TZF7 and TZF10) are MAPK substrates. So, it would be interesting to validate other TZFs as MAPK substrate and to analyse the effect of phosphorylation on their localization/stability/binding to mRNA. Overall, this would be a novel aspect of MAPK mediated post-transcriptional regulation through CCCH-TZF proteins.

4.8 CCCH-TZFs are involved in stress-response: a future perspective

CCCH-type tandem zinc-finger proteins have been associated with several plant stress responses with only a few reports demonstrating the role of TZFs specifically in biotic stress. For example, *tzf9* mutant showed attenuated defense against *Pseudomonas syringae*, and TZF9 is a biotic stimuli-responsive gene (Maldonado-Bonilla et al., 2014). However, a number of studies suggest related members of TZF family are also responsive to abiotic stimuli. For example, four ankyrin repeat containing TZFs of subfamily IX, TZF7/9/10/11, are proposed to work redundantly in activating oxidative stress tolerance and preventing stress-induced flowering (Blanvillain et al., 2011). It is also plausible that TZF9 regulates drought or other abiotic responses. As TZFs could be redundant in function, so *tzf9* mutant was crossed with *tzf7*, *tzf8*, *tzf10*, *tzf11* lines to generate double mutants in our laboratory. The resulting four lines, *tzf9/tzf7*, *tzf9/tzf8*, *tzf9/tzf10*, *tzf9/tzf11* can be selected further for homozygosity and in near future used to study stress responses. For example, *tzf7* mutant lines were shown to have compromised oxidative burst while *tzf9* mutant lines also showed attenuated ROS accumulation in two independent studies (Blanvillain et al., 2011; Maldonado-Bonilla et al., 2014). So, it would be interesting to check and compare ROS accumulation in *tzf7/tzf9* double mutant as compared to single mutants post biotic stress. A quantitative value might indicate whether the effect is cumulative or additive. Since *tzf7* mutant also shows insensitivity to ABA and stress-induced flowering, and a *tzf10* mutant showed sensitivity to ABA in the process of germination (AbuQamar et al., 2006). It will be intriguing to perform these assays with *tzf9* and the double mutants (*tzf9/tzf7* and *tzf9/tzf10* mutants respectively). Also, *tzf10* and *tzf11* have been shown to be compromised in salt stress and *tzf10/tzf11* double mutant are more sensitive to salt stress than the single mutants (Sun et al., 2007). The sensitivity to salt stress can be checked for *tzf9*, *tzf9/tzf10*, *tzf9/tzf11*. Also, the expression of TZF10 was induced upon necrotrophic pathogen *Botrytis cinerea* infection and mutant *tzf10* plants were more susceptible to *Botrytis cinerea* (AbuQamar et al., 2006). However, based on previous bioassay experiments performed in the lab using *Botrytis cinerea*, *tzf9* mutant shows no significant difference in terms of fungal growth. However, this bioassay experiment can be repeated possibly with weaker strains of *Botrytis* that may reveal minor quantitative differences (Liu et al., 2017). In this context, a triple mutant (*tzf9/tzf10/tzf11*) was also generated in our laboratory by crossing *tzf9* to double mutant *tzf10/tzf11*, which could also be included in the respective

experiments. Additionally, polysomal profiling and translational study can also be performed on RPL18/*tzf7*, RPL18/*tzf8*, RPL18/*tzf10*, RPL18/*tzf11* which were generated by RPL18-*tzfs* crosses. Overall, these mutants (generated during this study) offers a platform to study, characterize and understand stress-related role of *TZF9* and related genes.

Not only the ankyrin repeat containing *TZFs* (*TZF7,-8,-9,10,11*), but all 11 members of the subfamily IX CCCH-*TZFs* in *Arabidopsis* are known to be involved in a variety of biotic and abiotic responses. For example, overexpression of *TZF1* enhances cold, drought and salt (NaCl) stress tolerance as compared to wild-type (Lin et al., 2011; Han et al., 2014). Also, *TZF1* is a positive regulator of abscisic acid (ABA) and sugar signaling while it is a negative regulator for Gibberellic acid (GA) responses. Besides, overexpression of *TZF1* resulted in compact and late flowering, suggesting the involvement of *TZF1* in developmental phenotype as well. Hence, *TZF1* may serve as a mediator of cross-talk by integrating both nutrient and stress signals and modulating the downstream gene expression. Considering its role, it is plausible that *TZF1* might be having a role in biotic stress as well. Overexpression of *TZF2* and *TZF3* increases sensitivity to ABA and enhances drought tolerance in *Arabidopsis* (Lee et al., 2012). *TZF2* and -3 are also positive regulators of salt and oxidative stresses and negative regulators of methyl jasmonate (MeJA)-induced leaf senescence (Lee et al., 2012; Huang et al., 2011) (Huang et al., 2012). Seed-specific *TZF4* and -5 regulate seed germination by differential regulation of genes involved in ABA and GA metabolism and responses. *TZF4* and -5 upregulate ABA biosynthesis and GA catabolic genes but downregulate ABA catabolic genes and upregulate GA biosynthetic genes, thus enhancing ABA while reducing GA accumulation. Consequently, the *tzf4* knockout mutant showed low levels of ABA and elevated levels of GA (Bogamuwa and Jang 2013; Kim et al., 2008).

CCCH-*TZF* in other plants is also reported to be playing roles in stress responses. For example, a rice homolog, *OsTZF1*, is induced by drought, high salt, H₂O₂, MeJA, SA, and ABA. In *OsTZF1* overexpression lines genes related to stress, reactive oxygen species homeostasis, and metal homeostasis were differentially regulated. Moreover, overexpression of *OsTZF1* delayed seed germination and leaf senescence and also retarded seedling growth whereas RNAi knockdown plants show early germination, early leaf senescence (Jan et al., 2013). Overexpression of another rice *TZF* gene, *OsTZF2*, delayed MeJA-induced leaf senescence and RNAi knockdown of *OsTZF2* results an accelerated leaf senescence. So *OsTZF2* is believed to be a negative regulator of JA accumulation and response (Kong et al., 2006).

Taken together, while deciphering the involvement of *TZF9* in biotic signaling via post-transcriptional regulation, the present study offers many interesting questions regarding the involvement of *TZF9* (and related *TZFs*, some of which are potential MPK substrates) in (a)biotic stresses and in hormonal responsiveness.

5 Summary

In conclusion, a detailed study was performed to characterize the *Arabidopsis* tandem zinc finger protein TZF9. It was confirmed that it has a role in plant immunity and is a MPK3/6 substrate. Also, phosphorylation leads to the degradation of the protein which might be required for protein turn-over. TZF9 interacts with a calmodulin-binding cytoplasmic protein namely, putative RNA ligase via its Ankyrin domain. As putative RNA ligase is a poorly characterized protein, subsequent effect of cytoplasmic interaction between TZF9 with putative RNA ligase are yet to be ascertained. TZF9 localizes to processing bodies and requires CCCH motif to bind RNAs. So, TZF9 might be involved in degradation or stabilization of mRNA. The knockout mutant *tzf9* is attenuated in defense responses. Subsequently, omics analyses performed in this study suggested that genes responsive to stress and stimuli are deregulated in *tzf9* mutant. Those may directly or indirectly be involved in stress responses in wild-type plants during early-PTI. Also, the omics study suggested that flg22-induced gene expression in *tzf9* is biased at translational level. This biological evidence again supports the hypothesis that TZF9 regulates the expression of genes at post-transcriptional level. *In-vitro* studies such as RNA-EMSA and SELEX demonstrated that TZF9 binds mRNA in a sequence specific manner. Overall, this study successfully established that TZF9 affects post-transcriptional regulation – possibly in the control of mRNAs entering the translational cycle or partitioning into PB for storage or RNA processing. A simplified model depicting the overall possible role of TZF9 in cellular processes is shown in **Fig. 37**.

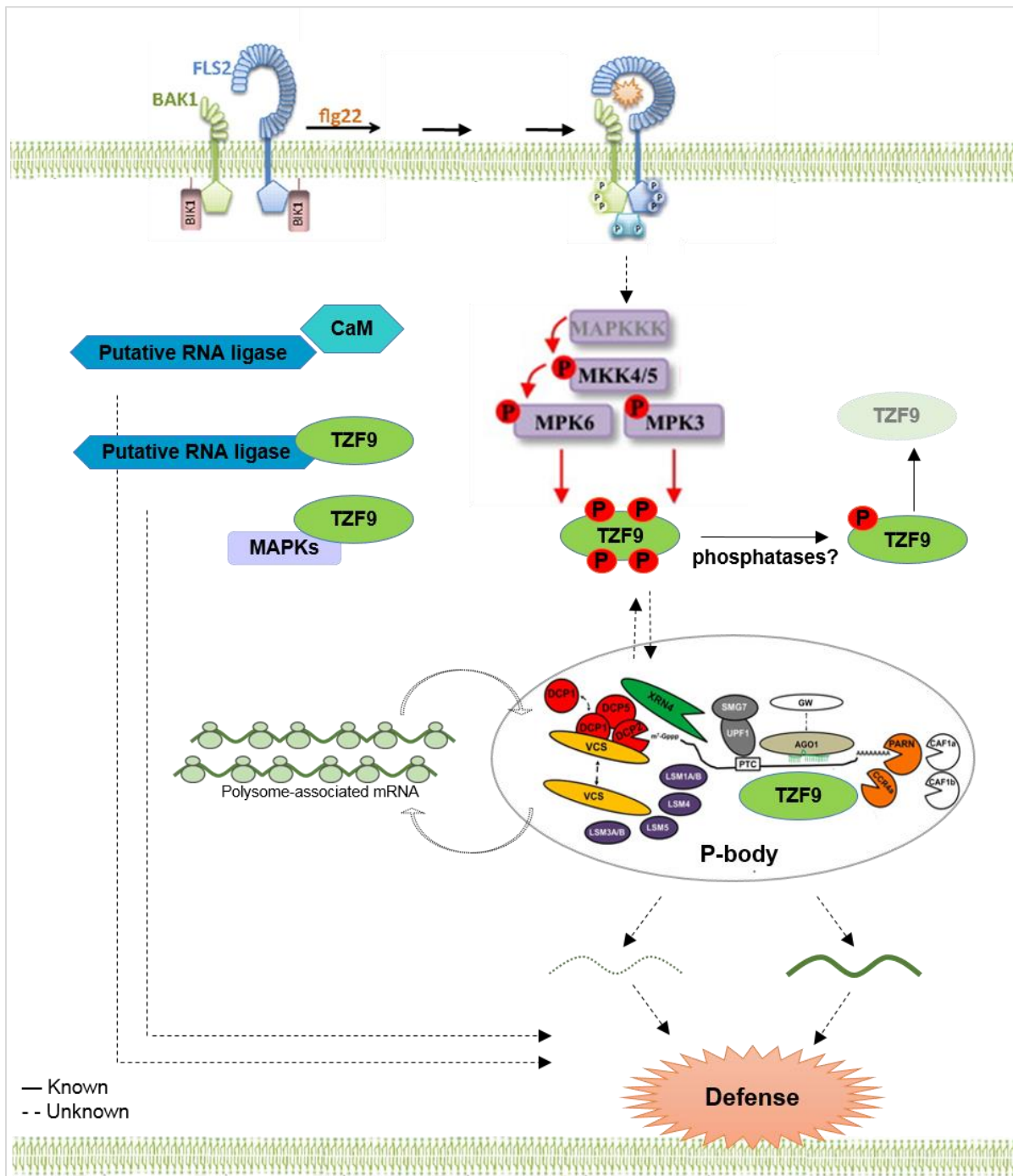


Fig. 37: A model depicts the possible roles of TZF9 in PTI. Upon flg22-elicitation, TZF9 is phosphorylated by MAPKs and degraded. Beside interaction with MPK3 and MPK6, TZF9 also interacts with a CaM binding protein RNA ligase. TZF9 localizes to the PB, binds RNA and thereby it might regulate defense responses. (Solid lines show known functions and dotted line shows unknown functions).

6 References

- AbuQamar S, Chen X, Dhawan R, Bluhm B, Salmeron J, Lam S, Dietrich RA, Mengiste T (2006) Expression profiling and mutant analysis reveals complex regulatory networks involved in Arabidopsis response to Botrytis infection. *The Plant journal : for cell and molecular biology* 48 (1):28-44. doi:10.1111/j.1365-313X.2006.02849.x
- Albert M (2013) Peptides as triggers of plant defence. *J Exp Bot* 64 (17):5269-5279. doi:10.1093/jxb/ert275
- Arabidopsis Interactome Mapping C (2011) Evidence for network evolution in an Arabidopsis interactome map. *Science (New York, NY)* 333 (6042):601-607. doi:10.1126/science.1203877
- Asai T, Tena G, Plotnikova J, Willmann MR, Chiu WL, Gomez-Gomez L, Boller T, Ausubel FM, Sheen J (2002) MAP kinase signalling cascade in Arabidopsis innate immunity. *Nature* 415 (6875):977-983. doi:10.1038/415977a
- Bardwell AJ, Flatauer LJ, Matsukuma K, Thorner J, Bardwell L (2001) A conserved docking site in MEKs mediates high-affinity binding to MAP kinases and cooperates with a scaffold protein to enhance signal transmission. *Journal of Biological Chemistry* 276 (13):10374-10386. doi:DOI 10.1074/jbc.M010271200
- Bendak K, Loughlin FE, Cheung V, O'Connell MR, Crossley M, Mackay JP (2012) A rapid method for assessing the RNA-binding potential of a protein. *Nucleic acids research* 40 (14):e105-e105. doi:10.1093/nar/gks285
- Benjamini Y, Hochberg Y (1995) Controlling the False Discovery Rate - a Practical and Powerful Approach to Multiple Testing. *J Roy Stat Soc B Met* 57 (1):289-300
- Bethke G, Pecher P, Eschen-Lippold L, Tsuda K, Katagiri F, Glazebrook J, Scheel D, Lee J (2012) Activation of the Arabidopsis thaliana mitogen-activated protein kinase MPK11 by the flagellin-derived elicitor peptide, flg22. *Molecular plant-microbe interactions : MPMI* 25 (4):471-480. doi:10.1094/MPMI-11-11-0281
- Bigeard J, Colcombet J, Hirt H (2015) Signaling mechanisms in pattern-triggered immunity (PTI). *Mol Plant* 8 (4):521-539. doi:10.1016/j.molp.2014.12.022
- Blackshear PJ, Lai WS, Kennington EA, Brewer G, Wilson GM, Guan XJ, Zhou P (2003) Characteristics of the interaction of a synthetic human tristetraprolin tandem zinc finger peptide with AU-rich element-containing RNA substrates. *Journal of Biological Chemistry* 278 (22):19947-19955. doi:10.1074/jbc.M301290200
- Blanvillain R, Wei S, Wei P, Kim JH, Ow DW (2011) Stress tolerance to stress escape in plants: role of the OXS2 zinc-finger transcription factor family. *The EMBO journal* 30 (18):3812-3822. doi:10.1038/emboj.2011.270
- Bogamuwa S, Jang JC (2013) The Arabidopsis tandem CCCH zinc finger proteins AtTZF4, 5 and 6 are involved in light-, abscisic acid- and gibberellic acid-mediated regulation of seed germination. *Plant, cell & environment* 36 (8):1507-1519. doi:10.1111/pce.12084
- Bogamuwa SP, Jang JC (2014) Tandem CCCH zinc finger proteins in plant growth, development and stress response. *Plant & cell physiology* 55 (8):1367-1375. doi:10.1093/pcp/pcu074
- Bogamuwa SP, Jang JC (2014) Tandem CCCH zinc finger proteins in plant growth, development and stress response. *Plant & cell physiology* 55 (8):1367-1375. doi:10.1093/pcp/pcu074
- Boller T, Felix G (2009) A renaissance of elicitors: perception of microbe-associated molecular patterns and danger signals by pattern-recognition receptors. *Annual review of plant biology* 60:379-406. doi:10.1146/annurev.arplant.57.032905.105346
- Boudsocq M, Willmann MR, McCormack M, Lee H, Shan L, He P, Bush J, Cheng SH, Sheen J (2010) Differential innate immune signalling via Ca(2+) sensor protein kinases. *Nature* 464 (7287):418-422. doi:10.1038/nature08794
- Brode M. (2014) Analyse der Proteininstabilität und die Identifikation von putativen RNA-Bindungsmotiven eines *Arabidopsis thaliana* Tandem Zinkfingerproteins (Master's thesis, MLU Halle, Unpublished).
- Brooks SA, Blackshear PJ (2013) Tristetraprolin (TTP): interactions with mRNA and proteins, and current thoughts on mechanisms of action. *Biochim Biophys Acta* 1829 (6-7):666-679. doi:10.1016/j.bbagr.2013.02.003
- Chen Y, Sun A, Wang M, Zhu Z, Ouwerkerk PB (2014) Functions of the CCCH type zinc finger protein OsGZF1 in regulation of the seed storage protein GluB-1 from rice. *Plant molecular biology* 84 (6):621-634. doi:10.1007/s11103-013-0158-5
- Cheng Y, Kato N, Wang W, Li J, Chen X (2003) Two RNA binding proteins, HEN4 and HUA1, act in the processing of AGAMOUS pre-mRNA in Arabidopsis thaliana. *Dev Cell* 4 (1):53-66
- Chrestensen CA, Schroeder MJ, Shabanowitz J, Hunt DF, Pelo JW, Worthington MT, Sturgill TW (2004) MAPKAP kinase 2 phosphorylates tristetraprolin on in vivo sites including Ser(178), a site

- required for 14-3-3 binding. *Journal of Biological Chemistry* 279 (11):10176-10184. doi:10.1074/jbc.M310486200
- Clement SL, Scheckel C, Stoecklin G, Lykke-Andersen J (2011) Phosphorylation of tristetraprolin by MK2 impairs AU-rich element mRNA decay by preventing deadenylase recruitment. *Mol Cell Biol* 31 (2):256-266. doi:10.1128/MCB.00717-10
- Delaney KJ, Xu R, Zhang J, Li QQ, Yun KY, Falcone DL, Hunt AG (2006) Calmodulin interacts with and regulates the RNA-binding activity of an Arabidopsis polyadenylation factor subunit. *Plant physiology* 140 (4):1507-1521. doi:10.1104/pp.105.070672
- Djamei A, Pitzschke A, Nakagami H, Rajh I, Hirt H (2007) Trojan horse strategy in Agrobacterium transformation: abusing MAPK defense signaling. *Science (New York, NY)* 318 (5849):453-456. doi:10.1126/science.1148110
- Dyson MR, Shadbolt SP, Vincent KJ, Perera RL, McCafferty J (2004) Production of soluble mammalian proteins in *Escherichia coli*: identification of protein features that correlate with successful expression. *BMC Biotechnol* 4:32. doi:10.1186/1472-6750-4-32
- Feilner T, Hultschig C, Lee J, Meyer S, Immink RG, Koenig A, Possling A, Seitz H, Beveridge A, Scheel D, Cahill DJ, Lehrach H, Kreuzberger J, Kersten B (2005) High throughput identification of potential Arabidopsis mitogen-activated protein kinases substrates. *Molecular & cellular proteomics : MCP* 4 (10):1558-1568. doi:10.1074/mcp.M500007-MCP200
- Felix, G., Duran, J.D., Volko, S. and Boller, T. (1999) Plants have a sensitive perception system for the most conserved domain of bacterial flagellin. *The Plant journal : for cell and molecular biology*, 18, 265-276.
- Fenger-Gron M, Fillman C, Norrild B, Lykke-Andersen J (2005) Multiple processing body factors and the ARE binding protein TTP activate mRNA decapping. *Molecular cell* 20 (6):905-915. doi:10.1016/j.molcel.2005.10.031
- Frank R (2002) The SPOT-synthesis technique: Synthetic peptide arrays on membrane supports—principles and applications. *Journal of Immunological Methods* 267 (1):13-26. doi:[http://dx.doi.org/10.1016/S0022-1759\(02\)00137-0](http://dx.doi.org/10.1016/S0022-1759(02)00137-0)
- Gomez-Gomez L, Boller T (2000) FLS2: an LRR receptor-like kinase involved in the perception of the bacterial elicitor flagellin in Arabidopsis. *Molecular cell* 5 (6):1003-1011
- Gregory BD, O'Malley RC, Lister R, Urich MA, Tonti-Filippini J, Chen H, Millar AH, Ecker JR (2008) A link between RNA metabolism and silencing affecting Arabidopsis development. *Developmental Cell* 14 (6):854-866. doi:10.1016/j.devcel.2008.04.005
- Group M (2002) Mitogen-activated protein kinase cascades in plants: a new nomenclature. *Trends in plant science* 7 (7):301-308
- Guo YH, Yu YP, Wang D, Wu CA, Yang GD, Huang JG, Zheng CC (2009) GhZFP1, a novel CCCH-type zinc finger protein from cotton, enhances salt stress tolerance and fungal disease resistance in transgenic tobacco by interacting with GZIRD21A and GZIPR5. *The New phytologist* 183 (1):62-75. doi:10.1111/j.1469-8137.2009.02838.x
- Halter T, Imkamp J, Mazzotta S, Wierzba M, Postel S, Bucherl C, Kiefer C, Stahl M, Chinchilla D, Wang XF, Nurnberger T, Zipfel C, Clouse S, Borst JW, Boeren S, de Vries SC, Tax F, Kemmerling B (2014) The Leucine-Rich Repeat Receptor Kinase BIR2 Is a Negative Regulator of BAK1 in Plant Immunity. *Current Biology* 24 (2):134-143. doi:10.1016/j.cub.2013.11.047
- Han G, Wang M, Yuan F, Sui N, Song J, Wang B (2014) The CCCH zinc finger protein gene AtZFP1 improves salt resistance in Arabidopsis thaliana. *Plant molecular biology* 86 (3):237-253. doi:10.1007/s11103-014-0226-5
- Hilpert K, Winkler DFH, Hancock REW (2007) Peptide arrays on cellulose support: SPOT synthesis, a time and cost efficient method for synthesis of large numbers of peptides in a parallel and addressable fashion. *Nature protocols* 2 (6):1333-1349. doi:10.1038/nprot.2007.160
- Hitti E, Iakovleva T, Brook M, Deppenmeier S, Gruber AD, Radzioch D, Clark AR, Blackshear PJ, Kotlyarov A, Gaestel M (2006) Mitogen-activated protein kinase-activated protein kinase 2 regulates tumor necrosis factor mRNA stability and translation mainly by altering tristetraprolin expression, stability, and binding to adenine/uridine-rich element. *Mol Cell Biol* 26 (6):2399-2407. doi:10.1128/MCB.26.6.2399-2407.2006
- Huang P, Chung MS, Ju HW, Na HS, Lee DJ, Cheong HS, Kim CS (2011) Physiological characterization of the Arabidopsis thaliana oxidation-related zinc finger 1, a plasma membrane protein involved in oxidative stress. *J Plant Res* 124 (6):699-705. doi:10.1007/s10265-010-0397-3
- Huang P, Ju HW, Min JH, Zhang X, Chung JS, Cheong HS, Kim CS (2012) Molecular and physiological characterization of the Arabidopsis thaliana Oxidation-related Zinc Finger 2, a plasma membrane protein involved in ABA and salt stress response through the ABI2-mediated signaling pathway. *Plant & cell physiology* 53 (1):193-203. doi:10.1093/pcp/pcr162
- Jan A, Maruyama K, Todaka D, Kidokoro S, Abo M, Yoshimura E, Shinozaki K, Nakashima K, Yamaguchi-Shinozaki K (2013) OstZFP1, a CCCH-tandem zinc finger protein, confers delayed

- senescence and stress tolerance in rice by regulating stress-related genes. *Plant physiology* 161 (3):1202-1216. doi:10.1104/pp.112.205385
- Jang, J.C. (2016) Arginine-rich motif-tandem CCCH zinc finger proteins in plant stress responses and post-transcriptional regulation of gene expression. *Plant science : an international journal of experimental plant biology*, 252, 118-124
- Jones JD, Dangl JL (2006) The plant immune system. *Nature* 444 (7117):323-329. doi:10.1038/nature05286
- Kanchiswamy CN, Takahashi H, Quadro S, Maffei ME, Bossi S, Berteza C, Zebelo SA, Muroi A, Ishihama N, Yoshioka H, Boland W, Takabayashi J, Endo Y, Sawasaki T, Arimura G (2010) Regulation of Arabidopsis defense responses against *Spodoptera littoralis* by CPK-mediated calcium signaling. *BMC plant biology* 10:97. doi:10.1186/1471-2229-10-97
- Kedar VP, Darby MK, Williams JG, Blackshear PJ (2010) Phosphorylation of human tristetraprolin in response to its interaction with the Cbl interacting protein CIN85. *PLoS one* 5 (3):e9588. doi:10.1371/journal.pone.0009588
- Kedersha N, Stoecklin G, Ayodele M, Yacono P, Lykke-Andersen J, Fitzler MJ, Scheuner D, Kaufman RJ, Golan DE, Anderson P (2005) Stress granules and processing bodies are dynamically linked sites of mRNP remodeling. *Journal of Cell Biology* 169 (6):871-884
- Kim DH, Yamaguchi S, Lim S, Oh E, Park J, Hanada A, Kamiya Y, Choi G (2008) SOMNUS, a CCCH-type zinc finger protein in Arabidopsis, negatively regulates light-dependent seed germination downstream of PIL5. *The Plant cell* 20 (5):1260-1277. doi:10.1105/tpc.108.058859
- Kim WC, Kim JY, Ko JH, Kang H, Kim J, Han KH (2014) AtC3H14, a plant-specific tandem CCCH zinc-finger protein, binds to its target mRNAs in a sequence-specific manner and affects cell elongation in Arabidopsis thaliana. *The Plant journal : for cell and molecular biology* 80 (5):772-784. doi:10.1111/tpj.12667
- Kinoshita E, Kinoshita-Kikuta E, Takiyama K, Koike T (2006) Phosphate-binding tag, a new tool to visualize phosphorylated proteins. *Molecular & Cellular Proteomics* 5 (4):749-757. doi:10.1074/mcp.T500024-MCP200
- Kloth, K.J., Wieggers, G.L., Busscher-Lange, J., van Haarst, J.C., Kruijer, W., Bouwmeester, H.J., Dicke, M. and Jongsma, M.A. (2016) AtWRKY22 promotes susceptibility to aphids and modulates salicylic acid and jasmonic acid signalling. *J Exp Bot*, 67, 3383-3396.
- Kong Z, Li M, Yang W, Xu W, Xue Y (2006) A novel nuclear-localized CCCH-type zinc finger protein, OsDOS, is involved in delaying leaf senescence in rice. *Plant physiology* 141 (4):1376-1388. doi:10.1104/pp.106.082941
- Kulkarni M, Ozgur S, Stoecklin G (2010) On track with P-bodies. *Biochemical Society transactions* 38 (Pt 1):242-251. doi:10.1042/BST0380242
- Kunze G, Zipfel C, Robatzek S, Niehaus K, Boller T, Felix G (2004) The N terminus of bacterial elongation factor Tu elicits innate immunity in Arabidopsis plants. *The Plant cell* 16 (12):3496-3507. doi:10.1105/tpc.104.026765
- Lai WS, Carballo E, Thorn JM, Kennington EA, Blackshear PJ (2000) Interactions of CCCH zinc finger proteins with mRNA. Binding of tristetraprolin-related zinc finger proteins to Au-rich elements and destabilization of mRNA. *The Journal of biological chemistry* 275 (23):17827-17837. doi:10.1074/jbc.M001696200
- Lassowskat I, Bottcher C, Eschen-Lippold L, Scheel D, Lee J (2014) Sustained mitogen-activated protein kinase activation reprograms defense metabolism and phosphoprotein profile in Arabidopsis thaliana. *Front Plant Sci* 5:554. doi:10.3389/fpls.2014.00554
- Lee J, Eschen-Lippold L, Lassowskat I, Bottcher C, Scheel D (2015) Cellular reprogramming through mitogen-activated protein kinases. *Front Plant Sci* 6:940. doi:10.3389/fpls.2015.00940
- Lee SJ, Jung HJ, Kang H, Kim SY (2012) Arabidopsis zinc finger proteins AtC3H49/AtTZF3 and AtC3H20/AtTZF2 are involved in ABA and JA responses. *Plant & cell physiology* 53 (4):673-686. doi:10.1093/pcp/pcs023
- Li F, Zhao N, Li Z, Xu X, Wang Y, Yang X, Liu SS, Wang A, Zhou X (2017) A calmodulin-like protein suppresses RNA silencing and promotes geminivirus infection by degrading SGS3 via the autophagy pathway in *Nicotiana benthamiana*. *PLoS pathogens* 13 (2):e1006213. doi:10.1371/journal.ppat.1006213
- Li G, Meng X, Wang R, Mao G, Han L, Liu Y, Zhang S (2012) Dual-level regulation of ACC synthase activity by MPK3/MPK6 cascade and its downstream WRKY transcription factor during ethylene induction in Arabidopsis. *PLoS genetics* 8 (6):e1002767. doi:10.1371/journal.pgen.1002767
- Li Z, Thomas TL (1998) PEI1, an embryo-specific zinc finger protein gene required for heart-stage embryo formation in Arabidopsis. *The Plant cell* 10 (3):383-398
- Lin PC, Pomeranz MC, Jikumaru Y, Kang SG, Hah C, Fujioka S, Kamiya Y, Jang JC (2011) The Arabidopsis tandem zinc finger protein AtTZF1 affects ABA- and GA-mediated growth, stress

- and gene expression responses. *The Plant journal : for cell and molecular biology* 65 (2):253-268. doi:10.1111/j.1365-313X.2010.04419.x
- Liu S, Ziegler J, Zeier J, Birkenbihl RP, Somssich IE (2017) Botrytis cinerea B05.10 promotes disease development in Arabidopsis by suppressing WRKY33-mediated host immunity. *Plant, cell & environment* 40 (10):2189-2206. doi:10.1111/pce.13022
- Liu S, Ziegler J, Zeier J, Birkenbihl RP, Somssich IE (2017) Botrytis cinerea B05.10 promotes disease development in Arabidopsis by suppressing WRKY33-mediated host immunity. *Plant, cell & environment* 40 (10):2189-2206. doi:10.1111/pce.13022
- Lu DP, Wu SJ, Gao XQ, Zhang YL, Shan LB, He P (2010) A receptor-like cytoplasmic kinase, BIK1, associates with a flagellin receptor complex to initiate plant innate immunity. *Proceedings of the National Academy of Sciences of the United States of America* 107 (1):496-501. doi:10.1073/pnas.0909705107
- Lykke-Andersen J, Wagner E (2005) Recruitment and activation of mRNA decay enzymes by two ARE-mediated decay activation domains in the proteins TTP and BRF-1. *Genes & development* 19 (3):351-361. doi:10.1101/gad.1282305
- Macho AP, Zipfel C (2014) Plant PRRs and the activation of innate immune signaling. *Molecular cell* 54 (2):263-272. doi:10.1016/j.molcel.2014.03.028
- Maldonado-Bonilla LD (2014) Composition and function of P bodies in Arabidopsis thaliana. *Front Plant Sci* 5:201. doi:10.3389/fpls.2014.00201
- Maldonado-Bonilla LD, Eschen-Lippold L, Gago-Zachert S, Tabassum N, Bauer N, Scheel D, Lee J (2014) The Arabidopsis tandem zinc finger 9 protein binds RNA and mediates pathogen-associated molecular pattern-triggered immune responses. *Plant & cell physiology* 55 (2):412-425. doi:10.1093/pcp/pct175
- Meng X, Zhang S (2013) MAPK cascades in plant disease resistance signaling. *Annual review of phytopathology* 51:245-266. doi:10.1146/annurev-phyto-082712-102314
- Mohr, P.G. and Cahill, D.M. (2007) Suppression by ABA of salicylic acid and lignin accumulation and the expression of multiple genes, in Arabidopsis infected with Pseudomonas syringae pv. tomato. *Funct Integr Genomics*, 7, 181-191.
- Mustroph A, Zanetti ME, Jang CJH, Holtan HE, Repetti PP, Galbraith DW, Girke T, Bailey-Serres J (2009) Profiling translomes of discrete cell populations resolves altered cellular priorities during hypoxia in Arabidopsis. *Proceedings of the National Academy of Sciences* 106 (44):18843-18848. doi:10.1073/pnas.0906131106
- Nitta Y, Ding P, Zhang Y (2014) Identification of additional MAP kinases activated upon PAMP treatment. *Plant signaling & behavior* 9 (11):e976155. doi:10.4161/15592324.2014.976155
- Osbourn AE (1996) Preformed Antimicrobial Compounds and Plant Defense against Fungal Attack. *The Plant cell* 8 (10):1821-1831. doi:10.1105/tpc.8.10.1821
- Palm-Forster MA, Eschen-Lippold L, Lee J (2012) A mutagenesis-based screen to rapidly identify phosphorylation sites in mitogen-activated protein kinase substrates. *Anal Biochem* 427 (2):127-129. doi:10.1016/j.ab.2012.05.015
- Parker R, Sheth U (2007) P bodies and the control of mRNA translation and degradation. *Molecular cell* 25 (5):635-646. doi:10.1016/j.molcel.2007.02.011
- Pecher P, Eschen-Lippold L, Herklotz S, Kuhle K, Naumann K, Bethke G, Uhrig J, Weyhe M, Scheel D, Lee J (2014) The Arabidopsis thaliana mitogen-activated protein kinases MPK3 and MPK6 target a subclass of 'VQ-motif'-containing proteins to regulate immune responses. *The New phytologist* 203 (2):592-606. doi:10.1111/nph.12817
- Pieterse CMJ, Leon-Reyes A, Van der Ent S, Van Wees SCM (2009) Networking by small-molecule hormones in plant immunity. *Nature chemical biology* 5 (5):308-316. doi:10.1038/nchembio.164
- Pomeranz M, Lin PC, Finer J, Jang JC (2010a) AtTZF gene family localizes to cytoplasmic foci. *Plant signaling & behavior* 5 (2):190-192
- Pomeranz M, Zhang L, Finer J, Jang JC (2011) Can AtTZF1 act as a transcriptional activator or repressor in plants? *Plant signaling & behavior* 6 (5):719-722
- Pomeranz MC, Hah C, Lin PC, Kang SG, Finer JJ, Blackshear PJ, Jang JC (2010b) The Arabidopsis tandem zinc finger protein AtTZF1 traffics between the nucleus and cytoplasmic foci and binds both DNA and RNA. *Plant physiology* 152 (1):151-165. doi:10.1104/pp.109.145656
- Qiu JL, Fiil BK, Petersen K, Nielsen HB, Botanga CJ, Thorgrimsen S, Palma K, Suarez-Rodriguez MC, Sandbech-Clausen S, Lichota J, Brodersen P, Grasser KD, Mattsson O, Glazebrook J, Mundy J, Petersen M (2008a) Arabidopsis MAP kinase 4 regulates gene expression through transcription factor release in the nucleus. *The EMBO journal* 27 (16):2214-2221. doi:10.1038/emboj.2008.147
- Qiu JL, Zhou L, Yun BW, Nielsen HB, Fiil BK, Petersen K, Mackinlay J, Loake GJ, Mundy J, Morris PC (2008b) Arabidopsis mitogen-activated protein kinase kinases MKK1 and MKK2 have

- overlapping functions in defense signaling mediated by MEKK1, MPK4, and MKS1. *Plant physiology* 148 (1):212-222. doi:10.1104/pp.108.120006
- Qu J, Kang SG, Wang W, Musier-Forsyth K, Jang JC (2014) The Arabidopsis thaliana tandem zinc finger 1 (AtTZF1) protein in RNA binding and decay. *The Plant journal : for cell and molecular biology* 78 (3):452-467. doi:10.1111/tpj.12485
- Ritchie ME, Phipson B, Wu D, Hu YF, Law CW, Shi W, Smyth GK (2015) limma powers differential expression analyses for RNA-sequencing and microarray studies. *Nucleic acids research* 43 (7). doi:ARTN e4710.1093/nar/gkv007
- Rodriguez MC, Petersen M, Mundy J (2010) Mitogen-activated protein kinase signaling in plants. *Annual review of plant biology* 61:621-649. doi:10.1146/annurev-arplant-042809-112252
- Roux M, Schwessinger B, Albrecht C, Chinchilla D, Jones A, Holton N, Malinovsky FG, Tor M, de Vries S, Zipfel C (2011) The Arabidopsis leucine-rich repeat receptor-like kinases BAK1/SERK3 and BKK1/SERK4 are required for innate immunity to hemibiotrophic and biotrophic pathogens. *The Plant cell* 23 (6):2440-2455. doi:10.1105/tpc.111.084301
- Roux ME, Rasmussen MW, Palma K, Lolle S, Regue AM, Bethke G, Glazebrook J, Zhang W, Sieburth L, Larsen MR, Mundy J, Petersen M (2015) The mRNA decay factor PAT1 functions in a pathway including MAP kinase 4 and immune receptor SUMM2. *The EMBO journal* 34 (5):593-608. doi:10.15252/embj.201488645
- Sasabe M, Kosetsu K, Hidaka M, Murase A, Machida Y (2011) Arabidopsis thaliana MAP65-1 and MAP65-2 function redundantly with MAP65-3/PLEIADE in cytokinesis downstream of MPK4. *Plant signaling & behavior* 6 (5):743-747
- Segonzac C, Feike D, Gimenez-Ibanez S, Hann DR, Zipfel C, Rathjen JP (2011) Hierarchy and Roles of Pathogen-Associated Molecular Pattern-Induced Responses in *Nicotiana benthamiana*. *Plant physiology* 156 (2):687-699. doi:10.1104/pp.110.171249
- Sheikh AH, Eschen-Lippold L, Pecher P, Hoehenwarter W, Sinha AK, Scheel D, Lee J (2016) Regulation of WRKY46 Transcription Factor Function by Mitogen-Activated Protein Kinases in Arabidopsis thaliana. *Front Plant Sci* 7:61. doi:10.3389/fpls.2016.00061
- Somerville C, Bauer S, Brininstool G, Facette M, Hamann T, Milne J, Osborne E, Paredez A, Persson S, Raab T, Vorwerk S, Youngs H (2004) Toward a systems approach to understanding plant cell walls. *Science (New York, NY)* 306 (5705):2206-2211. doi:10.1126/science.1102765
- Souquere S, Mollet S, Kress M, Dautry F, Pierron G, Weil D (2009) Unravelling the ultrastructure of stress granules and associated P-bodies in human cells. *Journal of cell science* 122 (20):3619-3626. doi:10.1242/jcs.054437
- Steffens A, Brautigam A, Jakoby M, Hulskamp M (2015) The BEACH Domain Protein SPIRRIG Is Essential for Arabidopsis Salt Stress Tolerance and Functions as a Regulator of Transcript Stabilization and Localization. *Plos Biology* 13 (7). doi:ARTN e1002188 10.1371/journal.pbio.1002188
- Su YL, Wang SC, Chiang PY, Lin NY, Shen YF, Chang GD, Chang CJ (2012) Tristetraprolin inhibits poly(A)-tail synthesis in nuclear mRNA that contains AU-rich elements by interacting with poly(A)-binding protein nuclear 1. *PloS one* 7 (7):e41313. doi:10.1371/journal.pone.0041313
- Sun, J., Huang, G., Fan, F., Wang, S., Zhang, Y., Han, Y., Zou, Y. and Lu, D. (2017) Comparative study of Arabidopsis PBS1 and a wheat PBS1 homolog helps understand the mechanism of PBS1 functioning in innate immunity. *Sci Rep*, 7, 5487
- Sun J, Jiang H, Xu Y, Li H, Wu X, Xie Q, Li C (2007) The CCCH-type zinc finger proteins AtSZF1 and AtSZF2 regulate salt stress responses in Arabidopsis. *Plant & cell physiology* 48 (8):1148-1158. doi:10.1093/pcp/pcm088
- Sun Y, Li L, Macho AP, Han Z, Hu Z, Zipfel C, Zhou JM, Chai J (2013) Structural basis for flg22-induced activation of the Arabidopsis FLS2-BAK1 immune complex. *Science (New York, NY)* 342 (6158):624-628. doi:10.1126/science.1243825
- Takekawa M, Tatebayashi K, Saito H (2005) Conserved docking site is essential for activation of mammalian MAP kinase kinases by specific MAP kinase kinase kinases. *Molecular cell* 18 (3):295-306. doi:10.1016/j.molcel.2005.04.001
- Tebaldi T, Re A, Viero G, Pegoretti I, Passerini A, Blanzieri E, Quattrone A (2012) Widespread uncoupling between transcriptome and translome variations after a stimulus in mammalian cells. *BMC Genomics* 13 (1):220. doi:10.1186/1471-2164-13-220
- Tena G, Asai T, Chiu WL, Sheen J (2001) Plant mitogen-activated protein kinase signaling cascades. *Current opinion in plant biology* 4 (5):392-400
- Tierens KF, Thomma BP, Brouwer M, Schmidt J, Kistner K, Porzel A, Mauch-Mani B, Cammue BP, Broekaert WF (2001) Study of the role of antimicrobial glucosinolate-derived isothiocyanates in resistance of Arabidopsis to microbial pathogens. *Plant physiology* 125 (4):1688-1699

- Tyanova S, Temu T, Sinitcyn P, Carlson A, Hein MY, Geiger T, Mann M, Cox J (2016) The Perseus computational platform for comprehensive analysis of (prote)omics data. *Nat Meth* 13 (9):731-740. doi:10.1038/nmeth.3901
- Tzfira T, Vaidya M, Citovsky V (2001) VIP1, an Arabidopsis protein that interacts with Agrobacterium VirE2, is involved in VirE2 nuclear import and Agrobacterium infectivity. *Embo Journal* 20 (13):3596-3607. doi:DOI 10.1093/emboj/20.13.3596
- Wang D, Guo Y, Wu C, Yang G, Li Y, Zheng C (2008) Genome-wide analysis of CCCH zinc finger family in Arabidopsis and rice. *BMC Genomics* 9:44. doi:10.1186/1471-2164-9-44
- Weber C, Nover L, Fauth M (2008) Plant stress granules and mRNA processing bodies are distinct from heat stress granules. *The Plant journal : for cell and molecular biology* 56 (4):517-530. doi:10.1111/j.1365-3113X.2008.03623.x
- Xu G, Greene GH, Yoo H, Liu L, Marques J, Motley J, Dong X (2017) Global translational reprogramming is a fundamental layer of immune regulation in plants. *Nature* 545 (7655):487-490. doi:10.1038/nature22371
- Xu J, Chua NH (2009) Arabidopsis Decapping 5 Is Required for mRNA Decapping, P-Body Formation, and Translational Repression during Postembryonic Development. *The Plant cell* 21 (10):3270-3279. doi:10.1105/tpc.109.070078
- Xu J, Chua NH (2012) Dehydration stress activates Arabidopsis MPK6 to signal DCP1 phosphorylation. *The EMBO journal* 31 (8):1975-1984. doi:10.1038/emboj.2012.56
- Xu J, Yang JY, Niu QW, Chua NH (2006) Arabidopsis DCP2, DCP1, and VARICOSE form a decapping complex required for postembryonic development. *The Plant cell* 18 (12):3386-3398. doi:10.1105/tpc.106.047605
- Xu J, Zhang S (2015) Mitogen-activated protein kinase cascades in signaling plant growth and development. *Trends in plant science* 20 (1):56-64. doi:10.1016/j.tplants.2014.10.001
- Yamaguchi Y, Huffaker A (2011) Endogenous peptide elicitors in higher plants. *Current opinion in plant biology* 14 (4):351-357. doi:10.1016/j.pbi.2011.05.001
- Yeats TH, Rose JK (2013) The formation and function of plant cuticles. *Plant physiology* 163 (1):5-20. doi:10.1104/pp.113.222737
- Yeh YH, Panzeri D, Kadota Y, Huang YC, Huang PY, Tao CN, Roux M, Chien HC, Chin TC, Chu PW, Zipfel C, Zimmerli L (2016) The Arabidopsis Malectin-Like/LRR-RLK IOS1 Is Critical for BAK1-Dependent and BAK1-Independent Pattern-Triggered Immunity. *The Plant cell* 28 (7):1701-1721. doi:10.1105/tpc.16.00313
- Zanetti ME, Chang IF, Gong F, Galbraith DW, Bailey-Serres J (2005) Immunopurification of polyribosomal complexes of Arabidopsis for global analysis of gene expression. *Plant physiology* 138 (2):624-635. doi:10.1104/pp.105.059477
- Zhang J, Li W, Xiang T, Liu Z, Laluk K, Ding X, Zou Y, Gao M, Zhang X, Chen S, Mengiste T, Zhang Y, Zhou JM (2010) Receptor-like cytoplasmic kinases integrate signaling from multiple plant immune receptors and are targeted by a *Pseudomonas syringae* effector. *Cell Host Microbe* 7 (4):290-301. doi:10.1016/j.chom.2010.03.007

7 Appendix I

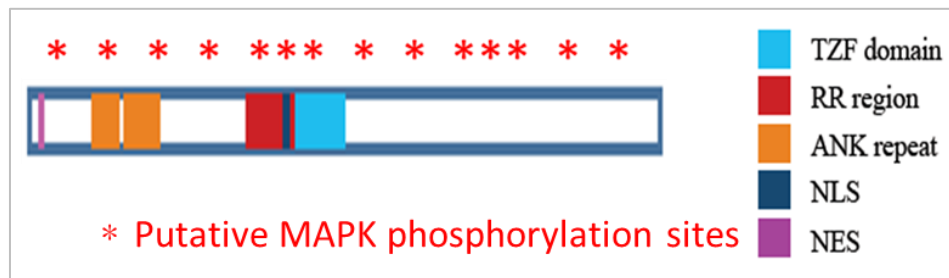


Fig. A1: Representation of domains in TZF9

1	MGVDELSHLK	FSLLESSAC	NDSLGFKSLV	EEEGLESIDG	SGLWYGRRLG
51	SKKMGFEER	T PLMIAALFGS	KEVVDYIIST	GLVDVNRSCG	SDGATALHCA
101	V SGLSANSLE	IVTLLKGS	NPDSCTDAYGN	K GDVIFPCL	SP VFSARMKV
151	LERLLKGNDD	LNEVNGQEEES	EPEVEVEVEV	SP PRGSRERKE	YPVDPTLPDI
201	KNGVYGTDEF	RMYAFKIKPC	SRAYSHDWTE	CPFVHPGENA	RRRDRPKYHY
251	SCV PC PEFRK	GSC SRGDT CE	YAH GIFECWL	HPA QYRTRL C	KDETNC SRRV
301	CFFAHK PEEL	RPLYPSTGSG	VP SP RSSFSS	CNSSTAFDMG	PI SP LPIGAT
351	TP PL SP NGV	SP IGGGK TW	MNWPNI TP PA	LQLPGSRLKS	ALNAREIDFS
401	EEMQSL TSP T	TWNN TPMS SP	FSGKGMNRLA	GGAM SP VNSL	SDMFGTEDNT
451	SGLQIRRSVI	NPQLHSNSLS	SP VGANS LF	SMDSSAVLAS	RAAEFAKQRS
501	QSFIERNNGL	NHHPAISSMT	TTCLNDWGSL	DGKLDWSVQG	DELQKLRKST
551	SFRLRAGGME	SRLPNEG TGL	EEPDVSWVEP	LVKEPQETRL	APVWMEQSYM
601	ETEQTVA				

■ Ankyrin repeat region
■ CCCH-TZF domain
SP/TP putative MPK phosphorylation site

Fig. A2: TZF9 peptide sequence showing Ankyrin region and TZF domain. Red letters are the putative MAPK phosphorylation sites

PhosPhAt

Experiment data: Basic search | Experiment data: Advanced search | Prediction

Proteins to predict: AT2G38280.1, At5g43280.1

Amino acid sequence (online prediction): Prediction by peptide sequence

Multiple online prediction: Select file

Time slot for prediction (hh:mm): 00:30

Insert one or more AGI codes to predict. Example: AT2G38280.1, At5g43280.1

Motif search | Kinase targets: Basic search | Kinase targets: Advanced search | Family search

About **AT5G58620.1** | SQ(pS)FIER | SQ(pS)FIER

Species: Arabidopsis thaliana
 Protein: AT5G58620.1
 Description: zinc finger (CCCH-type) family protein
 MapMan: 27.3.12 RNA.regulation of transcription.C3H zinc finger family
 Substrate for Kinase: AT2G43790.1 - ATPMK6, MPK6, MAPK6, ATMAPK6; MAP kinase 6
 AT3G45640.1 - ATPMK3, MPK3, ATMAPK3; mitogen-activated protein kinase 3

Sequence

```

1..54  M G V D E L S H L A F S L L L E S S A G N D L S G F K S L V E F F G L E S I D G S G L W Y G R R L G
51..100 S K K M G F E E R T P L M I A A L F G S K E V Y D Y I I S T G L Y D V M R S C G S D G A T A L H C A
101..150 V S G L S A N S L E L V T L L L K G S A N P D S O D A Y G N K P G D V I F P C L S P V F S A R M K V
151..200 L E R L L K G N D D L N E V N G Q E E S E P E V E V E V E S P P R G S E R K E Y P V D P T L P D I
201..250 K N G V Y G T D E F R M Y A F K I K P C S R A Y S H D W T E C P F V H P G E N A R R R D P R K Y H Y
251..300 S C V P C P E F R K Q S C S R G T T E Y A T G I F F C W L H P A Q Y R T R L C K D F T I N C S R R V
301..350 C F A H K G E E L R P L Y P S T S V S P R S S F S S O N S S I A F D M G P L S P L P I G A T
351..400 T T P P L S P M G V S S P I G S G K T W M M W P N I T P A L Q L P S R L K S A L I A R E I D F S
401..450 E F M Q S L T S P T T W N I T P M S S P F S K G M H R L A G A M S P V N S L S D M F G T E D N I
451..500 S G L Q T R R S V I N P Q L H S N L S S S P V G A N S L F S M D S S A V L A S R A A E F A K Q R S
501..550 Q S E I E R N N G L N H H P A I S S M T T T C L N D W G S L D G K L D W S V Q G D E L Q L R K S T
551..600 S F R L R A G G M E S R L P N E G T G L E E P D V S W V E P L V K E P Q E T R L A P V W M E Q S Y M
601..654 E T E Q T V A

```

Experiment data for AT5G58620.1

Peptide	Peptide w. Mod	Precursor	Charge	No. pSTY	Search engine	Score	Bins
SQSFIER	SQ(pS)FIER	625.8076172	2	1	other	27.3.12	
SQSFIER	SQ(pS)FIER	625.8076172	2	1	other	27.3.12	
SQSFIER	SQ(pS)FIER	473.7051293	2	1	Sequest	0.78569	27.3.12

Page 1 of 1 | Experiment data 1 - 3 of 3

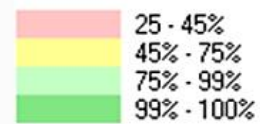
Fig. A3: *In-Silico* prediction of phosphosites inTZF9. Any experimental data was not available (Source: <http://phosphat.uni-hohenheim.de/>)

Identified phosphorylation sites in TZF9 by MPK6: S³²³ and S⁴³⁵

1	11	21	31	41	51	61	71	81	91	101
1	MGVDLSHLK FSLLESSAC NDLSCFKSLV EEEGLESIDG SGLWYCRRLG SIKMGFEERT PLMIAALFCS KEVVDTIIST GLVDVNRSCG SDGATALHCA VSGLSANSL									
111	IVTLLKGS A NPDS CDAYGN KPGDVIFFCL SPVFSARMKV LERLLKQND LNEVNGQES EPEVEVEVEV SPPRCSEK E YPVDPLPDI KNGVYGTDEF RMYAFKIKPC									
221	SPRYSHDWTE CPFVHFGENA RRDPPKHY SCVPCPEERK GSCSGDTCE YANGIFECWL MPAQYRTRLC KDETNCRRV CFFAHKPEEL RPLYPSTGSG VSP ^P SSFS									
331	CNSSTAFDMG PISPLPIGAT TTPPLSPNGV SSPIGGGKTV IONWPNITPPA LQLPGSRKLS ALNAREIDFS EEMQSLTSPT TWNTPMSSP FSGKCHNPLA GGAM ^P SP ^P NSL									
441	SDIQTEDNT SGLQIRRSVI NPQLMSNLS SSPVGNLSL SMDSSAVLRS RAAEFARQPS QSEIERNNGL NQDPRISSMT TTCLNDWGLS DGKLBWSVQG DELQKLRKST									
551	SERLRAGGHE SERLNEGTGL EEPDVSUVEP LVKEPQETRL APVWHEQSYH ETEQTVA									

1	11	21	31	41	51	61	71	81	91	101
1	MGVDLSHLK FSLLESSAC NDLSCFKSLV EEEGLESIDG SGLWYCRRLG SIKMGFEERT PLMIAALEGS KEVVDTIIST GLVDVNRSCG SDGATALHCA VSGLSANSL									
111	IVTLLKGS A NPDS CDAYGN KPGDVIFFCL SPVFSARMKV LERLLKQND LNEVNGQES EPEVEVEVEV SPPRCSEK E YPVDPLPDI KNGVYGTDEF RMYAFKIKPC									
221	SPRYSHDWTE CPFVHFGENA RRDPPKHY SCVPCPEERK GSCSGDTCE YANGIFECWL MPAQYRTRLC KDETNCRRV CFFAHKPEEL RPLYPSTGSG VSP ^P SSFS									
331	CNSSTAFDMG PISPLPIGAT TTPPLSPNGV SSPIGGGKTV IONWPNITPPA LQLPGSRKLS ALNAREIDFS EEMQSLTSPT TWNTPMSSP FSGKCHNPLA GGAM ^P SP ^P NSL									
441	SDIQTEDNT SGLQIRRSVI NPQLMSNLS SSPVGNLSL SMDSSAVLRS RAAEFARQPS QSEIERNNGL NQDPRISSMT TTCLNDWGLS DGKLBWSVQG DELQKLRKST									
551	SERLRAGGHE SERLNEGTGL EEPDVSUVEP LVKEPQETRL APVWHEQSYH ETEQTVA									

PTM Site Probabilities:



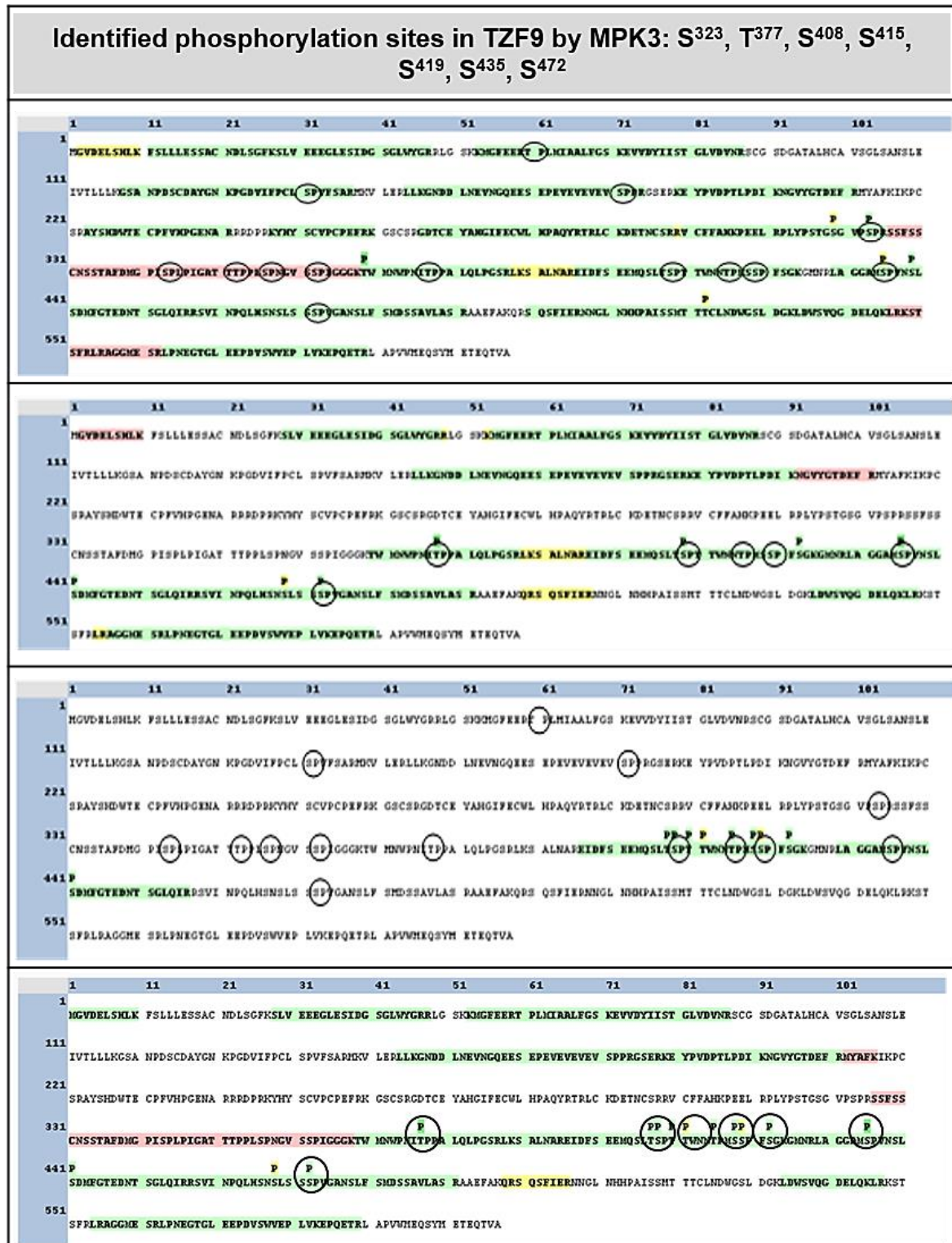
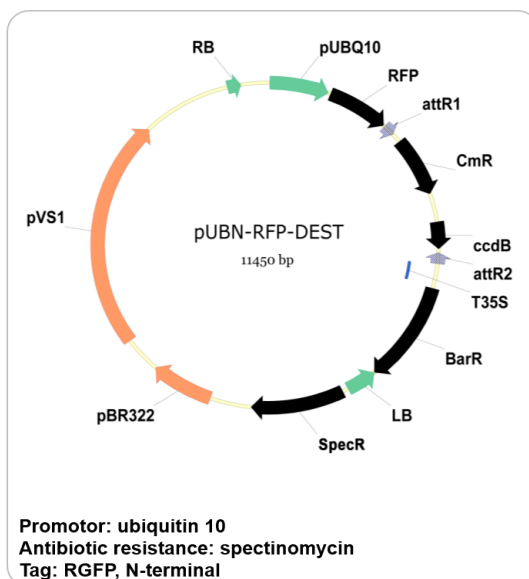
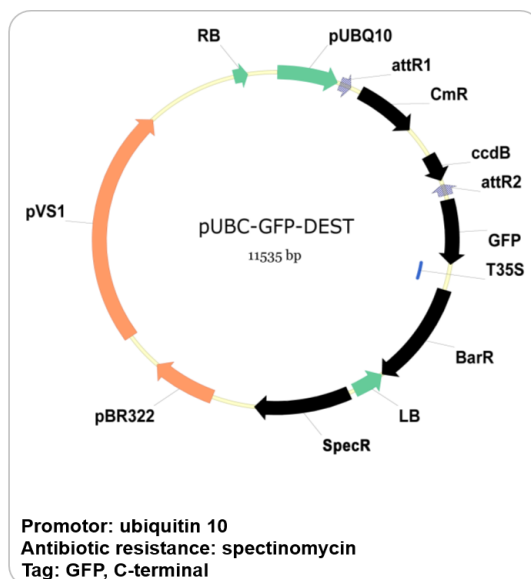
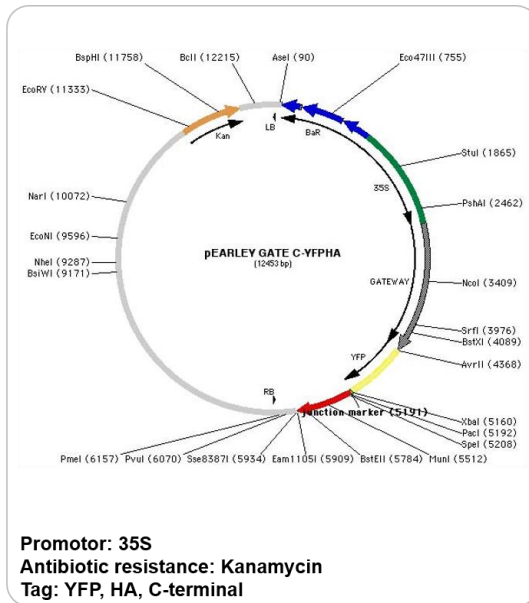
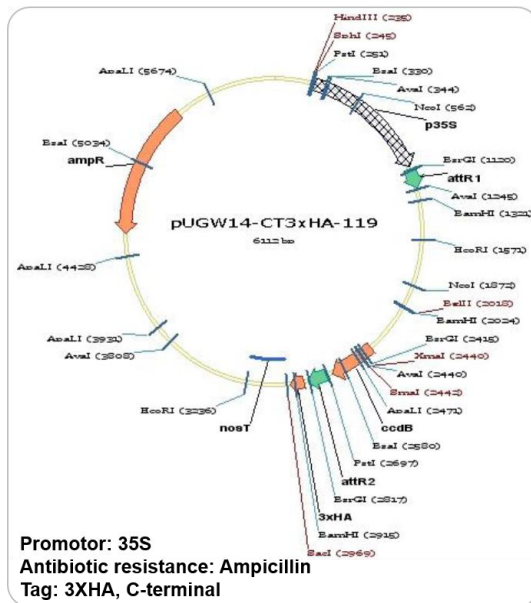
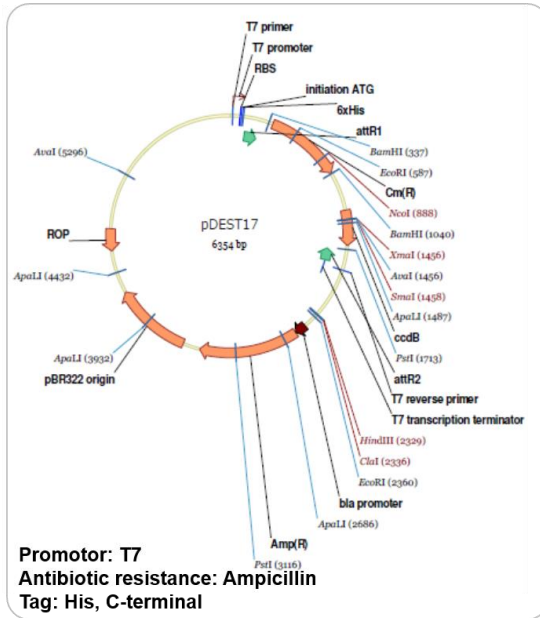
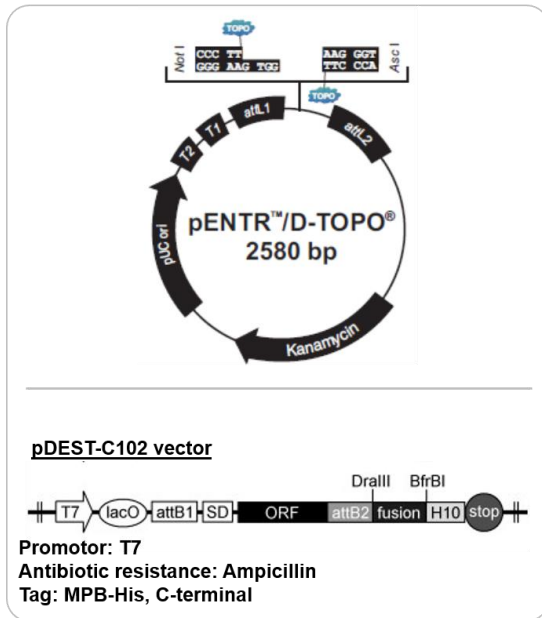


Fig. A4: Summary of phosphorylation sites detected by mass spectrometry. These measurements were performed several times in collaboration with Dr. Hoehenwarter (Leibniz IPB, Halle) but never performed as part of this thesis.



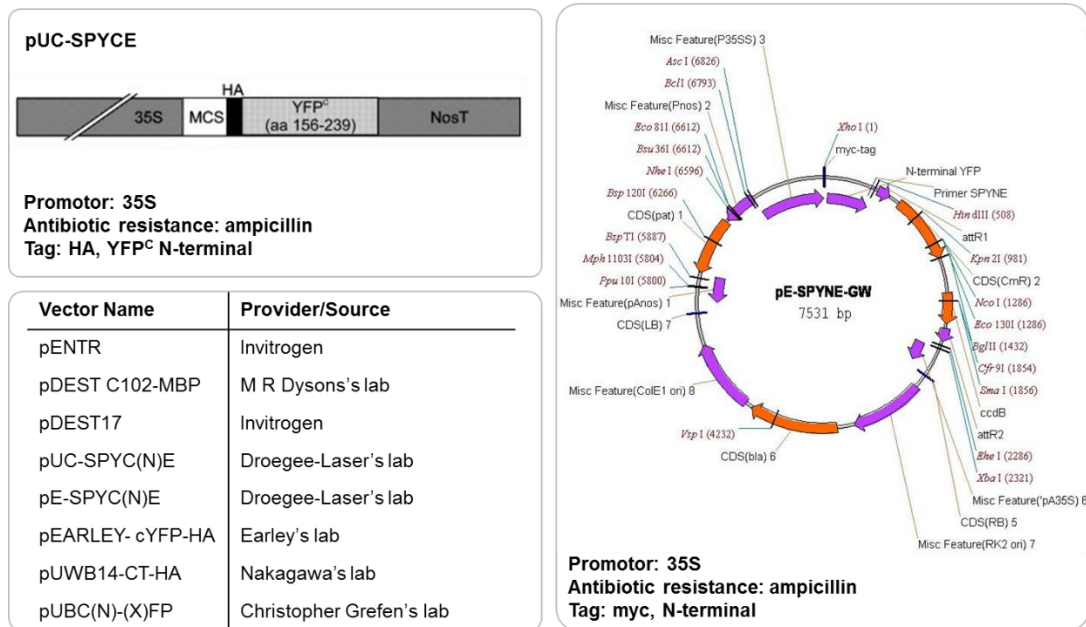


Fig. A5: Vector used in this study

Sequence of 12 Pentaprobates (Bendak, Loughlin et al. 2012)	
PP1	5' -CGGAATTCTA CGAATTTTTC TTTTGTAT TTCCTTTCGC TTTGCTTCTC TTCCTTCGT TCTGTTCCGT TTTACCTTGT CTTGCCTTAT CTTACTTTA-3'
PP2	5' -TATCTTACTT TAGTTTCATT TAATTGTGTT GTACTCTCCT CTGCGTTTAC TTAGCTTAAC TTGGTTTGGC TTGATTGAC TTCAGTTGCG CTCTATTCTA-3'
PP3	5' -CGCTCTATT TACTGTCTG TGCATTCAAT CGTTGAGTTC GATCTAGTCT CGTCTAACC TCCCTGCTC CGTGGTCTG GCCTCGCCTA TCCTACCCAT-3'
PP4	5' -TATCCTACCC ATTGGGCTCA TCTGATCCAT CCGGTCCCGT CCACTCGGCT ATGTTATGCT GTATTGCAGT CGTGTCCGCT CGAGCTGCC TAATCCCACC-3'
PP5	5' -CTAATCCCA CCTAGCGTAT CGGGTCATGT AGTGCTACGT TACGGCCCCG CCCGGCATCA TATTATATCA CCCAGTGA ATGTGGTGTG AGGTTGGAG-3'
PP6	5' -GTGAGGTTGG AGTCCGACCT GGAATCTCAG CTTGACGTGC CATGCGGTGC GATGTCACGC CGCGCCACGG TATAGTATGG TACGGGATCC CG-3'
PP7	5' -TAAAGTAAGA TAAGGCAAGA CAAGGTA AAA CGGAACAGAA CCGAAGGGAA GAGAAGCAA GCGAAAGGAA ATAAACAAA GAAAAATTC TAGAATCCG-3'
PP8	5' -TAGAATAGAG CGCAACTGAA GTCAAATCAA GCCAAACCA GTTAAGCTAA GTGAACGACG AGGAGAGTAC AACACAATTA AATGAACTA AAGTAAGATA-3'
PP9	5' -ATGGGTAGGA TAGCGGAGGC CAGACCAGCG GAGCAGGGGA GGGTTAGACG AGACTAGATC GAACTCAACG ATTGAATGCA CAGGACAGTA GAATAGAGCG-3'
PP10	5' -GGTGGGATTA GGCAGCTCG ACGCAGACAG ACTGCAATAC AGCATAACAT AGCCGAGTGG ACGGGACCG ATGGATCAGA TGAGCCCAAT GGGTAGGATA-3'
PP11	5' -CTCCAACCTC ACACCACATT ACACTGGGT GATATAATAT GATGCCGGG GGGGGCGTA ACGTAGCACT ACATGACCCG ATACGCTAGG TGGATTAGG-3'
PP12	5' -CGGGATCCCG TACCATACTA TACCGTGCG CGCGTGACA TCGACCAGCA TGGCAGTCA GGCTGAGATT CCAGGTCGGA CTCCAACCTC AC-3'

Fig. A6: Nucleotide sequence of pentaprobates (PP1 to PP12)

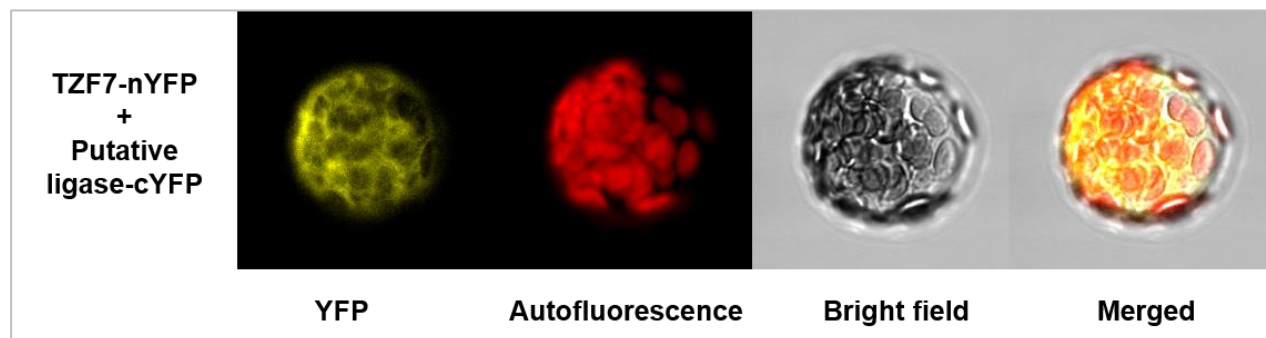


Fig. A7: BiFC showing interaction between TZF7 and putative RNA ligase (At5G58620)

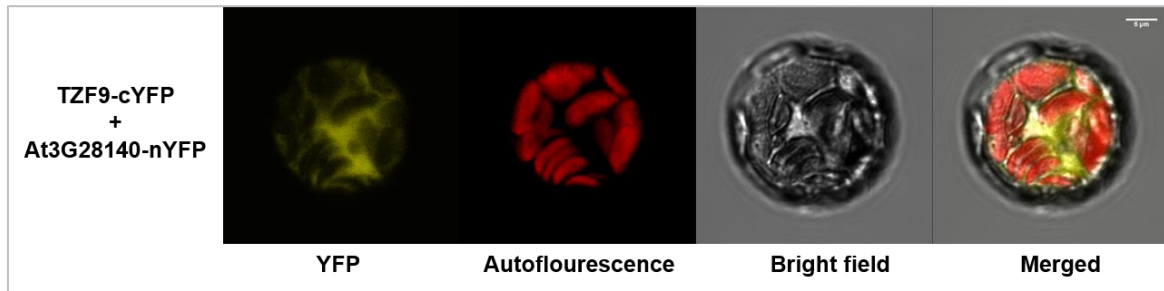


Fig. A8: BiFC showing interaction between TZF9 and homologous putative RNA ligase (At3G28140)

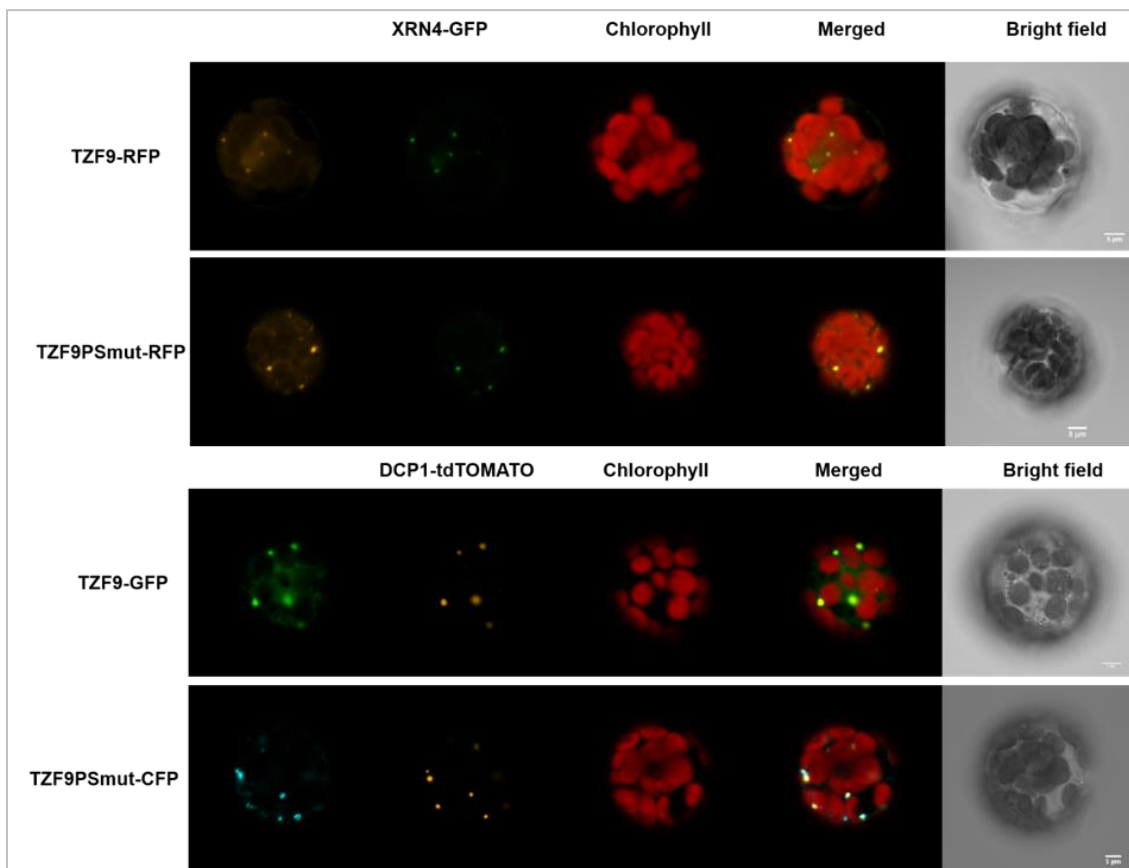


Fig. A9: TZF9-WT and TZF9-PS mutant colocalizes with PB marker protein

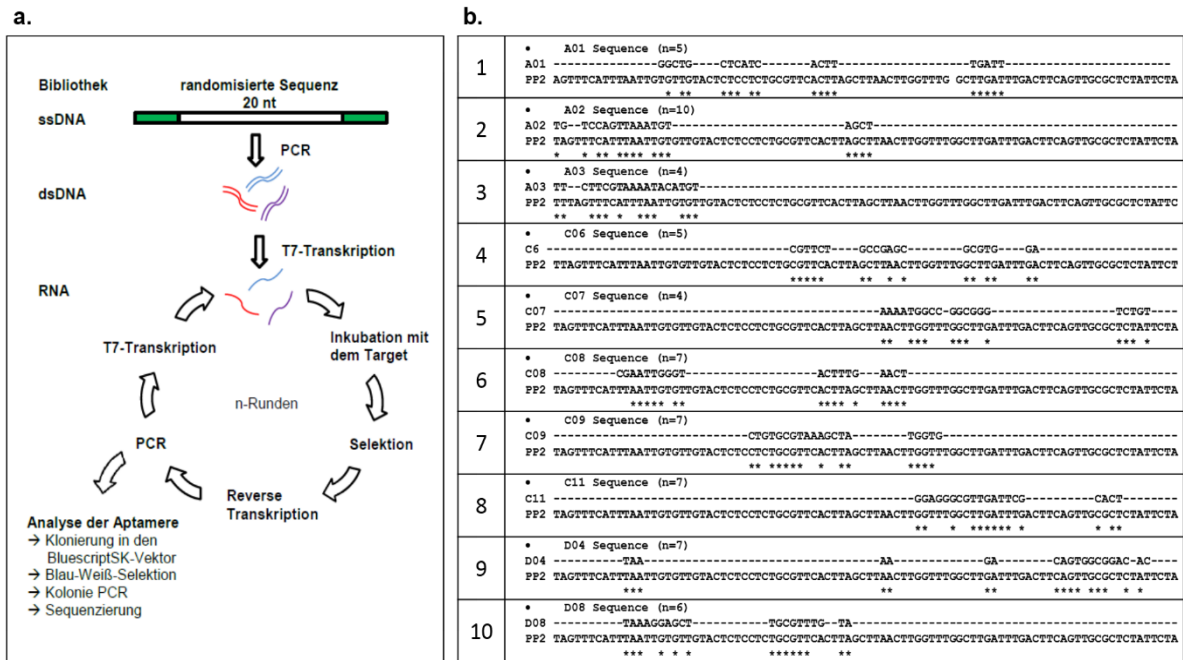


Fig. A10: (a) Method of SELEX experiment. (Source master thesis, Martina Brode). **(b)** Alignment of pentaprobe 2 to SELEX sequences

Table A1: List of primers with Tm

Purpose	Name of the primers	Oligonucleotide sequence	Tm (°C)
	AT5G40190F	5'-CACCATGTCAGAAGGCTACGCAA-3'	62.4
	AT5G40190R-with stop	5'-TCAAGACTCCAAAGTGTTACCAAGA-3'	59.7
	AT5G40190R-no stop	5'-AGACTCCAAAGTGTTACCAAGA-3'	59.7
Cloning and sequencing	At3G28140_fwd	5'-TCCACCTCCTTCTTCGATTCAACG-3'	62.7
	At3G28140_rev	5'-ACAGAGAAAGCCTCAGCCATACGA-3'	62.7
	TZF9_Int_F	5'-TGTTTCTTTGCCACAAACC-3'	55.2
	TZF9_Int_R	5'-GGTTTGTGGGCAAAGAAACA-3'	55.2
	M13 F	5'-GTA AACGACGGCCAGT-3'	52.8
	M13 R	5'-GGAAACAGCTATGACCATG-3'	54.5
	LBa1	5'-TGGTTCACGTAGTGGCCATCG-3'	64
	TZF9-LPNSC	5'-TGTGTCCCTTGTCTGAATTC-3'	60
	TZF9-RPNSC	5'-GACTTTGCTTCTTGTGGAACG-3'	60
	35S promoter-F	5'-CTATCCTTCGCAAGACCCTTC-3'	59.8
Genotyping	FLAG-R	5'-CTTGTCATCGTCATCCTTGTAATC-3'	59.3
	SALK_084396_LP	5'-TAAGAAACGCGCATCATTGTC-3'	55.9
	SALK_084396_RP	5'-CGACTTTGACTACAACACAGAGC-3'	60.6
	SALK_084402_LP	5'-TTGCCTTTTGTGTTTACGTCC-3'	55.9
	SALK_084402_RP	5'-CGAACAGGAGAAAACCTCAACG-3'	57.9

	qRT-PUB22-LP	5'-CAGAGAGAAGGAATTCAGAGATGG-3'	59
	qRT-PUB22-RP	5'-CCTTCTGCGCACTGACATAA-3'	59
	qRT-WRKY22-LP	5'-CCAGTGGCTCCAATACCTCT-3'	59
	qRT-WRKY22-RP	5'-ATGCCCAGACATCGGAGTT-3'	59
	qRT-ERF019-LP	5'-CGTGACCGTCTCTGGTTAGG-3'	59
	qRT-ERF019-RP	5'-CAGAAGAAAGCAACGTCGTG-3'	59
	qRT-chitinase-LP	5'-TTCTACACTCGCCAGGCTTT-3'	59
Quantitative real	qRT-chitinase-RP	5'-GGTTCCTTTATAGGCGTCGAA-3'	59
time PCR	qRT-PBS1-LP	5'-CAATAACATATCTGGACTCCCTTCA-3'	59
	qRT-PBS1-RP	5'-TCCTCCATTGGTCTTTGAGC-3'	59
	qRT-BIK1-LP	5'-TCCGATCTCCGTTCCACATCT-3'	59
	qRT-BIK1-RP	5'-TTCAACCCACAAGGCAAAA-3'	59
	qRT-FRK1-LP	5'-GAGACTATTTGGCAGGTAAAAGGT-3'	59
	qRT-FRK1-RP	5'-AGGAGGCTTACAACCATTGTG-3'	59
	qRT-IOS1-LP	5'-ATCCCTGCAACTCTCCTTGA-3'	59
	qRT-IOS1-RP	5'-GAACAAAGCCCGGTATTTCC-3'	59

	S472A-5	5'-TCGCCTGTGGGAGCCAATTCTCTG-3'	66.1
	S141A-3	5'-ACCGGCGCCAAACAAGGGAAAATC-3'	64.4
	S141A-5	5'-AGGCCGGTTTTTAGCGCGAGG-3'	63.7
Generation of	S323A-3	5'-CGCGGCGCCGGAACACCTGATCC-3'	71.3
phosphonull	S323A-5	5'-TCGCCGCGGTCTTCCTTCTCATC-3'	66
mutant (site	T352A/s356A/S362A-		
directed	3	5'-ACCGTTAGGCGCCAAAGGAGGTGCGGTTG-3'	72.3
mutagenesis)	T352A/s356A/S362A-		
	5	5'-CTAACGGTGTATCCGCTCCAATAG-3'	62.7
	S472A-3	5'-ACAGGCGCCGAAGAAAGACTGTTGGA-3'	66.4

	A60T-F (M1F)	5'-aaaaaaGAAGACACGCCTTATGATTGCTGCC-3'	59.8
	A60T-R (M1R)	5'-aaaaaaGAAGACAGAGGCTCCCTCCTCAAAACCC-3'	70.6
	A141S-F (M2F)	5'-aaaaaaGAAGACAGTCCGGTTTTTAGCGCGAGG-3'	68.2
Generation of	A141S-R (M2R)	5'-aaaaaaGAAGACACCGGACTCAAACAAGGGAAAATC-3'	67.2
one WT	A181S-F (M3F)	5'-aaaaaaGAAGACTCGCCTCCTCGGGGTCTGAGAG-3'	71.3
phosphosite	A181S-R (M3R)	5'-aaaaaaGAAGACGGAGGCGAAACCTCAACCTCAACC-3'	70.6
(site directed	A323S-F (M4F)	5'-aaaaaaGAAGACTCGCCGCGGTCTTCCTTCTCATC-3'	70.6
mutagenesis)	A323S-R (M4R)	5'-aaaaaaGAAGACCGGGGACGGAACACCTGATCC-3'	73
	G343S-F (M5F)	5'-aaaaaaGAAGACAGTCCGCTTCTATCGGAGCAAC-3'	69.5
	G343S-R (M5R)	5'-aaaaaaGAAGACAGCGGACTAATCGGTCCCATGTGCG-3'	70.6
	A352S-F (M6F)	5'-aaaaaaGAAGACCTAACGGTGTATCCgCTCCAATAG-3'	64.6

A352S-R (M6R)	5'- aaaaaaGAAGACACCGTTAGGCGCCAAAGGAGGTGTGGTTG- 3'	73.4
A356S-F (M7F)	5'-aaaaaaGAAGACCTAACGGTGTATCCGCTCCAATAG-3'	64.6
A356S-R (M7R)	5'- aaaaaaGAAGACACCGTTAGGACTCAAAGGAGGTGcGGTTG- 3'	72.4
A362S-R (M8R)	5'-aaaaaaGAAGACCTAACGGTGTATCCTCTCCAATAG-3'	67.2
A362S-R (M8R)	5'- aaaaaaGAAGACACCGTTAGGCGCCAAAGGAGGTGcGGTTG- 3'	72.3
G377T-F (M9F)	5'-aaaaaaGAAGACACCCCTCCTGCATTGCAGCT-3'	68.2
G377T-R (M9R)	5'-aaaaaaGAAGACGGAGGGTTATGTTAGGCCAG-3'	68.2
A408S-F (M10F)	5'- aaaaaaGAAGACGGAACAACGCGCCAATGTCAGCTCCATTCT CC-3'	72
A408S-R (M10R)	5'-aaaaaaGAAGACGTTGTTCCATGTAGTTGGAGAAGTAAG-3'	67.4
A415T-F (M11F)	5'- aaaaaaGAAGACGGAACAACACGCCAATGTCAGGCTCCATTC TCC-3'	73.2
A415T-R (M11R)	5'-aaaaaaGAAGACGTTGTTCCATGTAGTTGGCGCAGTAAG-3'	65
A419S-F (M12F)	5'- aaaaaaGAAGACGGAACAACGCGCCAATGTCATCTCCATTCT C-3'	72.3
A419S-R (M12R)	5'-aaaaaaGAAGACGTTGTTCCATGTAGTTGGCGCAGTAAG-3'	66.6
A435S-F (M13F)	5'-aaaaaaGAAGACAGCCCGGTGAATAGTCTCAGTGAT-3'	68.3
A435S-R (M13R)	5'-aaaaaaGAAGACACCGGGCTCATTGCTCCTCCT-3'	69.5
A472S-F (M14F)	5'-aaaaaaGAAGACTCACCTGTGGGAGCCAATTCTCTG-3'	69.5
A472S-R (M14R)	5'-aaaaaaGAAGACACAGGTGATGAAGAAAGACTGTTGGA-3'	67.3

Table A2: PCR condition for genotyping

Steps	Temperature (°C)	Time
Initial denaturation	95	3'
Denaturation	95	30''
Annealing	55	30''
Extension	74	1-2'
Final extension	74	5'

Table A3: Condition for colony PCR

Steps	Temperature (°C)	Time
Initial denaturation	95	3'
Denaturation	95	30''
Annealing	-	30''
Extension	74	1min/kb
Final extension	74	5'

Table A4: Condition for gene amplification (cloning)

Steps	Temperature (°C)	Time
Initial denaturation	98	30''
Denaturation	98	10''
Annealing	-	30''
Extension	74	30s/kb
Final extension	74	5'

Table A5: Condition for qRT PCR

Steps	Temperature (°C)	Time
Enzyme activation	95	15''
PCR (40)	95	15''
	64	40''
	95	2'
Melting curve	55	30'
	95	30''

Table A6: GO term enrichment of genes upregulated in *tzf9* (Transcriptome, uninduced)

GO_acc	Term	Query item [#]	Query total ^{##}	Bg item [*]	Bg total ^{**}	P value	FDR
GO:0006950	response to stress	69	318	2320	37767	7.50E-20	7.20E-17
GO:0050896	response to stimulus	91	318	4057	37767	2.20E-18	1.10E-15
GO:0010033	response to organic substance	44	318	1342	37767	3.50E-14	1.10E-11
GO:0042221	response to chemical stimulus	54	318	2085	37767	3.50E-13	8.30E-11
GO:0010200	response to chitin	16	318	151	37767	1.00E-12	2.00E-10
GO:0009743	response to carbohydrate stimulus	17	318	240	37767	7.60E-11	1.20E-08
GO:0009611	response to wounding	14	318	197	37767	3.50E-09	4.80E-07
GO:0005982	starch metabolic process	8	318	41	37767	7.20E-09	8.70E-07
GO:0009251	glucan catabolic process	6	318	15	37767	1.60E-08	1.50E-06
GO:0009719	response to endogenous stimulus	30	318	1068	37767	1.70E-08	1.50E-06
GO:0005983	starch catabolic process	6	318	15	37767	1.60E-08	1.50E-06
GO:0009628	response to abiotic stimulus	36	318	1471	37767	1.80E-08	1.50E-06
GO:0006970	response to osmotic stress	18	318	408	37767	2.60E-08	1.90E-06
GO:0044247	cellular polysaccharide catabolic process	6	318	17	37767	2.90E-08	2.00E-06
GO:0009607	response to biotic stimulus	22	318	638	37767	5.10E-08	3.10E-06
GO:0000272	polysaccharide catabolic process	6	318	19	37767	5.00E-08	3.10E-06
GO:0009651	response to salt stress	16	318	366	37767	1.80E-07	9.90E-06
GO:0009605	response to external stimulus	17	318	429	37767	2.70E-07	1.50E-05
GO:0009617	response to bacterium	13	318	247	37767	3.50E-07	1.70E-05
GO:0051707	response to other organism	20	318	599	37767	3.40E-07	1.70E-05
GO:0009753	response to jasmonic acid stimulus	12	318	215	37767	5.50E-07	2.50E-05
GO:0042742	defense response to bacterium	11	318	177	37767	6.00E-07	2.60E-05

GO:0048583	regulation of response to stimulus	11	318	188	37767	1.10E-06	3.70E-05
GO:0002376	immune system process	15	318	368	37767	9.90E-07	3.70E-05
GO:0044262	cellular carbohydrate metabolic process	16	318	417	37767	9.30E-07	3.70E-05
GO:0006952	defense response	22	318	766	37767	1.00E-06	3.70E-05
GO:0006955	immune response	15	318	367	37767	9.60E-07	3.70E-05
GO:0006073	cellular glucan metabolic process	8	318	87	37767	1.40E-06	4.60E-05
GO:0009737	response to abscisic acid stimulus	15	318	378	37767	1.40E-06	4.60E-05
GO:0009725	response to hormone stimulus	25	318	982	37767	1.60E-06	5.00E-05
GO:0044042	glucan metabolic process	8	318	89	37767	1.60E-06	5.10E-05
GO:0034641	cellular nitrogen compound metabolic process	17	318	506	37767	2.40E-06	7.20E-05

#Bg total: Total number of genes in background

##Bg item: Number of genes enriched for the given category in background

*Query total: Total number of DEGs in input list

**Query item: Number of DEGs enriched for a given category in input list

Table A6.1. Some representative defense/stress responsive genes upregulated in *tzf9* Transcriptome, uninduced)

Gene_ids	Desc.TAIR10	SP.Function.	Coef.mu_ctrl .wt_ctrl
AT5G45110.1	NPR1-like protein 3	May act as a substrate-specific adapter of an E3 ubiquitin-protein ligase complex (CUL3-RBX1-BTB) which mediates the ubiquitination and subsequent proteasomal degradation of target proteins (By similarity). Involved in the regulation of basal defense responses against pathogens. {ECO:0000250, ECO:0000269 PubMed:17076807}.	1.426

AT1G29690.1	MAC/Perforin domain-containing protein	Negatively controls the salicylic acid (SA)-mediated pathway of programmed cell death in plant immunity. {ECO:0000269 PubMed:15799997}.	1.026
AT2G38470.1	WRKY DNA-binding protein 33	Transcription factor. Interacts specifically with the W box (5'-TTGAC[CT]-3'), a frequently occurring elicitor-responsive cis-acting element. Involved in defense responses. Required for resistance to the necrotrophic fungal pathogen <i>B.cinerea</i> (PubMed:17059405, PubMed:21990940). Regulates the antagonistic relationship between defense pathways mediating responses to the bacterial pathogen <i>P. syringae</i> and the necrotrophic pathogen <i>B.cinerea</i> (PubMed:17059405). Required for the phytoalexin camalexin synthesis following infection with <i>B.cinerea</i> . Acts as positive regulator of the camalexin biosynthetic genes PAD3 (CYP71B15) and CYP71A13 by binding to their promoters (PubMed:21498677, PubMed:22392279). Acts downstream of MPK3 and MPK6 in reprogramming the expression of camalexin biosynthetic genes, which drives the metabolic flow to camalexin production (PubMed:21498677). Functions with WRKY25 as positive regulator of salt stress response and abscisic acid (ABA) signaling (PubMed:18839316). Functions with WRKY25 and WRKY26 as positive regulator of plant thermotolerance by partially participating in ethylene-response signal transduction pathway (PubMed:21336597). The DNA-binding activity of WRKY33 is increased by SIB1 and SIB2 (PubMed:21990940). {ECO:0000269 PubMed:18839316, ECO:0000269 PubMed:21336597, ECO:0000269 PubMed:21498677, ECO:0000269 PubMed:21990940, ECO:0000269 PubMed:22392279}.	2.324
AT1G27730.1	salt tolerance zinc finger	Transcriptional repressor involved in abiotic stress responses. Can repress the stress responsive genes DREB1A and LTI78. Probably involved in jasmonate (JA) early signaling response. May regulate the expression of the JA biosynthesis gene LOX3 and control the expression of TIFY10A/JAZ1, a key repressor in the JA signaling cascade. {ECO:0000269 PubMed:12032082, ECO:0000269 PubMed:15333755, ECO:0000269 PubMed:17112521, ECO:0000269 PubMed:18216250, ECO:0000269 PubMed:20140232, ECO:0000269 PubMed:8662738}.	1.557
AT1G21326.1	VQ motif-containing protein	Regulator of plant defense response. May contribute to MPK4-regulated defense activation by coupling the kinase to specific WRKY transcription factors. {ECO:0000269 PubMed:15990873}.	1.202

AT3G15210.1	ethylene responsive element binding factor 4	Acts as a transcriptional repressor. Binds to the GCC-box pathogenesis-related promoter element. Involved in the regulation of gene expression by stress factors and by components of stress signal transduction pathways, and could also regulate other AtERFs. {ECO:0000269 PubMed:10715325, ECO:0000269 PubMed:11487705, ECO:0000269 PubMed:9756931}.	1.2
AT3G55980.1	salt-inducible zinc finger 1	Involved in salt stress response. May positively modulate plant tolerance to salt stress. {ECO:0000269 PubMed:17609218}.	1.101
AT5G66070.1	RING/U-box superfamily protein	May be involved in the early steps of the plant defense signaling pathway.	1.042
AT5G47220.1	ethylene responsive element binding factor 2	Acts as a transcriptional activator. Binds to the GCC-box pathogenesis-related promoter element. Involved in the regulation of gene expression by stress factors and by components of stress signal transduction pathways. Involved in disease resistance pathways. {ECO:0000269 PubMed:10715325, ECO:0000269 PubMed:12805630, ECO:0000269 PubMed:9756931}.	1.289
AT1G28370.1	ERF domain protein 11	Involved in the regulation of gene expression by stress factors and by components of stress signal transduction pathways. Transcription factor that binds to the GCC-box pathogenesis-related promoter element. Acts as a transcriptional inhibitor and may regulate other AtERFs (By similarity). {ECO:0000250, ECO:0000269 PubMed:11487705}.	1.163
AT2G31880.1	Leucine-rich repeat protein kinase family protein	Dual specificity kinase acting on both serine/threonine- and tyrosine-containing substrates. Promotes the activation of plant defense and cell death. Functions as an inhibitor/regulator of abscission, probably by regulating membrane trafficking during abscission. {ECO:0000269 PubMed:19616764, ECO:0000269 PubMed:20081191}.	1.372
AT4G37910.1	mitochondrial heat shock protein 70-1	In cooperation with other chaperones, Hsp70s stabilize preexistent proteins against aggregation and mediate the folding of newly translated polypeptides in the cytosol as well as within organelles. These chaperones participate in all these processes through their ability to recognize nonnative conformations of other proteins. They bind extended peptide segments with a net hydrophobic character exposed by polypeptides during translation and membrane translocation, or following stress-induced damage (By similarity). {ECO:0000250}.	1.054

AT4G19660.1	NPR1-like protein 4	May act as a substrate-specific adapter of an E3 ubiquitin-protein ligase complex (CUL3-RBX1-BTB) which mediates the ubiquitination and subsequent proteasomal degradation of target proteins (By similarity). Involved in the regulation of basal defense responses against pathogens, and may be implicated in the cross-talk between the SA- and JA-dependent signaling pathways. {ECO:0000250, ECO:0000269 PubMed:15634206, ECO:0000269 PubMed:17076807}.	1.54
AT1G52400.1	beta glucosidase 18	Hydrolyzes abscisic acid glucose ester (ABA-GE) which represents the predominant form of conjugated ABA (biologically inactive). No activity with beta-D-glucopyranosyl zeatin. The hydrolysis of ABA-GE in the endoplasmic reticulum (ER) forms free ABA and contributes to increase its cellular levels under dehydration conditions. ABA-GE hydrolyzing activity is enhanced by dehydration stress-induced polymerization into higher molecular weight forms. The ABA produced by BGLU18 contributes to the initiation of intracellular signaling as well as the increase in the extracellular ABA level. {ECO:0000269 PubMed:16990135, ECO:0000269 PubMed:17923167}.	1.817
AT2G39030.1	Acyl-CoA N-acyltransferases (NAT) superfamily protein	Acetyltransferase that converts ornithine to N5-acetylornithine, which is likely used in plant defense. {ECO:0000269 PubMed:21917546}.	1.911

Table A7: GO term enrichment of genes downregulated in *tzf9* (Transcriptome, uninduced)

GO_acc	Term	query item	query total	bg item	bg total	p value	FDR
GO:0050896	response to stimulus	50	152	4057	37767	2.30E-13	1.30E-10
GO:0009698	phenylpropanoid metabolic process	12	152	175	37767	1.60E-11	4.40E-09
GO:0009699	phenylpropanoid biosynthetic process	11	152	141	37767	3.20E-11	4.40E-09
GO:0019748	secondary metabolic process	17	152	489	37767	2.70E-11	4.40E-09
GO:0009628	response to abiotic stimulus	26	152	1471	37767	3.00E-10	3.30E-08
GO:0042398	cellular amino acid derivative biosynthetic process	12	152	233	37767	3.70E-10	3.40E-08

GO:0006575	cellular amino acid derivative metabolic process	13	152	315	37767	8.90E-10	6.40E-08
GO:0006950	response to stress	32	152	2320	37767	9.30E-10	6.40E-08
GO:0019438	aromatic compound biosynthetic process	11	152	237	37767	5.80E-09	3.60E-07
GO:0009058	biosynthetic process	46	152	5118	37767	8.00E-08	4.30E-06
GO:0042221	response to chemical stimulus	27	152	2085	37767	8.40E-08	4.30E-06
GO:0006725	cellular aromatic compound metabolic process	12	152	399	37767	1.20E-07	5.40E-06
GO:0044249	cellular biosynthetic process	44	152	4925	37767	2.00E-07	8.80E-06
GO:0006519	cellular amino acid and derivative metabolic process	14	152	682	37767	9.20E-07	3.60E-05
GO:0010033	response to organic substance	19	152	1342	37767	2.40E-06	9.00E-05

Bg total: Total number of genes in background

Bg item: Number of genes enriched for the given category in background

Query total: Total number of DEGs in input list

Query item: Number of DEGs enriched for a given category in input list

Table A7.1. Some representative defense/stress responsive genes downregulated in *tzf9* (Transcriptome, uninduced)

Gene_ids	Desc.TAIR10	SP.Function	Coef.mu_ctrl .wt_ctrl
AT2G43620.1	Chitinase family protein	Defense against chitin-containing fungal pathogens.	-2.291
AT4G01250.1	WRKY family transcription factor	Transcription factor involved in the expression of defense genes in innate immune response of plants. Interacts specifically with the W box (5'-(T)TGAC[CT]-3'), a frequently occurring elicitor-responsive cis-acting element. Activates WRKY 29, SIRK and its own promoters. {ECO:0000269 PubMed:11875555}.	-2.266
AT3G52450.1	plant U-box 22	E3 ubiquitin-protein ligase that negatively regulates water stress response. May control in coordination with PUB23 a drought signaling pathway by ubiquitinating cytosolic RPN12a. Acts as negative regulator of the immunity triggered by the pathogen-associated molecular patterns (PAMPs), in	-2.173

		association with PUB23 and PUB24. {ECO:0000269 PubMed:18664614, ECO:0000269 PubMed:18771922}.	
AT5G64120.1	Peroxidase superfamily protein	Removal of H ₂ O ₂ , oxidation of toxic reductants, biosynthesis and degradation of lignin, suberization, auxin catabolism, response to environmental stresses such as wounding, pathogen attack and oxidative stress. These functions might be dependent on each isozyme/isoform in each plant tissue.	-2.148
AT5G05440.1	Polyketide cyclase/dehydrase and lipid transport superfamily protein	Receptor for abscisic acid (ABA) required for ABA-mediated responses such as stomatal closure and germination inhibition. Inhibits the activity of group-A protein phosphatases type 2C (PP2Cs) in an ABA-independent manner but more efficiently when activated by ABA. Confers enhanced sensitivity to ABA (PubMed:19407143, PubMed:19624469, PubMed:23844015, PubMed:21658606). Can be activated by both (-)-ABA and (+)-ABA (PubMed:23844015). {ECO:0000269 PubMed:19407143, ECO:0000269 PubMed:19624469, ECO:0000269 PubMed:21658606, ECO:0000269 PubMed:23844015}.	-1.862
AT3G54420.1	homolog of carrot EP3-3 chitinase	Defense against chitin-containing fungal pathogens.	-1.837
AT1G22810.1	Integrase-type DNA-binding superfamily protein	Probably acts as a transcriptional activator. Binds to the GCC-box pathogenesis-related promoter element. May be involved in the regulation of gene expression by stress factors and by components of stress signal transduction pathways (By similarity). {ECO:0000250}.	-1.576
AT4G17090.1	chloroplast beta-amylase	Beta-amylase activity. No alpha-amylase activity. Involved in cold resistance. Mediates the accumulation of maltose upon freezing stress, thus contributing to the protection of the photosynthetic electron transport chain. Plays a role in the circadian-regulated starch degradation and maltose metabolism in chloroplasts, especially at night. More active on phosphorylated glucan. Interacts directly with starch or other alpha-1,4-glucan. {ECO:0000269 PubMed:10652124, ECO:0000269 PubMed:16055686, ECO:0000269 PubMed:16297066, ECO:0000269 PubMed:17631522, ECO:0000269 PubMed:18390594, ECO:0000269 PubMed:19664588}.	-1.506

AT4G37770.1	1-amino-cyclopropane-1-carboxylate synthase 8	1-aminocyclopropane-1-carboxylate synthase (ACS) enzymes catalyze the conversion of S-adenosyl-L-methionine (SAM) into 1-aminocyclopropane-1-carboxylate (ACC), a direct precursor of ethylene.	-1.388
AT3G30775.1	Methylenetetrahydrofolate reductase family protein	Converts proline to delta-1-pyrroline-5-carboxylate. {ECO:0000269 PubMed:20403182, ECO:0000269 PubMed:9847097}.	-1.374
AT5G39580.1	Peroxidase superfamily protein	Removal of H ₂ O ₂ , oxidation of toxic reductants, biosynthesis and degradation of lignin, suberization, auxin catabolism, response to environmental stresses such as wounding, pathogen attack and oxidative stress. These functions might be dependent on each isozyme/isoform in each plant tissue.	-1.344
AT1G17100.1	SOUL heme-binding family protein	Can promote mitochondrial permeability transition and facilitate necrotic cell death under different types of stress conditions. Does not bind hemin. {ECO:0000269 PubMed:17098234}.	-1.308
AT1G70000.2	myb-like transcription factor family protein	Binds selectively to the DNA sequence 5'-[GA]GATAA-3' and may act as a transcription factor involved in the regulation of drought-responsive genes. Enhances stomatal closure in response to abscisic acid (ABA). Confers drought and salt tolerance. {ECO:0000269 PubMed:21030505}.	-1.301
AT3G08730.1	protein-serine kinase 1	Downstream effector of TOR signaling pathway involved in osmotic stress response. Could be involved in the control of plant growth and development. Phosphorylates the ribosomal proteins P14, P16 and S6. Functions as a repressor of cell proliferation and required for maintenance of chromosome stability and ploidy levels through the RBR1-E2F pathway. {ECO:0000269 PubMed:20683442}.	-1.288
AT2G44940.1	Integrase-type DNA-binding superfamily protein	Probably acts as a transcriptional activator. Binds to the GCC-box pathogenesis-related promoter element. May be involved in the regulation of gene expression by stress factors and by components of stress signal transduction pathways (By similarity). {ECO:0000250}.	-1.13

Table A8: GO term enrichment of genes upregulated in *tzf9* (Translatome, uninduced)

GO_acc	Term	Query item	Query total	Bg item	Bg total	p-value	FDR
GO:0050896	response to stimulus	145	576	4057	37767	3.70E-22	4.80E-19
GO:0042221	response to chemical stimulus	89	576	2085	37767	7.80E-18	5.00E-15
GO:0010033	response to organic substance	67	576	1342	37767	1.10E-16	4.80E-14
GO:0009611	response to wounding	24	576	197	37767	5.70E-14	1.80E-11
GO:0006950	response to stress	86	576	2320	37767	7.50E-14	1.90E-11
GO:0009605	response to external stimulus	32	576	429	37767	1.10E-12	2.00E-10
GO:0009719	response to endogenous stimulus	52	576	1068	37767	9.30E-13	2.00E-10
GO:0009725	response to hormone stimulus	40	576	982	37767	5.00E-08	8.10E-06
GO:0016054	organic acid catabolic process	12	576	98	37767	1.10E-07	1.30E-05
GO:0046395	carboxylic acid catabolic process	12	576	98	37767	1.10E-07	1.30E-05
GO:0009743	response to carbohydrate stimulus	18	576	240	37767	9.10E-08	1.30E-05
GO:0044248	cellular catabolic process	31	576	746	37767	1.10E-06	0.00012
GO:0009620	response to fungus	13	576	158	37767	2.10E-06	0.00021
GO:0009753	response to jasmonic acid stimulus	15	576	215	37767	2.50E-06	0.00023
GO:0010200	response to chitin	12	576	151	37767	7.30E-06	0.00063
GO:0009063	cellular amino acid catabolic process	7	576	47	37767	1.60E-05	0.0013
GO:0006631	fatty acid metabolic process	14	576	225	37767	1.80E-05	0.0014
GO:0009310	amine catabolic process	7	576	49	37767	2.00E-05	0.0015
GO:0051707	response to other organism	24	576	599	37767	3.10E-05	0.0021
GO:0009755	hormone-mediated signaling pathway	16	576	321	37767	6.10E-05	0.0034
GO:0031407	oxylipin metabolic process	6	576	39	37767	5.50E-05	0.0034
GO:0034641	cellular nitrogen compound metabolic process	21	576	506	37767	6.00E-05	0.0034

GO:0032870	cellular response to hormone stimulus	16	576	321	37767	6.10E-05	0.0034
GO:0009607	response to biotic stimulus	24	576	638	37767	8.00E-05	0.0043
GO:0032787	monocarboxylic acid metabolic process	18	576	408	37767	9.60E-05	0.0043
GO:0043436	oxoacid metabolic process	29	576	859	37767	9.60E-05	0.0043
GO:0009414	response to water deprivation	13	576	229	37767	8.60E-05	0.0043
GO:0006082	organic acid metabolic process	29	576	860	37767	9.80E-05	0.0043
GO:0019752	carboxylic acid metabolic process	29	576	859	37767	9.60E-05	0.0043

Bg total: Total number of genes in background

Bg item: Number of genes enriched for the given category in background

Query total: Total number of DEGs in input list

Query item: Number of DEGs enriched for a given category in input list

Table A8.1. Some representative defense/stress responsive genes upregulated in *tzf9* (Translatome, uninduced)

Gene_ids	Desc.TAIR10	SP.Function	Coef.mu_ctrl .wt_ctrl
AT1G62300.1	WRKY family transcription factor	Transcription factor involved in the control of processes related to senescence and pathogen defense. Interacts specifically with the W box (5'-(T)TGAC[CT]-3'), a frequently occurring elicitor-responsive cis-acting element. Activates the transcription of the SIRK gene and represses its own expression and that of the WRKY42 genes. {ECO:0000269 PubMed:12000796}.	2.739
AT4G12490.1	Bifunctional inhibitor/lipid- transfer protein/seed storage 2S albumin superfamily protein	Probable lipid transfer protein (LTP). May improve freezing survival. Seems to control the flowering process and lignin synthesis. Confers resistance to <i>Botrytis cinerea</i> . {ECO:0000269 PubMed:17257167, ECO:0000269 PubMed:17786468, ECO:0000269 PubMed:21815977}.	2.691

AT5G06870.1	polygalacturonase inhibiting protein 2	Inhibitor of fungal polygalacturonase. It is an important factor for plant resistance to phytopathogenic fungi.	2.672
AT1G57630.1	Toll-Interleukin-Resistance (TIR) domain family protein		2.642
AT3G15356.1	Legume lectin family protein	Plays a role in defense responses triggered by jasmonate, ethylene and chitin. {ECO:0000269 PubMed:19214436}.	2.386
AT2G39030.1	Acyl-CoA N-acyltransferases (NAT) superfamily protein	Acetyltransferase that converts ornithine to N5-acetylornithine, which is likely used in plant defense. {ECO:0000269 PubMed:21917546}.	2.324
AT5G67080.1	mitogen-activated protein kinase kinase 19	Functions in the NACK-PQR (NPK1-NQK1/MEK1-NRK1) MAP kinase signaling pathway, which is essential for somatic cell cytokinesis, especially for the cell-plate formation and its expansion, and depends on NACK1 and NACK2 kinesin-related proteins. Functions in the regulation of resistance gene-mediated resistance responses such as the N-mediated resistance to tobamovirus (TMV) and the Rx-mediated hypersensitive response (HR) to potato virus X (PVX). {ECO:0000269 PubMed:11159915, ECO:0000269 PubMed:11955449, ECO:0000269 PubMed:12194859, ECO:0000269 PubMed:22006334, ECO:0000269 PubMed:9790195}.	2.111
AT4G19700.1	SBP (S-ribonuclease binding protein) family protein	E3 ubiquitin-protein ligase involved in the regulation of pathogen and abiotic stress responses by facilitating degradation of MYB108/BOI. Attenuates cell death by preventing caspase activation. Has no effect on the stability of the DELLA proteins. Not regulated by MYB108/BOI. {ECO:0000269 PubMed:20921156, ECO:0000269 PubMed:21926169, ECO:0000269 PubMed:23482857}.	2.090
AT3G54420.1	homolog of carrot EP3-3 chitinase	Defense against chitin-containing fungal pathogens.	1.983

AT2G39660.1	botrytis-induced kinase1	Required to activate the resistance responses to necrotrophic pathogens. Phosphorylates FLS2 and BAK1. {ECO:0000269 PubMed:16339855, ECO:0000269 PubMed:20404519}.	1.918
AT2G37130.1	Peroxidase superfamily protein	Removal of H ₂ O ₂ , oxidation of toxic reductants, biosynthesis and degradation of lignin, suberization, auxin catabolism, response to environmental stresses such as wounding, pathogen attack and oxidative stress. These functions might be dependent on each isozyme/isoform in each plant tissue.; FUNCTION: Might function as heat shock-like defense protein. May be implicated in the systemic acquired resistance response.	1.738
AT4G01250.1	WRKY family transcription factor	Transcription factor involved in the expression of defense genes in innate immune response of plants. Interacts specifically with the W box (5'-(T)TGAC[CT]-3'), a frequently occurring elicitor-responsive cis-acting element. Activates WRKY 29, SIRK and its own promoters. {ECO:0000269 PubMed:11875555}.	1.544
AT5G45250.1	Disease resistance protein (TIR-NBS-LRR class) family	Disease resistance (R) protein that specifically recognizes the AvrRps4 type III effector avirulence protein from P.syringae. Resistance proteins guard the plant against pathogens that contain an appropriate avirulence protein via an indirect interaction with this avirulence protein. That triggers a defense system including the hypersensitive response, which restricts the pathogen growth. The combined presence of both regular and alternative RPS4 transcripts with truncated open reading frames (ORFs) is necessary for function (PubMed:17951452). RPS4 function is regulated at multiple levels, including gene expression, alternative splicing, and protein stability (PubMed:17951452). When over-expressed, confers temperature-conditioned EDS1-dependent auto-immunity (PubMed:24146667). Heterodimerization with RRS1 is required to form a functional complex to recognize AvrRps4 and PopP2 (PubMed:24744375). Abscisic acid deficiency enhances nuclear accumulation of RPS4 and its cell death-inducing activity (PubMed:22454454). {ECO:0000269 PubMed:10571887, ECO:0000269 PubMed:15469494, ECO:0000269 PubMed:22454454, ECO:0000269 PubMed:24146667, ECO:0000269 PubMed:24744375, ECO:0000305 PubMed:17951452, ECO:0000305 PubMed:19519800}.	1.406
AT5G39190.1	germin-like protein 2	May play a role in plant defense. Probably has no oxalate oxidase activity even if the active site is conserved.	1.400

AT4G03110.1	RNA-binding protein-defense related 1	RNA-binding protein that may be involved in the regulation of pre-mRNA alternative splicing. {ECO:0000250}.	1.311
-------------	---------------------------------------------	----------------------------------------------------------------------------------------------------------------	-------

Table A9: GO term enrichment of genes downregulated in *tzf9* (Translatome, uninduced)

GO_acc	Term	Query item	Query total	Bg item	Bg total	p-value	FDR
GO:0006412	translation	55	341	1445	37767	6.00E-19	5.70E-16
GO:0044237	cellular metabolic process	148	341	8722	37767	1.40E-16	6.70E-14
GO:0008152	metabolic process	167	341	10614	37767	4.30E-16	1.40E-13
GO:0044249	cellular biosynthetic process	100	341	4925	37767	3.40E-15	8.10E-13
GO:0044238	primary metabolic process	147	341	8995	37767	5.30E-15	1.00E-12
GO:0009058	biosynthetic process	101	341	5118	37767	1.40E-14	2.30E-12
GO:0019538	protein metabolic process	85	341	4009	37767	8.30E-14	1.10E-11
GO:0044267	cellular protein metabolic process	77	341	3487	37767	2.30E-13	2.80E-11
GO:0009987	cellular process	169	341	11684	37767	7.80E-13	8.20E-11
GO:0009266	response to temperature stimulus	26	341	485	37767	1.50E-12	1.40E-10
GO:0009409	response to cold	21	341	328	37767	9.80E-12	8.40E-10
GO:0043170	macromolecule metabolic process	117	341	7127	37767	1.50E-11	1.20E-09
GO:0034645	cellular macromolecule biosynthetic process	75	341	3661	37767	1.80E-11	1.30E-09
GO:0009059	macromolecule biosynthetic process	75	341	3685	37767	2.50E-11	1.70E-09
GO:0042254	ribosome biogenesis	18	341	241	37767	2.90E-11	1.80E-09
GO:0044260	cellular macromolecule metabolic process	108	341	6447	37767	4.20E-11	2.50E-09
GO:0022613	ribonucleoprotein complex biogenesis	18	341	253	37767	6.10E-11	3.40E-09
GO:0044085	cellular component biogenesis	24	341	571	37767	1.20E-09	6.30E-08

GO:0010467	gene expression	74	341	3962	37767	1.60E-09	7.80E-08
GO:0034404	nucleobase, nucleoside and nucleotide biosynthetic process	5	341	8	37767	6.80E-08	3.00E-06
GO:0034654	nucleobase, nucleoside, nucleotide and nucleic acid biosynthetic process	5	341	8	37767	6.80E-08	3.00E-06
GO:0009628	response to abiotic stimulus	36	341	1471	37767	1.10E-07	4.60E-06
GO:0034641	cellular nitrogen compound metabolic process	18	341	506	37767	1.50E-06	5.90E-05
GO:0055086	nucleobase, nucleoside and nucleotide metabolic process	12	341	221	37767	1.50E-06	5.90E-05
GO:0006950	response to stress	45	341	2320	37767	1.60E-06	5.90E-05
GO:0050896	response to stimulus	66	341	4057	37767	2.10E-06	7.70E-05
GO:0044271	cellular nitrogen compound biosynthetic process	15	341	394	37767	5.20E-06	0.00018
GO:0044262	cellular carbohydrate metabolic process	15	341	417	37767	9.90E-06	0.00033
GO:0009116	nucleoside metabolic process	6	341	50	37767	1.10E-05	0.00036
GO:0006457	protein folding	12	341	275	37767	1.30E-05	0.00039

Bg total: Total number of genes in background

Bg item: Number of genes enriched for the given category in background

Query total: Total number of DEGs in input list

Query item: Number of DEGs enriched for a given category in input list

Table A9.1. Some representative defense/stress responsive genes downregulated in *tzf9* (Translatome, uninduced)

Gene_ids	Desc.TAIR10	SP.Function	Coef.mu_ctl rl.wt_ctrl
AT1G09350.1	galactinol synthase 3	Galactinol synthase involved in the biosynthesis of raffinose family oligosaccharides (RFOs) that function as osmoprotectants. May promote plant stress tolerance (By similarity). {ECO:0000250}.	-1.635
AT2G22190.1	Haloacid dehalogenase-like	Removes the phosphate from trehalose 6-phosphate to produce free trehalose. Trehalose accumulation in plant may improve abiotic stress tolerance (By similarity). {ECO:0000250}.	-1.346

	hydrolase superfamily protein		
AT3G21950.1	S-adenosyl-L-methionine-dependent methyltransferase superfamily protein	Methyltransferase involved in the biosynthesis of methylsalicylate in response to stresses. Utilizes salicylic acid (SA) more efficiently than benzoic acid (BA). Can also use anthranilic acid and m-hydroxybenzoic acid as substrate. {ECO:0000269 PubMed:14617060, ECO:0000269 PubMed:19669626, ECO:0000269 PubMed:19958141, ECO:0000269 PubMed:20407809}.	-1.473
AT4G37910.1	mitochondrial heat shock protein 70-1	In cooperation with other chaperones, Hsp70s stabilize preexistent proteins against aggregation and mediate the folding of newly translated polypeptides in the cytosol as well as within organelles. These chaperones participate in all these processes through their ability to recognize nonnative conformations of other proteins. They bind extended peptide segments with a net hydrophobic character exposed by polypeptides during translation and membrane translocation, or following stress-induced damage (By similarity). {ECO:0000250}.	-1.328
AT3G06730.1	Thioredoxin z	Thiol-disulfide oxidoreductase that plays a role in proper chloroplast development, most likely through regulating plastid-encoded polymerase (PEP) dependent chloroplast transcription. Acts as a component of the transcriptionally active plastid chromosome that is required for plastid gene expression. May be involved in cell death and defense responses (By similarity). {ECO:0000250 UniProtKB:Q9LKW0, ECO:0000269 PubMed:16326926, ECO:0000269 PubMed:20133584, ECO:0000269 PubMed:20511297, ECO:0000269 PubMed:21949211}.	-1.105
AT5G03350.1	Legume lectin family protein	Plays a positive role in the effector-triggered immunity (ETI) response (PubMed:19199050, PubMed:24006883). Involved in salicylic acid (SA)-mediated processes occurring in ETI response,	-1.764

but is not involved in the autophagy process (PubMed:24006883). Promotes systemic rather than local immunity (PubMed:24755512). Essential for systemic acquired resistance (SAR), but not necessary for immune signaling downstream of SA (PubMed:24755512). May act in parallel with SA (PubMed:24755512). {ECO:0000269|PubMed:19199050, ECO:0000269|PubMed:24006883, ECO:0000269|PubMed:24755512}.

AT1G74930.1	Integrase-type DNA-binding superfamily protein	Probably acts as a transcriptional activator. Binds to the GCC-box pathogenesis-related promoter element. May be involved in the regulation of gene expression by stress factors and by components of stress signal transduction pathways (By similarity). {ECO:0000250}.	-2.109
AT4G39260.1	cold, circadian rhythm, and RNA binding 1	Plays a role in RNA transcription or processing during stress. Binds RNAs and DNAs sequence with a preference to single-stranded nucleic acids. Involved in mRNA alternative splicing of numerous targets by modulating splice site selection. Negatively regulates the circadian oscillations of its own transcript as well as RBG7 transcript. Forms an interlocked post-transcriptional negative feedback loop with the RBG7 autoregulatory circuit. Both proteins negatively autoregulate and reciprocally crossregulate by binding to their pre-mRNAs and promoting unproductive splicing coupled to degradation via the NMD pathway. Target of the <i>Pseudomonas syringae</i> type III effector HopU1. {ECO:0000269 PubMed:18987006, ECO:0000269 PubMed:19527663, ECO:0000269 PubMed:23042250}.	-1.646
AT4G13850.1	glycine-rich RNA-binding protein 2	Plays a role in RNA transcription or processing during stress. Binds RNAs and DNAs sequence with a preference to single-stranded nucleic acids. Displays strong affinity to poly(U) sequence. Exerts cold and freezing tolerance, probably by exhibiting an RNA chaperone activity during the cold and freezing adaptation process. {ECO:0000269 PubMed:11972043, ECO:0000269 PubMed:16207746, ECO:0000269 PubMed:17376161}.	-1.155

AT5G61030.1	glycine-rich RNA-binding protein 3	Possibly has a role in RNA transcription or processing during stress. {ECO:0000250}.	-1.154
AT1G14320.1	Ribosomal protein L16p/L10e family protein	Ribosomal protein involved in translational regulation (PubMed:18694459). Contribute to general translation under UV-B stress (PubMed:20516338, PubMed:23886624). Involved in the NIK1-mediated defense response to geminivirus infection (PubMed:18789471, PubMed:19112492). Acts coordinately with LIMYB as a transcriptional repressor (PubMed:25707794). {ECO:0000269 PubMed:18694459, ECO:0000269 PubMed:18789471, ECO:0000269 PubMed:19112492, ECO:0000269 PubMed:20516338, ECO:0000269 PubMed:23886624, ECO:0000269 PubMed:25707794}.	-1.031
AT3G18130.1	receptor for activated C kinase 1C	Minor component of the RACK1 regulatory proteins that play a role in multiple signal transduction pathways. Involved in multiple hormone responses and developmental processes (PubMed:18947417). MAPK cascade scaffolding protein involved in the protease IV and ArgC signaling pathway but not the flg22 pathway (PubMed:25731164). {ECO:0000269 PubMed:18947417, ECO:0000269 PubMed:25731164}.	-1.318
AT5G35220.1	Peptidase M50 family protein	Membrane-associated and ATP-independent metalloprotease required for development of both thylakoid grana and well-organized lamellae in chloroplast. Required for the accumulation of chlorophyll and chlorophyll a/b binding (CAB) proteins (from both PS I and PS II) in chloroplast membranes, and for grana formation and normal chloroplast development. Involved in the regulation of nuclear gene expression in response to ammonium stress and interacts with ABA signaling. Carries out beta-casein degradation in an ATP-independent manner in vitro. {ECO:0000269 PubMed:15659096, ECO:0000269 PubMed:18097640, ECO:0000269 PubMed:23064408}.	-1.049

AT3G23990.1	heat shock protein 60	Implicated in mitochondrial protein import and macromolecular assembly. May facilitate the correct folding of imported proteins. May also prevent misfolding and promote the refolding and proper assembly of unfolded polypeptides generated under stress conditions in the mitochondrial matrix.	-1.856
AT1G35720.1	annexin 1	Has a peroxidase activity. May act in counteracting oxidative stress. May also mediate regulated, targeted secretion of Golgi-derived vesicles during seedling development. {ECO:0000269 PubMed:15368128, ECO:0000269 PubMed:16153598}.	-1.025
AT4G27585.1	SPFH/Band 7/PHB domain-containing membrane-associated protein family	Mitochondrial protein that probably regulates the biogenesis and the activity of mitochondria. Stimulates cardiolipin biosynthesis, binds cardiolipin-enriched membranes where it recruits and stabilizes some proteins including prohibitin and may therefore act in the organization of functional microdomains in mitochondrial membranes. Through regulation of the mitochondrial function may play a role into several biological processes including cell migration, cell proliferation, T-cell activation, calcium homeostasis and cellular response to stress. May play a role in calcium homeostasis through negative regulation of calcium efflux from mitochondria. Required for mitochondrial hyperfusion a pro-survival cellular response to stress which results in increased ATP production by mitochondria. May also regulate the organization of functional domains at the plasma membrane and play a role in T-cell activation through association with the T-cell receptor signaling complex and its regulation. {ECO:0000269 PubMed:19360003, ECO:0000269 PubMed:23028053}.	-1.410

Herewith, I declare that this thesis and its content was made solely based on my work as a PhD student at the Martin-Luther Universität Halle-Wittenberg. This work was done independently without any help from others. Other resources and support than those stated in the thesis were not used. All citations are correct and the sources are acknowledged accordingly in the thesis references.

I certify that this thesis has never been submitted to other faculties or universities for examination.

Halle, October 2017
Tabassum

Naheed

Curriculum Vitae

Personal details

Name: Naheed Tabassum
Address: D/O Md. Moinul Haque
Hatpara Rd, Barharwa
Dist.; Sahiganj, Jharkhand, India.
PIN:816101

Date and place of birth: 27th January 1989 in Jharkhand

Education

1992-2000 Primary School, Bal Vidya Niketan, Barharwa, India
2000-2003 St. Thomas Girls' High School, Barharwa, India
2003-2006 Intermediate of Science, J.D. Women's; College, Patna, India
2007-2010 Bachelor of Science, Patna Women's College, Patna, India
2010-2012 Master of Science, Jamia Millia Islamia, New Delhi, India
Mar-May 2013 Technical assistant, NIPGR, New Delhi, India
June 2013- 2017 PhD work, Leibniz Institute of Plant Biochemistry, Halle(S), Germany

Halle, October 2017

Naheed Tabassum

Parts of this thesis have been published in the following paper talk and posters.

Journal paper

Maldonado-Bonilla, L. D., Eschen-Lippold, L., Gago-Zachert, S., Tabassum, N., Bauer, N., Scheel, D., & Lee, J. (2014). The Arabidopsis tandem zinc-finger 9 protein binds RNA and mediates pathogen-associated molecular pattern-triggered immune responses. *Plant Cell Physiol*, 55(2), 412-425. doi:10.1093/pcp/pct175

Talk

The Tandem Zinc-finger Protein 9 (TZF9), a mitogen-activated protein kinase substrate, mediates immunity in *Arabidopsis thaliana*. IGC symposium Sept 26-27, 2017, Oeiras Portugal.

Posters

The Tandem Zinc-finger Protein 9 (TZF9), a mitogen-activated protein kinase substrate, mediates immunity in *Arabidopsis thaliana*. PSSC, June, 2014, IPK, Gatersleben.

The Tandem Zinc-finger Protein 9 (TZF9), a mitogen-activated protein kinase substrate, mediates immunity in *Arabidopsis thaliana*. GARNet Sept 06-07, 2017, Cardiff, UK

Acknowledgements

I would like to convey my gratefulness to few people by honourably mentioning their names.

Prof. Dr. Dierk Scheel for granting me the rare opportunity to pursue to my doctorate degree in his lab under his kind supervision and encouragement.

Dr. Justin Lee for his excellent supervision and critical evaluation of my results. His knowledge and experiences greatly helped me nurture myself.

Without financial support of SFB648 and IPB, this work would not have been possible.

I would express my sincere appreciation to Dr. Arsheed Hussain Sheikh and Dr. Justin Lee and Prof. Dierk Scheel for editing this thesis.

Special thanks to my mentor, Dr. Selma P. Gago Zachert (MSV, IPB), who initially also helped me with RNA-EMSA experiment, Dr. Benedikt Athmer (SZB, IPB) for bioinformatics analysis, Dr. Wolfgang Hoehenwarter (Head of the proteomics group) for his help with Perseus, Dr. Luis Maldonado-Bonilla and Ms. Martina Brode for their wonderful jobs, Mr. Fabian Trempel for helping me with Luminometer, Mr. Hagen Stellmach (SZB, IPB) with microscope, Ms. Nicole Bauer and Dr. Arsheed Sheikh with learning techniques in my initial days, Dr. Lennart Eschen-Lippold and Mr. Martin Wehye for fruitful discussions, Dr. Alok Krishna Sinha for his kind concern and encouragement. I would like to thank each of my colleagues and friends in cellular signaling group, lab C119 and room C126 for a friendly comfortable environment.

My thanks to my families and friends for their patience and love. Special thanks to my Mother for always being there for me.

I am truly grateful to my husband for his unwavering support, encouragement and patience. This thesis is my dedication to you.

Appendix II (Data provided in CD)

